FINAL TECHNICAL REPORT

AWARD NUMBER: 08HQGR0029

Nonlinear Soil Behavior from Downhole Array Measurements and Site Response Modeling

Recipient / Primary Investigator

Youssef M. A. Hashash
Dept. of Civil & Environmental Engineering
Newmark Civil Engineering Laboratory
205 N Mathews Ave, Room 2230c
University of Illinois at Urbana-Champaign, Urbana IL 61801
Phone: (217) 333-6986. Fax: (217) 333-9464
E-mail: hashash@illinois.edu. URL: https://illinois.edu/~hashash

Program Elements:

Element 1: Technical Support for Seismic Practice and Code Development
Element 3: Problem-Focused Research and Technical Resources Development to Improve Seismic Engineering Practice

July 2010

Research supported by the U.S. Geological Survey (USGS), Department of the Interior, under USGS award number 08HQGR0029. The views and conclusions contained in this document are those of the author and should not be interpreted as necessarily representing the official policies, either expressed or implied, of the U.S. Government.

Abstract

Observations from earthquakes over the past 40 years have shown the importance of local site conditions on propagated ground motions. An increasing number of downhole arrays are deployed to measure motions at the ground surface and within the soil profile, along with pore pressure response within the soil profile. Recordings from these arrays are used to enhance our understanding of the wave propagation through these soils and hence to better characterize site effects. The available records have been used to calibrate and improve the available methodologies for site effects estimation. The USGS (e.g. through ANSS) and other agencies continue to make significant investments in the installation and maintenance of these arrays. New approaches are needed to maximize the benefit from these investments and that would result in a significant improvement in our ability to represent non-linear site response.

SelfSim, an inverse analysis framework, is employed to directly extract soil material behavior from downhole arrays that can be then be readily used in 1-D nonlinear site response analysis. The SelfSim, Self learning simulations, inverse analysis framework has been developed and employed for downhole arrays by the PI's research group with respect to total stress site response analysis. The successful performance of the total stress aspect of SelfSim is demonstrated using four synthetic vertical array recordings.

In this report we apply the developed SelfSim algorithm to extract total stress behavior from measurements from two field arrays - Lotung (Taiwan) and La Cienega (CA). Extensive evaluation of extracted soil behavior is described. The SelfSim algorithm is then extended to take advantage of both measured motions (acceleration and displacement) and pore pressure response obtained from downhole arrays. The successful performance of the expanded algorithm is demonstrated using four synthetic vertical array recordings and one case history recording from the original Wildlife Liquefaction Array, CA, which measured accelerations and excess pore pressure generation during the 1987 Superstition Hills earthquake. The resulting soil models and pore pressure models provide correct ground response and pore pressure generation capability, indicating that the extended algorithm is capable of extracting nonlinear soil behavior and pore pressure response using downhole array measurements.

Table of Contents

Abstract 2
1 Introduction 9
2 SelfSim (Self-Learning in Engineering Simulations) Methodology 11
2.1 SelfSim application to 1D seismic response - total stress analysis 11
2.2 SelfSim extension to 1D seismic response - fully coupled analysis 12
2.3 1D site response analysis procedure for Step 2a 13
2.4 1D site response analysis procedure for Step 2b 14
3 Use of NN to Represent Cyclic Soil Constitutive Behavior 16
3.1 Input variables and NN architecture for modeling of soil behavior and pore pressure response 16
3.2 Training and testing of NN material constitutive models 18
4 Application of SelfSim to Synthetically Generated Downhole Array Data - Total Stress Analysis, A brief review 19
5 SelfSim Learning of Field Array Measurements - Total Stress Analysis - Lotung Array, Taiwan 20
6 SelfSim applied to Field Array Measurements - Total Stress Analysis - La Cienega Array, CA 22
Method 1 Collect backbone curves 24
Method 2: Assume symmetric loops 24
Stage 3 Modulus reduction and damping curves 25
Stage 1 to Stage 3 evolution of extracted modulus reduction and damping 25
Evaluation of effect of number of cycles on soil behavior 25
Evaluation of effect of strain rates on soil behavior 26
7 Extension of SelfSim to Synthetically Generated Downhole Array Data - Coupled Analysis 28
7.1 Mesh discretization and analysis considerations for coupled analysis 28
7.2 Pore pressure dissipation and redistribution model 31
8 Application of SelfSim to Synthetically Generated Downhole Array Data - Coupled Analysis 32
8.1 Profile 1, single soil layer, sinusoidal motion 32
8.2 Profile 2, uniform soil profile with multiple layers, seismic motion 33
8.3 Profile 3, non-uniform soil profile, seismic motion 34
9 SelfSim Learning of Multiple Events at Profile 3 Vertical Array - Fully Coupled Analysis 35
9.1 Learning of individual events 35
9.2 Continued learning of three events 35
10 SelfSim applied to Field Array Measurements - Fully Coupled Analysis - Wildlife Liquefaction Array, CA 36
11 Discussion and Conclusions 38

12 Acknowledgments 39
13 References 40

List of Tables

Table 1 List of used events recorded by LLST 43
Table 2 List of used events recorded by La Cienaga array 44
Table 3 Parameters of Hyperbolic model used in DEEPSOIL to generate artificial array data 45
Table 4 Detail of the recording used to generate synthetic array 45

List of Figures

Figure 1 SelfSim algorithm applied to a downhole array. 46
Figure 2 A conventional site response analysis model: Acceleration is input at bedrock and converted to equivalent forces acting on lumped masses representing the soil column (from Tsai 2007, after Matasovic 1993). 47
Figure 3 Composite boundary condition of 1D site response analysis for Step 2(b) of SelfSim analysis, Figure 1. The force boundary from base acceleration is applied at the layers ($F=m\ddot{u}_g$) where no measurement (displacement) is available. 48
Figure 4 Illustration of (a) input parameters of general 3-point scheme and (b) the corresponding architecture of NN. (γ_i, τ_i) is current state of strain and stress. (γ_{i-1}, τ_{i-1}) and (γ_{i-2}, τ_{i-2}) are 2 history points which can be reverse points or immediate history points 49
Figure 5 1-Point model demonstrated for pore pressures (a); 3-point model demonstrated for stress-strain-pore pressure coupled behavior (b). Proposed NN architectures for (c) pore pressure response model, and (d) stress-strain model illustrating how the pore pressure output is given as input to the soil model..... 50
Figure 6 (a) Test results for NN pore water pressure model using the 1-point scheme, and (b) Test results for NN stress-strain model using the modified 3-point scheme..... 51
Figure 7 SelfSim learning of multiple events to improve SelfSim learning. Stage1: SelfSim learning of individual events. Stage2: combine data bases (DB) of extracted stress-strain behavior to train a new NN material model. Stage 3: SelfSim learning of individual events, and update of the combined data base used in retraining the NN material model. 52
Figure 8 Lotung DHB array geology and shear wave profile (Tang 1987). The profile shows the four NN material models used in SelfSim learning..... 53
Figure 9 Comparison of measured and computed displacement of LLST7 NS component prior to and after SelfSim Stage1 learning of LLST7 NS component. Total Stress SelfSim Learning - Lotung Array, Taiwan 54
Figure 10 Comparison of measured and computed response spectra of LLST7 NS component prior to and after Stage1 SelfSim learning of LLST7 NS component (right column) and prediction of response spectra of LLST7 EW components using NN material model extracted by Stage1 SelfSim learning of LLST7 NS component (left column). Total Stress SelfSim Learning - Lotung Array, Taiwan..... 55
Figure 11 Comparison of response spectra of LLST7 and LLST11 NS component computed by Stage 2 combined NN material model trained with combined data from LLST7 NS component and LLST11 NS component (Prior to SelfSim loop) and Stage 3 combined NN material model extracted after three more SelfSim learning loops using LLST11 NS component and LLST7 NS component. Total Stress SelfSim Learning - Lotung Array, Taiwan. 56
Figure 12 Prediction of surface response of LLST4, LLST7, LLST11, LLST12, LLST14, and LLST15 event using NN material model after Stage3 SelfSim learning of LLST7 NS component and LLST11 NS component. Total Stress SelfSim Learning - Lotung Array, Taiwan..... 57
Figure 13 Extracted stress-strain curves of four soil types from SelfSim Learning, Stage 1 and Stage 3, Lotung array. Total Stress SelfSim Learning - Lotung Array, Taiwan..... 58
Figure 14 Geology and shear wave profile of La Cienaga array (ROSRINE) and two assigned NN models according to the geology profile. C1-C3 indicates the location of the specimen used for lab tests. Total Stress SelfSim Learning..... 59

Figure 15 Comparison of surface response spectra of 3 events computed by Stage1 individual learning, Stage2 combined NN material model trained with combined data of (a) LC20 NS component, (d) LC4 EW component, and (e) LC18 NS component (Prior to SelfSim loop), and Stage3 combined NN material model extracted after four more SelfSim learning loops of (a) LC20 NS component, (d) LC4 EW component, and (e) LC18 NS component and prediction of four events using NN model after Stage3 SelfSim learning of LC20 NS component, LC4 EW component, and LC18 NS component, La Cienaga array. Total Stress SelfSim Learning - Lotung Array, Taiwan 60
Figure 16 Illustration of Method 1 to extract soil behavior. 61
Figure 17 Illustration of method 2 to extract soil behavior 61
Figure 18 Compare extracted behaviors by methods 1 and 2 with properties from laboratory tests (Anderson and Tang 1989) and those from system identification (Elgamal et al. 2001), Lotung array. 62
Figure 19 Compare extracted behaviors by methods 1 and 2 with the properties from laboratory tests (ROSRINE), La Cienaga array. 62
Figure 20 Evolution of extracted behaviors compared with the properties from laboratory tests (Anderson and Tang 1989) and those from system identification (Elgamal et al. 2001), Lotung array. 63
Figure 21 Evolution of extracted behaviors compared with the properties from lab test (ROSRINE), La Cienaga array. 64
Figure 22 Extracted behavior of Soil type 1 in terms of number of cycles, Lotung array 65
Figure 23 Extracted behavior of Soil Type 5 in terms of number of cycles, La Cienaga array 66
Figure 24 Comparison of soil degradation behavior extracted from downhole array and from lab test(Vucetic and Dobry 1988) 67
Figure 25 Extracted behavior of Soil Type 1 in terms of strain rate, Lotung array 68
Figure 26 Extracted behavior of Soil Type 5 in terms of strain rate, La Cienaga array 69
Figure 27 Comparison of strain-rate dependent behavior extracted from downhole array and from lab test (Matesic and Vucetic 2003) 70
Figure 28 SelfSim mesh generation for pore pressure transducer and accelerometer measurements located at the same depth. Layers with imposed pore pressures (Step 2a) are sub-divided to impose displacements in Step 2b. 71
Figure 29 Three synthetic vertical arrays considered for SelfSim analysis. 72
Figure 30 Learning of measured surface displacements, Profile 1, harmonic loading. 73
Figure 31 SelfSim learning of pore pressure measurements, Profile 1, harmonic loading. 74
Figure 32 Extracted soil behavior, Profile 1, harmonic loading. 75
Figure 33 SelfSim learning of surface displacements, Profile 2, Loma Gilroy broadband motion. 76
Figure 34 Evolution of surface response spectrum during SelfSim learning process from SelfSim learning (Pass 15), Profile 2. 77
Figure 35 Comparison of learned pore pressure response and extracted and target strain-stress curve of each layer, Profile 2. 78
Figure 36 Learning of (a) response spectra and (b) pore pressure generation in layer 5 for LG event, Profile 3 79
Figure 37 Comparison of extracted and target strain-stress curve and pore pressure response of 4 layers, Profile 3 80
Figure 38 SelfSim learning of multiple events to improve SelfSim learning. Stage1: SelfSim learning of individual events. Stage2: combine data bases (DB) of extracted stress-strain behavior to train a new NN

material model. Stage 3: SelfSim learning of individual events, and update of the combined data base used in retraining the NN material model. 81
Figure 39 Comparison of (a) ground response and (b) pore pressure generation in layer 5 for KK event. 82
Figure 40 Comparison of ground response for LY event. No excess pore pressures were generated during this event. 83
Figure 41 Predicted surface response spectra of a given event using SelfSim extracted NN material models from other events. 84
Figure 42 Comparison of surface response spectra (left column, a- c) and pore pressure response in Layer 5 (right column, d-e) of 3 events predicted by using a combined NN material model trained with combined data base (Prior to SelfSim loop) and combined NN material model extracted from SelfSim learning. 85
Figure 43 Soil profile at the Wildlife Site and the instrumentation (from Matasovic, 1993; after Benett et al., 1984). 86
Figure 44 Geology and shear wave profile of Wildlife Liquefaction Array and four assigned NN models according to the geology profile. Accelerometers are located at the top and bottom of the considered profile. Pore pressure measurement locations are denoted as P1, P2, and P3. 87
Figure 45 Comparison of surface response spectra of surface measurements, results from 1D site response analysis models, and the SelfSim algorithm for three scenarios (SH1, SH2, SH3) at the original Wildlife Site. 88
Figure 46 Comparison of pore pressure recordings with results from 1D site response analysis models, as well as the SelfSim algorithm for three scenarios (SH1, SH2, SH3). 89
Figure 47 Extracted soil behavior from the SH2 (D/M Initialization) case of SelfSim learning demonstrating the degradation of shear modulus. 90

1 Introduction

Observations from earthquakes over the past 40 years have shown the importance of local site conditions on propagated ground motions. Strong motion records from many earthquakes (e.g. 1957 San Francisco Earthquake, 1989 Loma Prieta Earthquake, 1999 Chi-Chi earthquake) show significant differences between soil sites and nearby rock sites response. The 1985 Mexico City earthquake showed that soft soils can amplify ground motions and result in significant damage even at large distances from the earthquake source.

Conventional site response analysis models are used to predict seismic site response at a site including acceleration, velocity and displacement at ground surface and within the soil column. Pore water pressure models are similarly used to predict the generation of excess pore water pressures within the soil column, which in turn effect the site response. The accuracy of these predictions highly depends on both the representation of cyclic soil behavior and pore water pressure response. Laboratory tests are often used to measure or evaluate dynamic soil behavior and pore water pressure response. The measured soil behavior and pore water pressures are used to develop cyclic soil constitutive models and pore pressure response models which are implemented in a site response analysis model. However, the loading paths from lab tests can be significantly different from those experienced by the soil in the field and are not necessarily completely representative of anticipated soil behavior or pore water pressure response under real shaking.

Significant investments in downhole arrays have been and continue to be made to measure motions at the ground surface and within the soil profile, with additional pore water pressure data measured throughout the same profile. These arrays provide the real data necessary to better understand local site effects, in situ dynamic soil behavior and pore water pressure response under earthquake loading. Downhole arrays also provide a check on the accuracy of site response analysis models. Ad-hoc approaches are sometimes adopted to adjust soil model properties to match field observations. The approaches are not always successful and do not necessarily provide additional insights into the seismic site response or nonlinear cyclic soil behavior.

SelfSim, an inverse analysis framework, is employed to directly extract soil material behavior from downhole arrays that can be then be readily used in 1-D nonlinear site response analysis. The SelfSim, Self learning simulations, inverse analysis framework has been developed and employed for downhole arrays by the PI's research group and is extensively verified using synthetically generated downhole array data (Tsai and Hashash 2008).

SelfSim integrates site response analysis and field measurements, by learning the observed measurements (accelerations and displacements time series) from a vertical array while extracting the underlying nonlinear soil behavior. The main advantages of this approach over existing parametric and nonparametric system identification methods are that there is no need to

assume a specific soil behavior apriori and that the extracted response can be readily employed in site response analysis.

As part of this work, SelfSim is applied to actual array recordings from the Lotung (Taiwan) and La Cienega (CA) arrays under total stress consideration. Multiple recordings are needed to define the nonlinear soil behavior. The extracted soil behavior can be examined for factors such as influence of number of non-uniform loading cycles and loading rates.

The SelfSim algorithm is further developed to take advantage of both measured motions (acceleration and displacement) and pore pressure response obtained from downhole arrays. The successful performance of the expanded algorithm is demonstrated using four synthetic vertical array recordings and one case history recording from the Wildlife Liquefaction Array, CA, which measured accelerations and excess pore pressure generation during the 1987 Superstition Hills earthquake. Through the extended SelfSim algorithm, the field measurements can be reproduced while the in-situ soil behavior and pore pressure response can be extracted.

The extracted soil behavior can be developed into a library that can be directly used in site response analyses. Alternately, the extracted soil behavior can be used to develop new conventional constitutive models that contain features of extracted in situ behavior. This approach represents a major shift in our approach to representing and characterizing non linear soil behavior for site response analysis.

2 SelfSim (Self-Learning in Engineering Simulations) Methodology

The SelfSim methodology is an extension of the autoprogressive algorithm originally proposed by Ghaboussi et al (1998). With the use of a neural network (NN) based material model, the autoprogressive method is used to extract material behavior from non-uniform material tests (Ghaboussi et al. 1998; Sidarta and Ghaboussi 1998) . In a similar manner, the algorithm employed in SelfSim extracts stress-strain material behavior using global load and deflection measurements. Hashash et al (2003) further developed this method to update constitutive models using measured deformations around an excavation. Using an incremental nonlinear finite element analysis, two sets of boundaries (forces/displacements) are imposed in parallel with a parallel analysis scheme. The parallel analyses yield stress-strain pairs that are used to train the NN material model. The procedure is repeated until there is an acceptable match between the two analyses. The resulting NN model can then be used in the forward analysis of new boundary value problems.

2.1 SelfSim application to 1D seismic response - total stress analysis

The SelfSim framework allows for the extraction of the stress-strain field of a material from a general boundary value problem and provides a rich data set in which to train a NN based model. Further research by Tsai and Hashash (2008) extended the framework to the extraction of the stress-strain field from dynamic problems that were limited to total stress analysis considerations. The concept of extending SelfSim from static to dynamic problems is realized by recognizing that the loading (e.g. construction) steps of static problems are analogous to the loading steps (equal to the number of time steps) of dynamic problems. Two parallel boundary condition site response analyses are performed with NN based constitutive models to simulate the soil behavior. Initially, the soil response is unknown and the NN soil models are pre-trained using stress-strain data that reflect viscous linear elastic response over a limited strain range.

In a typical 1D seismic site response problem, a seismic motion is propagated from the bottom of the soil profile to the ground surface. In a downhole array the ground response corresponding to base shaking is measured at selected depths within the soil profile. The input base shaking and the corresponding measurements within the soil profile yield complementary sets of field observations. SelfSim uses these measurements to extract the underlying dynamic soil behavior. The parallel boundary condition analyses performed within SelfSim consist of the force boundary conditions applied in one analysis, referred to as Step 2a, and displacement boundary conditions applied in the other analysis, referred to as Step 2b.

In Step 2a of SelfSim a site response analysis using the current NN soil model is performed simulating ground response given a base shaking. The measured acceleration from the deepest point in a vertical array is applied at the bottom of the soil column in a conventional time-domain nonlinear site response analysis. Stresses and strains are computed throughout the soil column based on dynamic equilibrium considerations. However, the computed displacements may not necessarily match recorded displacements of the downhole array. SelfSim

stipulates that since the applied boundary forces due to base acceleration are accurate then the corresponding computed equilibrium stresses provide an acceptable approximation of the true stress field experienced by the soil.

In Step 2b of SelfSim a parallel site response analysis using the same NN soil model is performed in which the measurements from a downhole array are imposed as additional displacement boundary conditions. Displacements integrated from recorded acceleration time series within the soil profile are imposed in a 1-D time domain nonlinear site response analysis. Again, the stresses and strains are computed throughout the soil column. SelfSim stipulates that since the applied displacements are accurate then the corresponding computed equilibrium strains provide an acceptable approximation of the true strain field experienced by the soil.

The stresses from Step 2a and the strains from Step 2b form stress–strain pairs that approximate the soil constitutive response. The material constitutive model is updated by training and retraining the NN based material model using the extracted stress-strain pairs. The entire process is repeated several times using the full ground motion time series until analyses of Step 2a provide ground response similar to the measured response. SelfSim has extracted sufficient information about the dynamic soil response to reproduce the field measurements. The numerical procedures for conducting analyses for Step 2a and Step 2b are described in detail by Tsai (2007b). The applicability of the framework to total stress site response analysis is demonstrated in both synthetic arrays (Tsai and Hashash 2008) as well as field arrays from the Lotung and La Cienaga arrays to extract and evaluate the in situ soil behavior. This report presents the extension of the SelfSim framework to fully coupled site response analysis.

2.2 SelfSim extension to 1D seismic response - fully coupled analysis

Similar to the application to total stress site response analysis, the dynamic problem can be treated as a number of incrementally applied loading steps equal to the number of time steps. Figure 1 shows the concept of SelfSim applied to the downhole array problem with inclusion of pore water pressure response. In Step 1, measurements of accelerations and pore pressures are gathered from the downhole array instrumentation. The displacement boundary condition is established from the double integration of acceleration measurements. Ground motion response is simulated using a modified version of the 1D nonlinear time domain component of the DEEPSOIL code (Hashash and Park 2001).

In order to implement SelfSim algorithm for fully-coupled seismic site response the following is needed:

1. A 1D site response analysis procedure for Step (2a) which includes the effects of pore pressures

2. A 1D site response analysis procedure for Step (2b) which includes the effects of pore pressures

3. A NN material model architecture that is capable of representing cyclic soil behavior and pore pressure response.

Site response analyses of Step 2a & 2b are again performed using a modified version of the 1-D non-linear time-domain component of the DEEPSOIL code (Hashash and Park 2001), www.illinois.edu/~deepsoil.

2.3 1D site response analysis procedure for Step 2a

In Step 2a, the measured acceleration from the deepest point in a vertical array is applied at the bottom of the soil column. This type of analysis is the same as a typical time-domain non-linear site response analysis that propagates the motion from the base of the soil column to the ground surface. Soil layers are represented by lumped masses, dashpots and springs (Figure 2) and the response of soil layers can be expressed using the equation of motion:

$$[M]\{\ddot{u}\} + [C]\{\dot{u}\} + [K]\{u\} = -[M]\{I\}\ddot{u}_g = \{F\} \tag{1}$$

Where $[M]$ is the mass matrix, $[C]$ is the damping matrix and $[K]$ is the stiffness matrix. Base acceleration $\ddot{u}_g$, as shown in Figure 2, can be converted to equivalent forces imposed on the lumped masses. The Newmark-β method (Chopra 1995) is used to solve Eq (1).

From time step *i* to *i+1*, Eq (1) can be simplified as

$$[K_i']\{\Delta u_i\} = \{P_i'\} \tag{2}$$

where

$$[K_i'] = \left[\frac{6[m]}{\Delta t^2} + \frac{3[c]}{\Delta t} + [k]_i\right] \tag{3}$$

$$\{P_i'\} = [m]\{I\}\left(\ddot{u}_{gi+1} - \ddot{u}_{gi}\right) + [m]\left[\frac{6}{\Delta t}\{\dot{u}\}_i + 3\{\ddot{u}\}_i\right] + \left[3\{\dot{u}\}_i + \frac{\Delta t}{2}\{\ddot{u}\}_i\right]$$

At time step i, $\{\ddot{u}\}_i$, $\{\dot{u}\}_i$, $\Delta\ddot{u}_{gi}$, $[m]$, $[c]$, and $[k]_i$, are given and $\{\Delta u\}_i$, is to be solved. Once $\{\Delta u\}_i$ is obtained, the displacement, velocity and acceleration at time step i+1 is

$$\{u\}_{i+1} = \{u\}_i + \{\Delta u\}_i \tag{4}$$
$$\{\dot{u}\}_{i+1} = \{\dot{u}\}_i + \{\Delta\dot{u}\}_i$$
$$\{\ddot{u}\}_{i+1} = \{\ddot{u}\}_i + \{\Delta\ddot{u}\}_i$$

In general, it is known that the generation of excess pore pressures will affect the stiffness of the soil column and must therefore be included in the equation of motion. In DEEPSOIL, the components of the stiffness matrix [k] for layer j are defined as:

$$k_j = \frac{G_j}{h_j} \tag{5}$$

Where G_j is the shear modulus and h_j is the thickness of layer j. For a nonlinear analysis, k_j is the tangent stiffness of the shear model, and G_j is the tangent shear modulus. When a neural network material model is employed, the tangent shear modulus is calculated as (Tsai and Hashash 2008):

$$G_{tan} = \frac{\tau_i - \tau_{i-1}}{\gamma_i - \gamma_{i-1}} \tag{6}$$

Where τ and γ are the shear stress and shear strain respectively. The tangent shear modulus is updated at every time step.

For the fully coupled analysis, the NN-based soil constitutive model must include states of pore water pressure as input to determine the next shear stress. Thus, the computed τ inherently includes the effect of the pore water pressure. By this inheritance the tangent shear modulus, stiffness matrix, and therefore the equation of motion incorporate the effect of pore water pressure on the stiffness of the soil layer. Thus, the calculation scheme of Step 2a is applicable to both the total stress and fully coupled analyses.

Similar to the application to total stress analysis, SelfSim stipulates that since the applied boundary forces due to base acceleration are accurate then the corresponding computed equilibrium stresses provide an acceptable approximation of the true stress field experienced by the soil. However, the computed displacements may not necessarily match recorded displacements of the downhole array. Since the generation of excess pore pressures in non-cohesive soils is primarily governed by the level of cyclic shear strain (Dobry 1982; Matasovic 1993), then the computed excess pore pressures generated may not necessarily match recorded pore pressures. Recorded pore pressures may be imposed in this step of the analysis, but no computed pore pressures from this analysis are used in training.

2.4 1D site response analysis procedure for Step 2b

In Step 2b displacements integrated from recorded acceleration time series at different depths are imposed in a 1-D time domain nonlinear site response analysis. Recorded data, however, are only available at certain depths as shown in Figure 3. The displacements of other layers are not readily known and need to be determined by solving the equation of motions. Therefore, the equivalent force due to base shaking are still imposed on the layers where no displacement measurements are available. This procedure is described for a 4-layer system (4 degrees of freedom system). The full matrix of Eq (2) can be expressed as

$$\begin{bmatrix} k'_{11} & k'_{12} & 0 & 0 \\ k'_{12} & k'_{22} & k'_{23} & 0 \\ 0 & k'_{23} & k'_{33} & k'_{34} \\ 0 & 0 & k'_{34} & k'_{44} \end{bmatrix} \begin{Bmatrix} \Delta u_1 \\ \Delta u_2 \\ \Delta u_3 \\ \Delta u_4 \end{Bmatrix} = \begin{Bmatrix} p'_1 \\ p'_2 \\ p'_3 \\ p'_4 \end{Bmatrix} \tag{7}$$

The matrix can be expanded in equation form to:

$$\begin{aligned} & k'_{11}\Delta u_1 + k'_{12}\Delta u_2 = p'_1 \\ & k'_{12}\Delta u_1 + k'_{22}\Delta u_2 + k'_{23}\Delta u_3 = p'_2 \\ & k'_{23}\Delta u_2 + k'_{33}\Delta u_3 + k'_{34}\Delta u_4 = p'_3 \\ & k'_{34}\Delta u_3 + k'_{44}\Delta u_4 = p'_4 \end{aligned} \tag{8}$$

Assume the measurement is available at layer 1 (surface) and layer 3, i.e. Δu_1 and Δu_3 are known and therefore P_1' and P_3' are redundant. The first and third equation which relate to P_1' and P_3' are eliminated and the rest of the equations are kept. Reassembling these equations yields

$$\begin{bmatrix} k'_{22} & 0 \\ 0 & k'_{44} \end{bmatrix} \begin{Bmatrix} \Delta u_2 \\ \Delta u_4 \end{Bmatrix} = \begin{Bmatrix} p'_2 - k'_{12}\Delta u_1 - k'_{23}\Delta u_3 \\ p'_4 - k'_{34}\Delta u_3 \end{Bmatrix} \tag{9}$$

Eq (9) implies that the available measurement Δu_1 provides the extra information (constraint, appearing on right side of equation) to solve the problem. The base acceleration imposes equivalent forces on the layers where no measurements are available as shown in Eq (9). Therefore, the site response analysis procedure for Step 2b solves the equations of motion with boundary condition composed of equivalent forces and displacements. Once $\{\Delta u\}_i$ is solved, the displacement, velocity and acceleration at the next time step can be also obtained.

Similar to the application to total stress analysis, SelfSim stipulates that since the applied displacements are accurate then the corresponding computed equilibrium strains provide an acceptable approximation of the true strain field experienced by the soil. Since the generation of excess pore pressures in non-cohesive soils is primarily governed by the level of cyclic shear strain (Dobry 1982; Matasovic 1993), then the computed excess pore pressures generated are also stipulated to provide an acceptable approximation of the pore pressure response in the field and are used in training. Recorded pore pressures are imposed in this step of the analysis, and both computed and imposed pore pressures are used in training.

3 Use of NN to Represent Cyclic Soil Constitutive Behavior

The work of Ghaboussi and his co-workers (Chou and Ghaboussi 1997; Ghaboussi et al. 1991) shows that a Neural Network, NN, can be used to define material constitutive relation through training using stress-strain data. If the data contains adequate relevant information, the trained neural network can interpolate or generalize material behavior to new loading cases. Many other researchers (Ellis et al. 1995; Penumadu and Zhao 1999; Zhu et al. 1998) have shown that NN are capable of representing soil nonlinear behavior for static problems, whereby only monotonic loadings are applied. For a cyclic loading-reloading, the data set contains one-to-many relationships. The direct mapping method is not efficient to capture such complex behavior. According to Basheer (2000), mapping techniques include: Function labeling, Function fragmentation, Quasi-sequential dynamic mapping, and Hybrid model. Quasi-sequential dynamic mapping is the most common technique to map cyclic behavior. It uses historical (prior) states of the function (or data) to predict future states. Wu and Ghaboussi (1993) used 3 history strain-stress data, 3-point scheme, to map concrete behavior in uniaxial cyclic compression. Yamamoto (1992) modeled Ramberg-Osgood type hysteretic loops with strains and stresses at the points where moving direction was most recently reversed. This is more like the function labeling method, which identifies the segments that restrict the function from being one-to-one by assigning distinctive indicators to them. Yun (2006) modeled hysteretic behavior of beam-column connections using one history point (Quasi-sequential dynamic) and three internal variables (function labeling) as input, which can be classified as hybrid model.

Using the 3-point scheme, Tsai (2007b) optimized the NN architecture by testing various combinations of history points until the NN could provide accurate cyclic soil constitutive behavior. The architecture of the NN along with the input parameters required for the 3-point scheme is illustrated in Figure 4b. The input parameters chosen to capture the cyclic constitutive behavior consist of 3 history points of stress-strain pairs along with the future state of strain. These input parameters provide the next state of stress as output. In the optimization of the NN architecture, Tsai (2007b) found that the use of 19 nodes in each of the two hidden layers of the NN provided the best results. It is from this 3-point scheme and NN architecture that additional developments are proposed to extend the NN capability to capture in-situ soil behavior as well as pore water pressure response.

3.1 Input variables and NN architecture for modeling of soil behavior and pore pressure response

It is procedurally desirable to couple the modeling of cyclic soil constitutive behavior with the generation/dissipation of pore water pressures in a single NN. The model used by Tsai and Hashash (2008) is modified to include three immediate history points of pore water pressure along with the current state of pore water pressure as input. The output is also modified to include the future state of pore water pressure. This architecture would allow a single model to be used to predict the future state of stress and pore water pressure from a single dataset of input. However, initial results suggest that the coupling of the two behaviors cannot be adequately

captured by the single NN model. Possible reasons for such results include that the generation of excess pore water pressure may primarily be dependent on the level of shear strain and not shear stress, and also that the next state of shear stress is dependent on the next state of pore water pressure. If the prior statements are assumed to be true then the future state of pore water pressure is required to determine the future state of shear stress. Thus, two separate NN models must be employed to capture both the dynamic behavior of soil as well as the pore water pressure response.

The NN architecture used by Tsai and Hashash (2008) is already proven to yield accurate results for total stress analyses – that is to say that the next state of shear stress is accurately determined from a given dataset. When considering a fully coupled analysis, the generation of excess pore water pressures will affect the state of shear stress experienced by the soil. Thus, the previous NN architecture is modified to include three immediate history points of pore water pressure along with the current state of pore water pressure as input. However, only the future state of shear stress is given as output.

Here it is important to note the manner in which the stiffness of the soil is calculated, Eq (6), as it has serious implication on the training of the NN soil model. Since the tangent shear modulus is calculated using a change in stress, this means that the initialized NN soil model must include some knowledge of degradation behavior. Without some initial suggestion of the degradation behavior, it is unlikely for any degradation behavior to be learned.

While developing the NN model for the capture of the pore water pressure response, the following observations were made:

1. The generation of excess pore water pressure is primarily dependent on the level of shear strain and not the level of shear stress (i.e. shear stress should not be included as input),
2. The amount of excess pore water pressure generated over a given time step is a function of the absolute change in shear strain $|\gamma_i - \gamma_{i-1}|$ in that time step,
3. The learning of the minimum required shear strain for excess pore pressures to be generated can be accommodated by providing a local reference shear strain – in this case, the absolute shear strain at the reversal point, $|\gamma_{rev}|$,
4. The γ_{rev} parameter can also be used to distinguish between loading/unloading conditions by setting it equal to zero when shear strains cross from positive to negative values (or vice versa), and
5. Since the NN model is intended to represent generation of excess pore water pressure, results of zero or negative excess pore pressure generation can be excluded from training.

From these assumptions, a 1-point scheme illustrated in Figure 5a is proposed to capture the pore water pressure response.

3.2 Training and testing of NN material constitutive models

To fully test how well the NN is trained, a recursive dynamic test is performed starting from a known initial condition to predict the next state, which in turn is used to predict the next state, and so on until the last stage. Therefore, a strain history and initial state of stress and pore water pressure are given. The resulting pore pressures and stresses of each step are input of the next step.

The NNs trained by different schemes described in Section 3.1 are tested using synthetic data generated by DEEPSOIL. Before the training of the NN to capture soil constitutive behavior can be tested, the training of the NN to capture pore pressure response must first be accurate as the output of the pore pressure response NN is an input to the soil behavior NN.

Results from the testing of the developed pore water pressure NN are shown in Figure 6a. In this case, Figure 6a indicates that the model has sufficiently learned both when excess pore water pressure is generated as well as the magnitude. Thus, the 1-point scheme is acceptable for capturing the pore water pressure response.

With an accurate pore pressure response model available, the training of the NN model for soil behavior is tested. For this test, the output of the pore pressure response model is provided as the current state of pore water pressure as input for the soil behavior model. The test result for the stress-strain model is shown in Figure 6b. The results correspond very well with the target stress-strain curves, suggesting that the modified Tsai and Hashash model is acceptable for modeling soil behavior in fully coupled analyses.

With the modeling schemes of the separate NNs established, the NN architecture of each model could be firmly established. The proposed architectures were illustrated in Figure 5.

Figure 5c shows the NN architecture for the capture of pore water pressure (pwp) response. The architecture consists of an input layer containing four nodes, two hidden layers each containing 19 nodes, and one output layer containing one node. The input layer consists of the most recent reversal strain, the next shear strain, and the difference between the next shear strain and previous shear strain. The inclusion of the most recent reversal strain allows the model to "learn" when the soil is experiencing a path of loading or unloading by providing a local point of reference strain. This plays a pivotal role in the pwp generation behavior in sands as the bulk of the pwp is generated during unloading.

Figure 5d illustrates the NN architecture for the capture of dynamic soil constitutive behavior including the effect of excess pwp. The architecture is similar to that developed by Tsai (2007b), with the exception that the input layer consists of 11 nodes, with a pwp history point (u^*) added to each stress-strain pair, and also the next state of pwp (u^*_{i+1}) as computed by the NN pwp model.

4 Application of SelfSim to Synthetically Generated Downhole Array Data - Total Stress Analysis, A brief review

The SelfSim learning of global measured responses while extracting the underlying soil behavior from downhole array measurements is demonstrated using synthetically generated downhole array data. The advantage of using synthetically generated array data is that soil behavior is known in advance and can be used to evaluate the extracted NN soil model. Development of synthetic vertical array data follows three steps:

Select a soil profile with known nonlinear soil behavior at the site. The hyperbolic model in DEEPSOIL describes the dynamic soil behavior. Model parameters of the hyperbolic model used for soil columns correspond to the nonlinear soil properties of the Mississippi embayment.

All tests follow the same procedure to generate synthetic array data:

1. Use DEEPSOIL to propagate a motion at bedrock through soil columns with known soil behavior using the hyperbolic soil model.
2. The output displacement, velocity, and acceleration are used as synthetic array data.

Three profiles are employed to demonstrate how SelfSim can be applied to extract dynamic soil behavior while capturing the measured site response from downhole measurements. The key finding from these analyses is that recordings from multiple earthquakes with varying amplitudes are necessary to learn the nonlinear soil behavior of a range of shear strains. The procedure for learning from multiple events is illustrated in Figure 7. Learning of individual events is conducted followed by combined learning of multiple events.

5 SelfSim Learning of Field Array Measurements - Total Stress Analysis - Lotung Array, Taiwan

In the early 1980s the US Electric Power Research Institute (EPRI) in cooperation with the Taiwan Power Company (TPC) conducted a Large-Scale Seismic Test (LSST) at a site near Lotung, within the southwestern quadrant of the SMART1 array (Tang 1987). A 1/4 scale containment structure modeling a nuclear power plant was instrumented. The sensors installed on the structure and beneath the ground provided the recording for the study of soil –structure interaction. Many earthquakes were recorded during the period 1985–1986.

Ground instrumentation of LLST includes two downhole arrays (DHA and DHB) that extend to a depth of 47 m below ground surface. Sensors containing three-component accelerometers oriented in the east-west (EW), north-south (NS), and up-down (UD) directions were installed at surface, 6m, 11m, 17m and 47m below the surface. DHA is located 3 m from the 1/4 scale structure, and DHB is located 47 m from the structure. Only DHB vertical array recordings are utilized in this paper since recorded motions more closely reflect free-field site response.

The geology of the Lotung site is summarized by Wen and Yeh (1984) and Tang (1987). The area consists of a recent alluvium layer 40-m to 50-m thick overlying a Pleistocene formation that varies from 150 to 500 m in thickness. Underlying the Pleistocene material is Miocene basement rock. Figure 8 shows the simplified soil profile consisting of inter-layered silty sand and sandy silt with some gravel, over clayey silt and silty clay. Ground-water level is about 1 m below ground surface. The shear wave velocity profile is based on the geophysical test results (Tang 1987).

Eighteen earthquakes were recorded between 1985 and 1986, including three moderate events (about 0.2 g peak lateral surface acceleration). Six events, listed in Table 1, are selected for SelfSim learning and prediction. One weak event (LLST14) is used to calibrate small strain linear soil properties (i.e. Vs profile and small strain damping). One strong event (LLST7) and one medium event (LLST11) are used for SelfSim learning. The rest of events are used to predict site response using extracted nonlinear material behavior.

Prior to SelfSim learning, an appropriate linear site response model has to be developed that can capture soil column response to very weak ground motions. LLST14, surface PGA=0.04 g, is used to calibrate the small strain properties used in site response model. The measurements at 47 m are propagated through the modeled soil column and the computed ground responses are compared with measurements at 0m, 6m, 11m, and 17m below ground surface. The soil below 47m is modeled as a rigid base since the input motion is a within motion (Kwok et al. 2006). A shear wave velocity (V_s) profile is proposed by Tang (1987). Two values for damping have been proposed in the literature, 1% damping suggested by Anderson and Tang (1989) based on laboratory tests and 5% suggested by Elgamal et al. (2001) based on system identification inverse analysis. The measurements of LLST14 are best matched using the V_s profile proposed

by (Tang 1987) and 3% small strain damping. These values are used in subsequent SelfSim learning.

Four NN material models are assigned to soil layers to reflect soil stratigraphy shown in Figure 8. The NN material models are initialized to represent the same small strain linear behavior. SelfSim learning is conducted in stages as shown in Figure 7. The best SelfSim performance in Stage 1 is achieved by adding sensor information one at a time from bottom to top of the array mimicking the wave propagation. After several passes all measurements are then imposed simultaneously.

Prior to SelfSim learning, the computed response at surface, 6m, 11m and 17m below surface given the NS motion at 47m using the initialized models is different from the measurements as shown in Figure 9 and the left column of Figure 10. SelfSim learning is required to improve the results. After 8 passes, SelfSim extracts sufficient information about the soil behavior to reproduce the ground motion measurements well.

The extracted NN material models from the SelfSim learning of LLST7-NS are then used in a site response analysis to predict the response for the LLST7-EW as shown in the right column of Figure 10. The measured ground motion response is well predicted indicating that extracted soil behavior is independent of the ground motion direction.

Similarly, Stage 1 SelfSim learning of LLST11-NS component is conducted and similar observations are made; (a) SelfSim extracts sufficient information about soil behavior to capture ground motion measurements well, and (b) the soil model extracted for SelfSim learning of LLST11-NS when used in a site response model can predict the LLST11-EW measured ground motion response well (Tsai 2007a).

During SelfSim Stage 1 learning of LLST7-NS and LLST11-NS stress-strain data bases for each of the soil layers are generated. In Stage 2, and for a given soil layer, the data bases from LLST7-NS and LLST11-NS are combined and used to train a new NN soil model for that layer.

Additional SelfSim Stage 3 learning which combines the two events (SelfSim loop) is carried out to enhance the extracted soil behavior and the combined learning of LLST7-NS and LLST11-NS. After 3 loops, SelfSim learning can simultaneously match the measured response of the two events very well as shown in Figure 11. Stage 3 learning improves the computed response after Stage 2 learning.

The four NN material models extracted from the SelfSim learning process of LLST7-NS and LLST11-NS are employed in site response analysis to predict the ground motion response for all events listed in Table 1. For LLST12 and LLST17 events, the deepest available measurement is at 17m. Therefore, site response analyses for these two events only are performed for the upper 17m using NN1, NN2, NN3 material models and the measurements at

17m are used as the input motions. For the rest of events, site response analyses are still performed for the entire soil column (47m) using NN1, NN2, NN3, and NN4 material models. The predicted surface response for all motions are shown in Figure 12. Details of the predictions for the other depths can be found in Tsai (2007a). The predicted responses for events approximate very well the measured responses. The extracted soil behavior from LLST7-NS and LLST11-NS was sufficient to predict the response for other events.

The extracted stress-strain histories at Stages 1 & 3 of SelfSim learning are shown in Figure 13. At stage 1 (individual event learning), the extracted NN material models from LLST7-NS have evolved sufficiently to represent nonlinear and hysteretic behavior of the soil, but those from LLST11-NS are still close to linear behavior. At stage 3 (combined learning), the extracted stress-strain loops of LLST7-NS shows greater nonlinearity. The stress-strain loops of LLST11 benefit significantly from the combined learning to reflect nonlinear and hysteretic behavior.

6 SelfSim applied to Field Array Measurements - Total Stress Analysis - La Cienega Array, CA

In 1989, the California Strong Motion Instrumentation Program (CSMIP) began instrumenting boreholes with strong-motion accelerometers to study site amplification effects including the La Cienega array. The array is located near the section of the Santa Monica freeway (I-10) at La Cienega that collapsed during the Northridge earthquake. Accelerometers are installed at surface, and at depths of 18, 100 m, and 252m (Graizer et al. 2000).

The geologic profile consists of recent fluvial deposits of about 30 m in thickness over marine deposits (sands, silts, clays and gravels). P-wave and S-wave velocity surveys were performed by Caltrans (suspension logging method) and the U.S. Geological Survey (averaging along the geologic layers). S-wave velocities are about 140 m/sec near the surface and increase to about 600 m/sec at 100 m depth. The obtained Vs profile of the upper 18m is shown in Figure 14 (Darragh et al. 1997).

Nineteen earthquakes with magnitudes 1.9<M<7.1 have been already recorded at this site, at the surface and at depths of 18 and 100 m. The latest few events, including the M7.1 Hector Mine and its M5.8 aftershock, were also recorded at the recently instrumented deepest hole (252m). The epicenters of these events, however, are distant from the La Cienega site and, consequently, the recorded motions at the site are not strong enough to induce significant nonlinear soil behavior. Only 3 events, listed in Table 2, which produce higher intensities at the sites are selected for SelfSim learning. One additional weak event (LC11) is used to calibrate small strain properties.

Only upper 18m soil column is used in SelfSim learning as site response analysis results of the entire soil column (252m) indicate that significantly greater nonlinear soil response is induced in the top 18m (note that the next recording point is at 100m). The weak event LC11, surface PGA=0.012g, is used to calibrate the V_s and small strain damping profiles of the soil column. Trial and error calibration shows that a soil profile with a shear wave velocity of $1.1V_s$ of Figure 14 and 2% damping provide the best match with measurements and are used in the site response analysis model for SelfSim learning.

Prior to SelfSim learning, two individual NN material models, initialized to represent the small strain linear behavior, are assigned to soil layers according to the geological profile as shown in Figure 14. SelfSim learning is performed in three stages:

1. SelfSim Stage 1 individual component learning: SelfSim learning is performed each of the three motions separately. Similar to the findings for the Loting array, the learned behavior from one event component (e.g. LC20-NS) can be used to reliably predicted the response of the other event component (e.g. LC20-EW) Details of the predictions for the other components can be found in (Tsai 2007a).
2. SelfSim Stage 2 combined learning: After SelfSim Learning of individual events, extracted stress-strain behavior is combined into a single data bases (DB) for each soil layer and is used to train a new NN material model for each of the layers. Figure 15a, d, e show computed results of 3 events using this combined NN material model (without additional SelfSim learning loops).
3. SelfSim Stage 3 combined learning: Additional SelfSim learning which combines the three events, SelfSim loop, is performed to enhance the results. No improvement in learning is achieved after 4 loops.

Figure 15a, d, e show the improvement in computed surface response at various SelfSim learning stages. Overall the computed response approximate the measured response very well. Additional details on SelfSim learning of LaCienaga array can be found in Tsai (2007a).

The NN material models extracted at the end of Selfsim learning are used in a site response analysis model to predict the remaining event components listed in Table 2. Figure 15b, c, f, g, h show that the learned behavior can reliability predict other events not used in the learning process. It appears that SelfSim successfully extracted relevant soil behavior and that the extracted soil behavior is independent of ground motion direction.

The preceding sections showed that SelfSim extracted soil behavior used in site response analysis provide a very good estimate of measured ground motions. An important by product of SelfSim is the ability to gain insights into soil behavior extracted from field recordings.

Nonlinear dynamic soil behavior is often characterized by modulus reduction and damping curves (Kramer 1996). These curves are constructed based on laboratory testing

whereby the soil sample is subjected to a sinusoidal harmonic motion. The influence of strain amplitude, number of cycles and loading rate and frequency on soil behavior are studied individually (Idriss et al. 1978; Isenhower and Stokoe 1981; Kim et al. 1991; Matesic and Vucetic 2003; Vucetic 1992; Vucetic and Dobry 1988).

However, the SelfSim extracted soil behavior is the result of general irregular motions that include a range of strain amplitudes, number of cycles and loading rate all combined together. Therefore it is challenging to separate these effects. This section presents two methods to interpret the extract soil behavior for selected soil layers from each array.

Method 1 Collect backbone curves

In this method a smoothed "backbone curve" is developed using extracted stress-strain data. The procedure is illustrated in Figure 16:

1. Re-assemble stress-strain loading paths (loops) between two reverse points as monotonic loading paths.
2. Find a best fit curve through the monotonic loading paths.
3. Construct loops at different strain levels by complementing the imaginary part of the fitted curve and assuming closed and symmetric loops.
4. Construct modulus reduction curve and damping curve based on these loops.

Different functions are tested for regression analysis and it is found that hyperbolic model provides the best curve fit in Step 2 of Figure 16. Darendeli (2001) and Roblee and Chiou (2004) also adopt hyperbolic model in regression analysis to fit modulus reduction curves obtained from lab tests. The method has been verified using synthetic generated stress-strain loops given known soil behaviour (e.g. hyperbolic model and Masing rule) by Tsai and Hashash (2008).

Method 2: Assume symmetric loops

While Method 1 provides a rational procedure to extract soil behaviour, it cannot provide insights into soil behaviour such as dependence on number of cycles of loading rate. Therefore, Method 2 is introduced and illustrated in Figure 17:

1. Construct loops between two reverse points of stress-strain loops by adding a complementary, imaginary, part of the stress-strain paths between two reverse points. Assume these loops are closed and symmetric.
2. Compute modulus reduction and damping from each of these.

Unlike Method 1, Method 2 does not aggregate stress-strain data to find a smooth curve. Instead, the stress-strain loops are processed individually in Method 2. Thus, more randomness and irregularity are expected yet more "realistic" soil behaviour can be interpreted. Only loading paths containing more than 3 points are used to calculate damping and secant modulus.

Stage 3 Modulus reduction and damping curves

Figure 18 compares the extracted soil behavior behaviors by Methods 1 & 2 with those from lab test (Anderson and Tang 1989) and those from system identification (Elgamal et al. 2001) for LLST. The soil behavior obtained from lab tests and from the system identification provides an average behavior for the entire soil column but SelfSim is able to extract behavior of different soil types. SelfSim learning failed if the same soil model is used for all four soil layers indicting differences in behavior between the various layers. The interpretation extracted soil behavior using Method 1 is closer to the results from system identification than from laboratory tests but show distinct differences. The results from Method 2 show significant scatter but do show a general trend of modulus reduction and increased damping with increasing strain amplitude.

Figure 19 provides a similar comparison of the LaCienega array. The extracted soil behavior, both Soil type 1 and type 2, are similar to the lab test results. Soil type 2 (gravel), however, shows greater normalized modulus reduction and damping compared to Soil type 1 (silty clay, loam). This is similar to the observation by others (Kramer 1996; Vucetic and Dobry 1991) that cohesive soil experiences less normalized modulus reduction and damping with strain increasing compared to granular soils.

Stage 1 to Stage 3 evolution of extracted modulus reduction and damping

Tsai and Hashash (2008) find that extracted soil behaviour from Stage 1 individual event learning reflects more of an "equivalent linear" behaviour and that combined event learning (stage 3) to capture the nonlinearity in soil behaviour. Figure 20 shows Method 2 interpretation of soil behavior of the Lotung array for Stages 1 and 3 learning. In Stage1, the learned behavior provides a reasonable estimate of modulus reduction and damping in the "equivalent" strain range corresponding to the level of shaking (event). For example, the extracted behavior from the weak motion (LLST11) is more accurate at small strains while the extracted behavior from the medium motion (LLST7) is more accurate at large strains. After combined learning (Stage3), the extracted behavior evolves to show a continuous nonlinear behavior over the entire strain range.

A similar observation can be made for the data from the La Cienega array shown in Figure 21.

In this section, soil behavior is simply interpreted as modulus reduction and damping curve. Both Method 1 and Method 2 show the capability of providing a reasonable interpretation of soil behavior. The extracted stress-strain loop, however, reveals more information rather than only two simple curves. Therefore, Method 2, which provides more capability, is adopted to further explore in-situ soil behavior in the next section.

Evaluation of effect of number of cycles on soil behavior

Cyclic degradation is the reduction of soil stiffness and strength parameters due to repeated cyclic loading. Experiments by Idriss et al (1978) revealed that both the initial stiffness

and the ordinates of the degraded backbone curves are reduced after several cycles. To quantify such degradation, Idriss et al (1978) introduced the concept of the degradation index, δ:

$$\delta = \frac{G_{sN}}{G_{s1}} \tag{10}$$

G_{sN} and G_{sl} is secant modulus after N cycles and at the first cycle, respectively. In general, granular soils are more likely to experience degradation and higher rate of degradation under cyclic loading compared to cohesive soils (Vucetic 1992; Vucetic and Dobry 1988).

In order to explore modulus degradation with number of cycles, the corresponding accumulated number of cycles are counted while determining the secant modulus and damping from stress-strain loops by Method 2. Figure 22 and Figure 23 present the extracted behavior of one soil layer in terms of number of cycles from LLST and LC respectively. Similar interpretation for the other soil layers can be found in Tsai (2007a). The stress-strain paths used in this interpretation are obtained from site response analyses of all events, listed in Table 1 and Table 2, for each of the sites. The interpreted behavior shows clearly the degradation of modulus with increased number of cycles. However, the interpreted behavior shows little dependency of damping on number of cycles. Given a strain amplitude, the degradation index δ corresponding to various number of cycles can be determined. Figure 24 shows the comparison of the interpreted degradation index δ from LLST and LC with lab testing results on clay (Vucetic and Dobry 1988). At the Lotung site where soil layers are mainly composed of silt and sand, higher degradation rates are interpreted compared to that of clay obtained from lab tests. At the La Cienega site, Soil type 6 (gravel) has a higher rate of degradation than Soil type 5 (clay), a trend that is in line with laboratory test reults. For all soil types, the rate of modulus degradation is nonlinear and increases with increase in number of cycles.

Evaluation of effect of strain rates on soil behavior

Several studies (Isenhower and Stokoe 1981; Kim et al. 1991; Matesic and Vucetic 2003) were conducted to explore the impact of strain rates and loading frequencies on soil behavior. The test results indicate that the shear modulus may increases with increase in the average shear strain rate, displaying a linear relationship with lognormal of the shear strain rate.

While modulus and damping of extracted soil behavior is obtained from stress-strain loops using Method 2, the corresponding strain rate can be determined as follows:

$$\dot{\gamma} = \frac{\gamma}{T} \tag{11}$$

Where γ is the total strain difference between two reverse points as shown in Figure 17 and T is the duration between them. Figure 25 and Figure 26 present the extracted behavior in terms of strain rates. Note that the extracted data points from LLST and LC at large strain (i.e. larger loop) do not necessary represent low strain-rate cycles as commonly obtained from lab testing. Instead,

those data points stand for the cycles with larger strain rate. The decrease in strain rate results in modulus reduction, which is similar to observations from laboratory test. However, the extracted behavior does not show much correlation between damping and strain rate.

The strain rate effect on shear modulus can be further quantified. Given an amplitude of cyclic strain, the obtained moduli at various strain rates are normalized to the modulus at the strain rate of 0.01%/s and are compared to lab test result as shown in Figure 27. Similar to the lab test results, the extracted behavior also shows the positive correlation between modulus and strain rate but the impact of strain rate is different at different ranges of cyclic strain. At small strain (0.001%), the effect of strain rate on modulus is small. Both extracted behavior and the lab test results are qualitatively consistent, however the interpreted behavior shows greater influence of strain rate on the shear modulus.

7 Extension of SelfSim to Synthetically Generated Downhole Array Data - Coupled Analysis

The extension of the SelfSim framework to coupled analysis requires careful consideration of how excess pore pressure time histories are to be imposed in the parallel analyses employed by the framework, and how the effect of dissipation/redistribution of the excess pore pressure can be modeled throughout the soil profile. This section discusses (1) mesh discretization and analysis considerations for application of both displacement and excess pore pressure measurements in analysis, and (2) the development of an excess pore pressure dissipation and redistribution model for analysis.

7.1 Mesh discretization and analysis considerations for coupled analysis

The successful inclusion of multiple data types within the SelfSim analysis framework first requires an understanding of how and where such data types are calculated within the modeled soil profile. By construction, there are two types of data considered within the analysis: (1) data calculated by solving the equation of motion [e.g. acceleration, velocity, and displacement], and (2) data calculated from the models employed in analysis [e.g. shear strain, shear stress, excess pore pressure]. The first data type is calculated at the top of each modeled layer in the analysis which is referred to as a computation node. The second data type is calculated at the mid-point of each modeled layer and is referred to as an integration point. By definition, a computation node cannot exist at the same location as an integration point.

The imposition of measured excess pore pressures and displacements in Step 2a and Step 2b respectively raises an analytical issue within the SelfSim framework if both measurements are available at similar depths within the soil profile. This is due to the fact that the determination of excess pore pressure, shear stress, and shear strain occurs at integration points located at the mid-point of each layer, while displacements occur at computational nodes located at the top of each layer. Thus, to make use of all available data, the mesh discretization for Step 2a and Step 2b must differ.

Measured pore pressures are imposed in Step 2a, while measured displacements are imposed in Step 2b. Thus, what will be an integration point in Step 2a will be a displacement node in Step 2b. This implies that integration points in the two analyses will not be consistent, and thus data from these points cannot be used for training. If a given soil layer is represented as a single layer in Step 2a, then it must be sub-divided into two layers in Step 2b. However, if this is done, the integration points for the layer will not match between analyses, and no training could occur for this layer. Additional sub-layers are required for these layers if any training is to occur. Layers which contain only a single type of measurement (i.e. displacement *or* pore pressure) do not need to be subdivided.

Figure 28 illustrates the development of the mesh generation for Step 2a and Step 2b for a downhole array with pore pressure and acceleration measurements located at similar depths in the soil profile. In this consideration, a downhole array profile consisting of 3 soils (Soil 1, Soil 2, Soil 3) has measurements of pore pressure and acceleration at the same depths in Soil 2 and Soil 3.

Mesh discretization begins with Step 2a, where only base excitation and pore pressure measurements are imposed. The discretization of Soil 1 remains intact as there are no measurements in this layer. For Soil 2 and Soil 3, the soil layers are each discretized into 3 sub-layers (Figure 28) which will each employ the soil-specific NN for each sub-layer. The pore pressure measurement is imposed in the second sub-layer and no data is extracted from this sub-layer. Training data for the soil is only extracted from the first and third sub-layers, as these integration points will match those of Step 2b.

Mesh discretization continues with Step 2b, where only base excitation and displacement measurements are imposed. The mesh discretization in Step 2b is similar to that of Step 2a, with the exception that sub-layers which contained pore pressure measurements in Step 2a must now be further sub-divided into two additional sub-layers of equal thickness in Step 2b (Figure 28) in order to impose displacements. The measured displacements are imposed between these two sub-layers, and no data is extracted from either sub-layer. Data is only extracted from the top and bottom sub-layers as their integration points will match those of Step 2a.

The result of the proposed mesh discretization procedure results in a learning process governed by neighboring behavior. For layers which contain measurements of pore pressure and displacement at the same depth, training data is only obtained from sub-layers where no measured values are imposed but whose behavior is affected by neighboring layers which do contain imposed measurements. In this case, the imposition of all available data is actually detrimental to learning the soil behavior and pore pressure response. Since pore pressure measurements are not actually used in training and the meshes of the two analyses differ, there can be no computational convergence check on pore pressure computations with respect to measurements in these layers. Similarly, there can be no convergence check on displacements at depth for these layers. Convergence is primarily governed by checking that the computations for layers containing only a single type of measurement for an analysis match those imposed in the complementary analysis. In the considered case, convergence would occur when the computed surface displacements from Step 2a match those imposed in Step 2b. While all available data can be readily imposed in a single SelfSim analysis for efficiency, it does not necessarily result in optimal learning of behavior. A sequential procedure is required.

The sequential method of SelfSim analysis is a lengthy procedure, but is developed to maximize the benefit of the recorded measurements in the learning process. In this method, 3 separate SelfSim analyses are employed:

SelfSim A:

For layers which contain both pore pressure and displacement measurements at the same depth, only displacement measurements are employed at these depths. The pore pressure measurements located at the same depth as displacement measurements are omitted in this analysis. This allows for the meshes of Step 2a and Step 2b to be equivalent. Layers which contain only pore pressure measurements may have such measurements imposed in Step 2a as integration points and displacement nodes will match between analyses. Analysis continues until the displacements computed in Step 2a match those imposed in Step 2b, and also until pore pressures computed in Step 2b match any imposed in Step 2a. The results of this analysis provide a reasonable approximation of the strain field experienced throughout the soil profile. The NNs developed in this analysis are extracted and employed in the next SelfSim analysis, SelfSim B.

SelfSim B:

For layers which contain both pore pressure and displacement measurements at the same depth, only pore pressure measurements are employed at these depths. The displacement measurements located at the same depth as pore pressure measurements are omitted in this analysis. Again, this allows for the meshes of Step 2a and Step 2b to be equivalent. Layers which contain only displacement measurements may have such measurements imposed in Step 2b as integration points and displacement nodes will match between analyses. Analysis continues until the pore pressures computed in Step 2b match those imposed in Step 2a, and also until displacements computed in Step 2a match any imposed in Step 2b. The results of this analysis provide a reasonable approximation of the pore pressure response of the soil. The NNs developed in this analysis are extracted and employed in the final SelfSim analysis, SelfSim C.

SelfSim C:

In this analysis, the meshes of Step 2a and Step 2b are developed as described above. The NNs developed from SelfSim B are employed in this analysis. Analysis continues until the computations of displacements in Step 2a match any appropriate applied measurements in Step 2b, and also until the computations of pore pressures in Step 2b match any appropriate applied measurements in Step 2a. At the conclusion of this analysis, the resulting NNs are applied to the SelfSim A and SelfSim B analyses to verify accuracy. The procedure is repeated until (1) computed displacements in SelfSim A match the imposed displacements, (2) computed pore pressures in SelfSim B match the imposed pore pressures, and (3) the computed pore pressures and displacements in SelfSim C match the imposed measurements at layers containing only a single measurement.

For profiles where measurements of displacements and excess pore pressures occur at different depths within the profile, the same mesh discretization may be used for both parallel analyses. In this case, the analysis framework is similar to the total stress analysis where the mesh discretizations employed yield corresponding computation nodes and integration points.

7.2 Pore pressure dissipation and redistribution model

During ground shaking, the generation and dissipation of excess pore pressures occurs simultaneously. A variety of models are available to model the generation of excess pore pressures, including the neural network material model described in this report. The dissipation/redistribution of excess pore pressures can be modeled by Terzaghi 1D consolidation theory:

$$\frac{\partial u}{\partial t} = c_v \left(\frac{\partial^2 u}{\partial z^2} \right) \tag{12}$$

where c_v is the coeffecient of vertical consolidation representing the rate at which a given soil can dissipate excess pore water pressure. The 1D consolidation equation can be approximated by finite difference formulae in which calculations occur at the midpoints of layers and it is assumed that the excess pore pressure in a given layer can be expressed at any time by a parabola. In 1D analysis, dissipation of the excess pore water pressure is assumed to occur only in the vertical direction.

8 Application of SelfSim to Synthetically Generated Downhole Array Data - Coupled Analysis

The SelfSim learning of global measured responses while extracting the underlying soil behavior from downhole array measurements is demonstrated using synthetically generated downhole array data. The advantage of using synthetically generated array data is that soil behavior is known in advance and can be used to evaluate the extracted NN soil model. Development of synthetic vertical array data follows three steps:

Select a soil profile with known nonlinear soil behavior at the site. The hyperbolic model in DEEPSOIL describes the dynamic soil behavior. The Dobry-Matasovic model is used to describe the pore pressure response. Model parameters of the hyperbolic model used for soil columns are listed in Table 3, and correspond to the nonlinear soil properties of Seed & Idriss curves for mean sands, with pore pressure parameters corresponding to the sands present at the Wildlife Site in California.

All tests follow the same procedure to generate synthetic array data:

1. Use DEEPSOIL to propagate a motion at bedrock through soil columns with known soil behavior using the hyperbolic soil model.
2. The output displacement, velocity, acceleration, and pore water pressure data of certain layers are used as synthetic array data.

Three profiles, illustrated in Figure 29, are employed to demonstrate how SelfSim can be applied to extract dynamic soil behavior while capturing the measured site response from downhole measurements.

8.1 Profile 1, single soil layer, sinusoidal motion

Profile 1 is subjected to a sinusoidal ground motion (2 Hz). The fundamental frequency of the site is 3.125 Hz, which is larger than the frequency of sinusoidal motion. Therefore, the sinusoidal wave will not be filtered out by the soil deposit.

Prior to SelfSim learning, the NN pore pressure generation model is initialized to represent cyclic generation of excess pore pressures over a limited shear strain range. The NN soil material model is similarly initialized to represent linear elastic behavior over the same limited shear strain range. The computed surface response using this initialized model is different from the measurements (target) as shown in Figure 30a. In order to learn global behavior gradually, SelfSim learning is divided into three windows as shown in Figure 30b. Once SelfSim learning can match the measurements within a given window, learning is continued over the next window:

SelfSim Learning, window 1: Over this window the dynamic loading includes one cycle of excess pore pressure generation. After 20 SelfSim learning passes (Figure 30c), calculated surface displacements approach the target measurements within this window. At this point, the period of oscillation has been learned well. However, the learned behavior is not sufficient to correctly predict the response over the entire recorded ground motion as illustrated in Figure 30c because the strain range obtained in the first window is limited as well is the amount of modulus degradation.

SelfSim Learning, window 2: Twenty additional SelfSim learning passes are then performed using the measurements in window 2 (through the 3rd cycle of excess pore pressure generation). The computed response matches the measurements very well (Figure 30d) over the learning window and can approximately predict the response at later shaking stages.

SelfSim Learning, window 3: Twenty additional SelfSim learning passes are then performed using the measurements in window 3 (the entire period of shaking). Figure 30e shows a very good match of SelfSim and measurements after a complete SelfSim learning process.

Figure 31 shows the SelfSim learning of excess pore pressure measurements, while Figure 32 shows the evolution of the extracted soil behavior due to SelfSim learning. Prior to SelfSim learning the soil behavior is nearly linear elastic with some initial suggestion of degradation behavior with increasing pore pressures. Through SelfSim learning from vertical array measurement, the extracted soil behavior is very close to the target soil behavior and able to represent nonlinear and hysteretic behavior, as well as excess pore pressure response.

8.2 Profile 2, uniform soil profile with multiple layers, seismic motion

A broadband input motion recorded during the Loma Prieta Earthquake, Table 4, which covers a wide range of frequencies, is used to generate the synthetic recordings in Profile 2 at the ground surface, Figure 29b. The 40ft soil column is subdivided into 4 layers so that the maximum propagated frequency is at least 25 Hz. Although soil properties are uniform at the site, soils within different sub-layers experience different loading paths.

Prior to SelfSim learning, the NN material models are initialized to represent linear elastic behavior with inclusion of degradation within a limited strain range. The same NN material models are used for all layers. The computed surface motion using the initialized model is different from the measurements (target) as shown in Figure 34 which plots the surface response spectra.

SelfSim learning is divided into 3 windows for this event based on the amplitude of the motion as shown in Figure 33a. Once SelfSim learning can match the measurement for a given window, then SelfSim learning is continued for the next window:

SelfSim Learning, window 1: After five SelfSim learning passes (Figure 33b), calculated surface displacements already approach the target measurements within this window. Five passes are sufficient to learn the behavior within this window because the shaking is not strong and the soil column response is nearly linear elastic with insignificant generation of excess pore pressures. The learned behavior is not sufficient to correctly predict the behavior over the entire recorded ground motion as illustrated in Figure 33b. Nevertheless the overall response is an improvement over the initial computed response shown in Figure 33a.

SelfSim Learning, window 2: Five additional SelfSim learning passes are then performed using window 2 data. The computed response (Pass 10) matches measurements very well (Figure 33c) over the learning window and can predict well response at later shaking stages.

SelfSim Learning, window 3: Five additional SelfSim learning passes are then performed using the window 3 data (the entire period of shaking). Figure 33d and Figure 34 show a very good match with measurements.

It appears that SelfSim is able to extract sufficient information about the soil behavior to accurately reproduce the field measurements.

The extracted stress-strain history and pore pressure response is compared to the known target soil response in Figure 35. Although the extracted behavior does not exactly match the target behavior there is an overall good match with the target response.

8.3 Profile 3, non-uniform soil profile, seismic motion

A broadband motion recorded during Loma Prieta Earthquake is used to generate the synthetic recordings in a two-layer soil profile with recordings at the ground surface and at the two layer interface as shown in Figure 29c.

The two soil layers are assigned two different sets of NN material models during SelfSim learning. Prior to SelfSim learning, the two sets of NN material models are initialized to represent linear elastic behavior with degradation effects. The computed surface motion and the motion at depth, using the initialized models are different from the measurements (target) as shown in Figure 36.

SelfSim learning is best accomplished by adding sensor information into the learning process one by one from bottom to top of the array mimicking the wave propagation. Measurements at lower layers are imposed first. After 4 SelfSim passes all measurements are then imposed simultaneously. Figure 36 shows the computed response spectra and pore pressure behavior in Layer 5. After a total of 5 passes, the measurements are reproduced well.

The extracted strain-stress history and pore pressure response of the 5th SelfSim pass is compared to the target soil response in Figure 37. Layer 1 and 3 represent soil 2 and Layer 5 and Layer 7 represent soil 3. The extracted NN material models have evolved sufficiently to

represent nonlinear and hysteretic behavior, while reasonably approximating excess pore pressure generation. Larger excess pore pressure generation was extracted for Layer 7, but overall there is a good match with target response.

9 SelfSim Learning of Multiple Events at Profile 3 Vertical Array - Fully Coupled Analysis

At most arrays recordings from multiple events are available for learning of soil behavior. It is assumed that recordings from 2 additional events (Table 4) are available at Profile 3 vertical array: (1) a recording from a weak motion (LY), and (2) a medium motion (KK). The SelfSim learning scheme using the multiple events is illustrated in Figure 38. Initial learning of individual events is conducted followed by combined learning of events.

9.1 Learning of individual events

Figure 39 and Figure 40 show the results of SelfSim learning of individual events KK and LY. The SelfSim learning for the LG event was shown in Figure 36. SelfSim learning is able to capture the measured surface response and pore pressure response in Layer 5.

In order to evaluate the predictive capability of the material models extracted from the individual events, site response analyses, using the material model extracted from a given event, are performed using input motions of the other three events as shown in Figure 41. As was observed earlier in this report, if the strain range experienced by the soil is within the strain range learned by the extracted constitutive model, then the predicted response is close to the measured response. For example, for the LY event, the models extracted from the KK and LG events (which are larger events) give a reasonable prediction of the surface response. However, for the KK and LG events, the LY event provides very poor prediction of the surface response.

9.2 Continued learning of three events

After SelfSim learning of individual events, extracted stress-strain behavior is combined into a single data base (DB) used to train a new set of NN material models (Figure 38, Stage 2). Figure 42 shows that the individual predictions of the 3 events using these combined NN material models (without additional SelfSim learning loops) have generally produced improved results.

Additional SelfSim learning which combines the three events, termed a SelfSim loop, is carried out to enhance the results as shown in Figure 38. A SelfSim loop includes sequential SelfSim passes. Each SelfSim pass is still performed separately for each event. The stress-strain data extracted from each individual event are used to update DB and combined with data from other events during each NN material model update. The updated NN material model from one event (pass) is used for the next event (pass). After 3 loops, SelfSim learning can simultaneously predict the measured response of all three events very well (Figure 42) as well as the pore pressure response in the soil.

10 SelfSim applied to Field Array Measurements - Fully Coupled Analysis - Wildlife Liquefaction Array, CA

The Wildlife liquefaction array in California is located in the flood plain of the Alamo River in the Imperial Valley. The original array was installed by the USGS in 1983. The array was installed in a stratigraphy consisting of flood plain deposits overlying a layer of liquefiable sands, which in turn overlay thick layers of overconsolidated clays as illustrated in Figure 43. The ground water table is located approximately 1.5 m from the ground surface.

The soil profile is broken into sub-layers utilizing four sets of NN models as illustrated in Figure 44. The first set of NN models (NN1) is for silt layers above the ground water table. It is assumed that no excess pore pressures are generated in these layers (i.e. the NN pore pressure material model is effectively set to zero in these layers). Silt layers below the ground water table use NN2. Sand termed as Wildlife Sand A (WSA) is modeled using NN3. Finally, sand termed as Wildlife Sand B (WSB) is modeled using NN4. All layers were modeled such that the minimum cutoff frequency was greater than 35 Hz for each layer.

The ground instrumentation includes two accelerometers located at the ground surface and immediately below the liquefiable material, as well as six (6) piezometers – five of which are located within the liquefiable material. Data from the 1987 Elmore Ranch and 1987 Superstition Hills earthquakes are currently available for this case study. However, the 1987 Elmore Ranch earthquake caused recorded PGA of 0.13 g with no significant excess pore pressures (and no available pore pressure measurements). In contrast, the 1987 Superstition Hills earthquake had recorded PGA of 0.21 g and generated significant excess pore pressures to the extent of liquefaction ($u^* = u'/\sigma'_{v0} = 1$).

The recordings offer a unique opportunity as often downhole arrays have more accelerometers than piezometers. Thus this investigation has the potential to give significant insight into factors affecting modulus degradation and generation of excess pore pressures for liquefiable sands.

Three scenarios using the Superstition Hills N-S earthquake measurements are considered in this investigation:

SH1 – Imposed Recordings, Linear Elastic NN Initialization,

In this case, the measured ground surface displacements and pore pressure recordings from the Superstition Hills Earthquake are implemented in SelfSim analysis to extract the underlying soil behavior. The NN material models are initialized to represent linear elastic behavior (with some degradation due to generation of excess pore pressures) over a limited strain range. Extracted behavior and ground response is compared with the recordings where available.

SH2 – Imposed Recordings; PDHM / D-M PWP Computed Values NN Initialization

In this case, the measured ground surface displacements and pore pressure recordings from the Superstition Hills Earthquake are imposed as in SH1. In this scenario, the NN material models are initialized using PDHM and D-M pore pressure results from a 1D analysis. The results are again compared as in SH1.

SH3 – Imposed Recordings; PDHM / GMP PWP Computed Values NN Initialization

In this case, the measured ground surface displacements and pore pressure recordings from the Superstition Hills Earthquake are once again implemented. The NN material models are initialized using PDHM and GMP pore pressure results from a 1D analysis. The results are again compared as in SH1.

Comparison of the surface response from surface measurements, 1D site response analysis models, and SelfSim scenarios SH1, SH2, and SH3 are shown in Figure 45. In general, it can be seen that the 1D site response analysis models have a tendency to slightly overestimate response at low period (T < 0.1 sec), greatly overestimate response at periods between 0.1 and 1 second, and then underestimate response at periods greater than 1 second. However, SelfSim is able to more accurately capture the measured surface response for all scenarios. In all SelfSim scenarios (SH1, SH2, SH3), the response has greatly improved for periods less than 1 second. Response is still underestimated at periods greater than 1 second, but does show vast improvement. It is interesting to note that the results of SH2 and SH3 provide the best results, with SH2 providing only a slightly better match, whereas the results of SH1 seem to be the least accurate of the three scenarios. The implications of these results are being investigated under current research.

Excess pore pressure response from actual measurements, 1D site response analysis models, and SelfSim scenarios SH1, SH2, and SH3 are shown in Figure 46. It can be seen that the 1D site response analysis models are unable to represent the pore pressure measurements for the complete duration. However, the D-M model does reasonably match measurements up to ~8 seconds of shaking. At this point, it should be noted that it is now believed (Holzer and Youd 2007) that the interference of surface waves have been the cause of delayed pore pressure response, followed by subsequent liquefaction of the sands after earthquake shaking had ended. Thus, it is difficult to ascertain the validity of the use of either model in this case. However, once again we find that the results of the SelfSim scenarios are able to more accurately learn the pore pressure generation behavior, though to varying degrees.

In Figure 46, it can be seen that SH1 results for NN3 and NN4 consistently overestimate the excess pore pressures, though they do manage to perform better at modeling the delayed pore pressure generation than either pore pressure response model (D-M, GMP). SH3 results from NN4 (WSB) also tend to greatly overestimate the pore pressure response at greater depths, though this may be due to the intense generation of pore pressures at the deepest measurement of WSB at 6.6 m. SH3 results from NN3 (WSA) however, display a marked improvement though

the pore pressure generation is still quite large through 35 seconds of shaking (after which the strong shaking has ceased).

The most unexpected and remarkable results are those of SH2 for both NN3 (WSA) and NN4 (WSB). The results for NN3 (WSA) almost exactly match the recordings. This is likely due to the fact that the imposed pore pressures are playing a more significant role in the learning process as NN3 consists of only three individual layers, but this does not explain why SH2 was not able to reach the same results. The current postulation is that the initialized training of the NN soil model included a more significant strain range which allowed the NN pore pressure model to more readily learn the pore pressure behavior, as well as good correlation of the D-M model with the measured results up to ~8 seconds of shaking. The results for NN4 (WSB) similarly show that the pore pressure generation behavior is well-learned, though in this case the overall behavior seems to be averaged between the measurements. In addition, the measurements, though separated by ~1.5 m of soil, show almost identical pore pressure generation behavior. Again, the fact that the D-M model showed good correlation with the recordings up to ~8 seconds of shaking, and the additional fact that the soil models experienced similar loading paths at these locations, likely played a role in the successful learning of the pore pressure generation behavior.

Figure 47 shows the preliminary results of the extracted behavior from the SH2 analysis for materials WSA (Figure 47a and Figure 47b), and WSB (Figure 47c and Figure 47d). It can be seen that the generation of excess pore pressures up to the point of liquefaction causes a wide scatter of the extracted behavior as the shear modulus degrades with excess pore pressure generation. As this occurs, the apparent damping also appears to be increasing to a greater extent than those measured from laboratory specimens. The correct interpretation of this data is ongoing, and will be further discussed in a future publication.

The application of SelfSim to the Wildlife Liquefaction Array - Superstition Hills earthquake records has shown SelfSim's capability in both capturing the soil response as well as the underlying soil behavior. Additional investigation will be performed with other actual field measurements to further explore the capabilities of SelfSim, as well as the behavior of soils due to earthquake motion.

11 Discussion and Conclusions

This report presents the development and application of the inverse analysis framework SelfSim, which provides a rational and systematic approach for integrating downhole measurements into numerical modeling of site response. SelfSim represents a major departure from general system identification methods from field observations and conventional methods for development and calibration of dynamic soil models and pore pressure models using laboratory measurements. SelfSim is capable of extracting nonlinear soil behavior with pore

pressure response using downhole array measurements unconstrained by prior assumptions of soil behavior.

The algorithm is successfully demonstrated using several synthetic downhole arrays profiles and measurements from actual field arrays for both total stress analysis and fully coupled analysis. The results show that SelfSim is able to gradually learn the measured global response while extracting the underlying soil behavior and pore pressure response. Recordings from multiple events are needed to extract nonlinear soil behavior over a wide strain range.

12 Acknowledgments

This work was supported by the U. S. Geological Survey, under Award Number 08HQGR0029,. Assistance provided by graduate research assistant David R. Groholski and Dr. Chi-chin Tsai is appreciated and acknowledged here. Any opinions, findings, conclusions and/or recommendations presented in this material are those of the author and do not necessarily reflect those of the funding agency.

13 References

Anderson, D. G., and Tang, Y. K. (1989). "Summary of soil characterization program for the Lotung large-scale seismic experiment." *NP-6154*, Electric Power Research Institute, Palo Alto, Calif.

Basheer, I. A. (2000). "Selection of methodology for neural network modeling of constitutive hystereses bahavior of soils." *Computer-Aided Civil and Infrastructure Engineering*, 15, 440-458.

Chopra, A. K. (1995). *Dynamics of structures : theory and applications to earthquake engineering*, Prentice Hall, Englewood Cliffs, N.J.

Chou, J. H., and Ghaboussi, J. "Structural damage detection and identification using genetic algorithm." *International Conference on Artificial Neural Networks in Engineering*, St. Louis, MO, 395-400.

Darendeli, M. B. (2001). "Development of a new family of normalized modulus reduction and material damping," The University of Texas, Austin.

Darragh, R., Graizer, V., and Shakal, A. (1997). "Site Characterization and Site Response Effects at CSMIP Stations: Tarzana and La Cienega Near the Santa Monica Freeway (I-10)." *OSMS 96-07*, Calif. Div. Mines and Geology.

Dobry, R., Ladd, R.S., Yokel, F.Y., Chung, R.M. and Powell, D. (1982). *Prediction of Pore Water Pressure Build-up and Liquefaction of Sands During Earthquakes by Cyclic Strain Method*, U.S. Department of Commerce, National Bureau of Standards, Washington, D.C.

Elgamal, A., Lai, T., Yang, Z., and He, L. "Dynamic soil properties, seismic downhole arrays and applications in practice." *4th International Conference on Recent Advances in Geotechnical Earthquake Engineering and Soil Dynamics*, San Diego, California, USA.

Ellis, G. W., Yao, C., Zhao, R., and Penumadu, D. (1995). "Stress-strain modeling of sands using artifiical neural network." *Journal of Geotechnical Engineering*, 429-435.

Ghaboussi, J., Garrett, J. H., and Wu, X. (1991). "Knowledge-based modeling of material behaviour with neural networks." *Journal of Engineering Mechanics Division*, 117(1), 132-153.

Ghaboussi, J., Pecknold, D. A., Zhang, M., and Haj-Ali, R. (1998). "Autoprogressive training of neural network constitutive models." *International Journal for Numerical Methods in Engineering*, 42(1), 105-126.

Graizer, V., Shakal, A., and Hipley, P. "Recent data recorded from downhole geotechnical arrays." *SMIP2000 Seminar on Utilization of Strong Motion Data*, Sacramento, California, USA.

Hashash, Y. M. A., Marulanda, C., Ghaboussi, J., and Jung, S. (2003). "Systematic update of a deep excavation model using field performance data." *Computers and Geotechnics*, 30(6), 477-488.

Hashash, Y. M. A., and Park, D. (2001). "Non-linear one-dimensional seismic ground motion propagation in the Mississippi embayment." *Engineering Geology*, 62(1-3), 185-206.

Holzer, T. L., and Youd, T. L. (2007). "Liquefaction, ground oscillation, and soil deformation at the Wildlife Array, California." *Bulletin of the Seismological society of America*, 97(3), 961-976.

Idriss, I. M., Dobry, R., and Singh, R. D. (1978). "Nonlinear behavior of soft clays during cyclic loading." *Journal of the Geotechnical Engineering Division*, 104(CT12), 1427-1447.

Isenhower, W., and Stokoe, K. "Strain-rate dependent shear modulus of San Francisco Bay Mud." *International Conference on Recent Advances in Geotechnical Earthquake Engineering and Soil Dynamics*, University of Missouri-Rolla.

Kim, D. S., Stokoe, K. H., and Hudson, W. R. (1991). "Deformational characteristics of soils at small to intermediate strains from cyclic tests." *1177-3*, Ceter for Transportation Research, Bureay of Engineering Research, Austin, Tex.

Kramer, S. L. (1996). *Geotechnical earthquake engineering*, Prentice Hall, Upper Saddle River, N.J.

Kwok, O.-L. A., Stewart, J. P., Hashash, Y. M. A., Matasovic, N., Pyke, R., Wang, Z., and Yang, Z. "Practical Implementation of Analysis Routines for Nonlinear Seismic Ground Response Analysis." *Eigth National Conference on Earthquake Engineering*, San Francisco, CA.

Matasovic, N. (1993). "Seismic response of composite horizontally-layered soil deposits," Ph.D. Thesis, University of California, Los Angeles.

Matesic, L., and Vucetic, M. (2003). "Strain-Rate Effect on Soil Secant Shear Modulus at Small Cyclic Strains." *Journal of Geotechnical and Geoenvironmental Engineering*, 129(6).
Penumadu, D., and Zhao, R. (1999). "Triaxial compression behavior of sand and gravel using artificial neural networks (ANN)." *Computers and Geotechnics*, 24(3), 207-230.
Roblee, C., and Chiou, B. (2004). "A PROPOSED GEOINDEX MODEL FOR DESIGN SELECTION OF NON-LINEAR PROPERTIES FOR SITE RESPONSE ANALYSES." Caltrans.
ROSRINE. "Resolution of Site Response Issues from the Northridge Earthquake." http://geoinfo.usc.edu/rosrine/.
Sidarta, D., and Ghaboussi, J. (1998). "Modelling constitutive behavior of materials from non-uniform material tests." *Computers and Geotechnics*, 22(1), 53-71.
Tang, H. T. (1987). "Large-scale soil structure interaction." *NP-5513-SR*, Electric Power Research Institute, Palo Alto, California.
Tsai, C.-C. (2007a). "Seismic site response and extraction of dynamic soil behavior from downhole array measurements," Ph. D., University of Illinois, Urbana.
Tsai, C.-C. (2007b). "Seismic Site Response and Interpretation of Dynamic Soil Behavior from Downhole Array Measurements," University of Illinois at Urbana-Champaign, Urbana.
Tsai, C.-C., and Hashash, Y. M. A. (2008). "A novel framework integrating downhole array data and site response analysis to extract dynamic soil behavior." *Soil Dynamics and Earthquake Engineering*, 28, 181-197.
Tsai, C.-C., and Hashash, Y. M. A. (2009). "Learning of Dynamic Soil Behavior from Downhole Arrays." *Journal of Geotechnical and Geoenvironmental Engineering*, 135(6), 745-757.
Vucetic, M. (1992). "Cyclic threshold shear strains in soil." *Journal of geotechincal engineering*, 120(12), 2208-2227.
Vucetic, M., and Dobry, R. (1988). "Degradation of marine clays under cyclic loading." *Journal of geotechincal and engineering*, 114(2), 133-149.
Vucetic, M., and Dobry, R. (1991). "Effect of soil plasticity on cyclic response." *Journal of Geotechnical Engineering*, 117(1), 87-107.
Wen, K. L., and Yeh, Y. T. (1984). "Seismic Velocity Structure Beneath the SMART1 Array." *Bulletin of the Insiture of Earth Science*, 4.
Wu, X., and Ghaboussi, J. "Modelling the cyclic behavior of the concrete using adaptive neural networks." *Asian Pacific conference on computational mechanics*.
Yamamoto, K. "Modeling of hysteretic behavior with neural network and its application to non-linear dynamic response." proceedings of the international conference in applications of artificial intelligence in engineering.
Yun, G. J. (2006). "modeling of hysteretic behavior of beam-column connections based on self learning simulation," University of Illinois at Urbana-Champaign, Urbana.
Zhu, J.-H., Zaman, M. M., and Anderson, S. A. (1998). "Modeling of soil behavior with a recurrent neural network." *Canadian Geotechnical Journal*, 35, 858-869.

Table 1 List of used events recorded by LLST

Selected event No.	Date (M/D/Y)	M_L	Epicenter Dist. (km)	Measurement	Components	PGA (g)	Purpose
LLST14	7/30/1986	4.2	5	0m, 6m, 11m, 17m, 47m	NS	0.04	Calibration of small strain properties
					EW	0.03	
LLST7	5/20/1986	6.2	66.2	0m, 6m, 11m, 17m, 47m	NS	0.2	SelfSim Learning
					EW	0.16	Prediction
LLST11	7/17/1986	4.3	6	0m, 6m, 11m, 17m, 47m	NS	0.11	SelfSim Learning
					EW	0.06	Prediction
LLST4	1/6/1986	6.1	23.7	0m, 6m, 11m, 47m	NS	0.23	Prediction
					EW	0.15	
LLST12	7/30/1986	5.8	5.2	0m, 6m, 11m, 17m	NS	0.2	Prediction
					EW	0.15	
LLST15	8/5/1986	4.2	4.7	0m, 6m, 11m, 17m	NS	0.09	Prediction
					EW	0.1	

Table 2 List of used events recorded by La Cienaga array

Selected event No.	Date (M/D/Y)	M_L	Epicenter Dist. (km)	Measurement	Components	PGA (g)	Purpose
LC11	6/17/1999	3.0	15.2	0m, 18m, 100m, 252m	NS	0.012	Calibration of small strain properties
					EW	0.012	
LC20	9/9/2001	4.2	2.7	0m, 18m, 100m, 252m	NS	0.49	SelfSim Learning
					EW	0.22	Prediction
LC4	4/4/1997	3.3	6.4	0m, 18m, 100m	NS	0.059	Prediction
					EW	0.078	SelfSim Learning
LC18	9/16//2000	3.3	7.9	0m, 18m, 100m, 252m	NS	0.033	SelfSim Learning
					EW	0.035	Prediction

Table 3 Parameters of Hyperbolic model used in DEEPSOIL to generate artificial array data

	Soil 1	**Soil 2**	**Soil 3**
Profiles	1,2	3	3
Nonlinear Model Parameters			
β	0.8	0.8	1.25
s	0.7	0.7	0.7
σ_{ref} (MPa)	0.18	0.18	0.18
γ_r (%)	0.03	0.02	0.06
b	0	0	0
c	1	1	1
d	0	0	0
Pore Pressure Generation Parameters			
f	2	2	2
p	1	1	0.7
F	0.73	0.73	0.73
s	1	1	1
γ_{tvp} (%)	0.02	0.02	0.02
ν	3.8	3.8	5

Table 4 Detail of the recording used to generate synthetic array

Symbol	Earthquake	Station	PGA(g)
LY	Loma Prieta	Yerba Buena	0.065
KK	Kobe	KJMA	0.4
LG	Loma Prieta	Gilroy	0.45

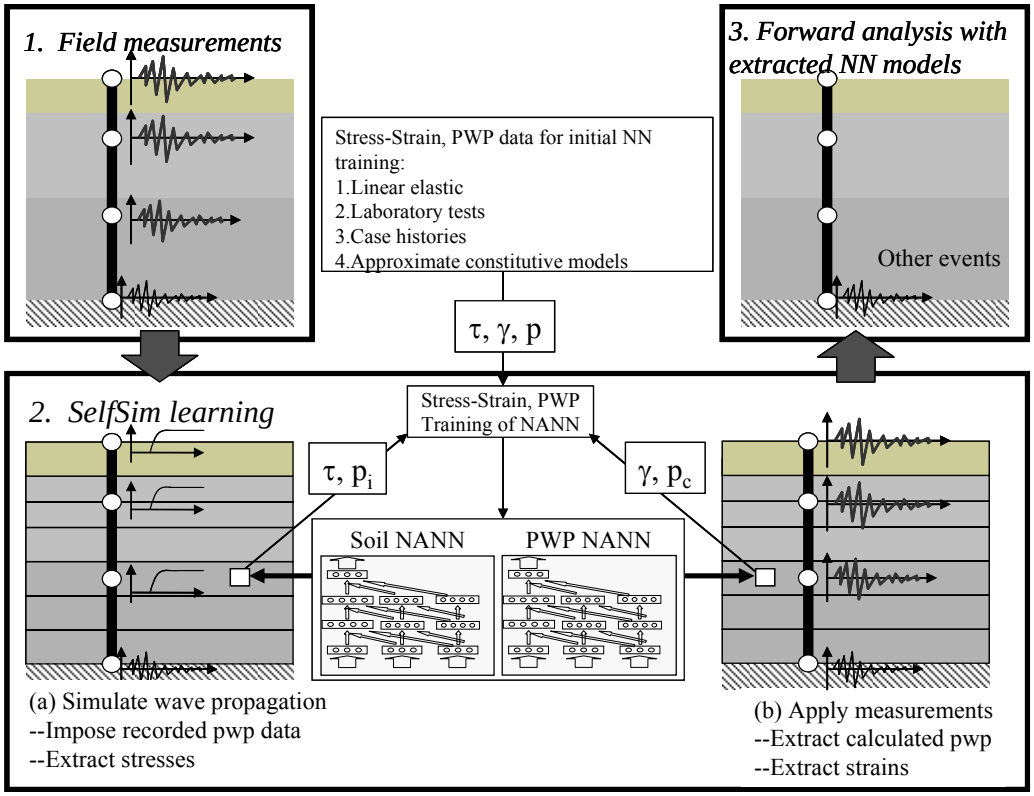

Figure 1 SelfSim algorithm applied to a downhole array.

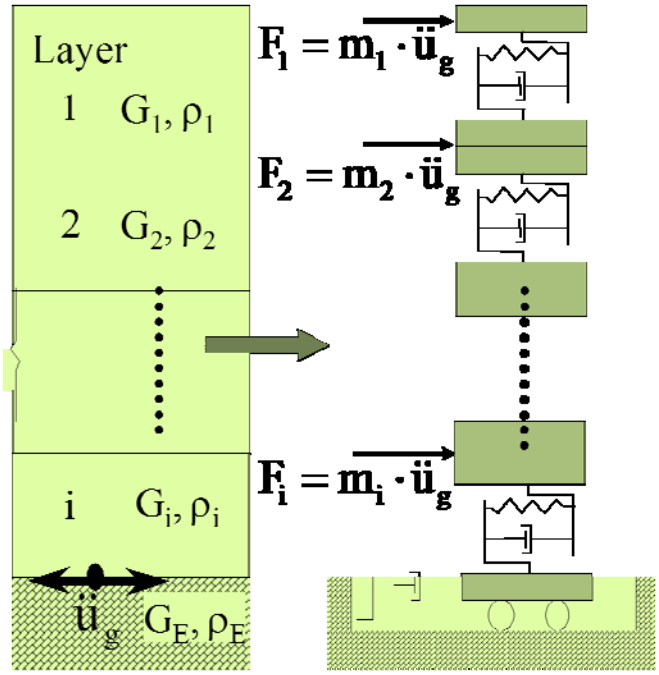

Figure 2 A conventional site response analysis model: Acceleration is input at bedrock and converted to equivalent forces acting on lumped masses representing the soil column (from Tsai 2007, after Matasovic 1993).

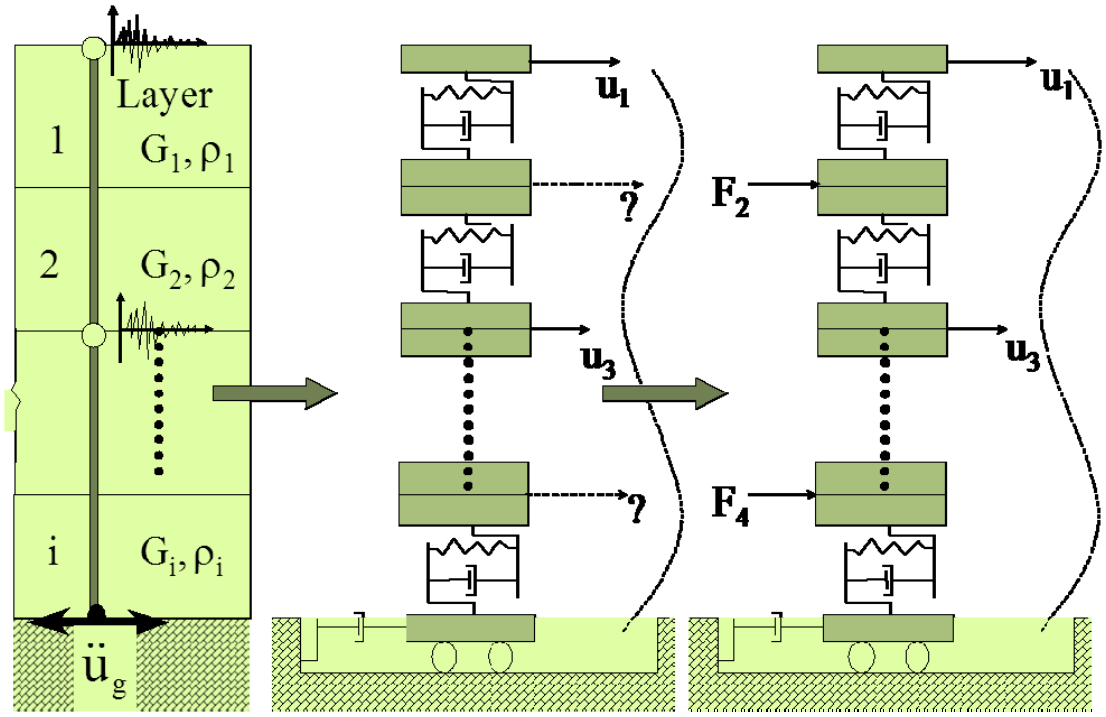

Figure 3 Composite boundary condition of 1D site response analysis for Step 2(b) of SelfSim analysis, Figure 1. The force boundary from base acceleration is applied at the layers ($F=m\ddot{u}_g$) where no measurement (displacement) is available.

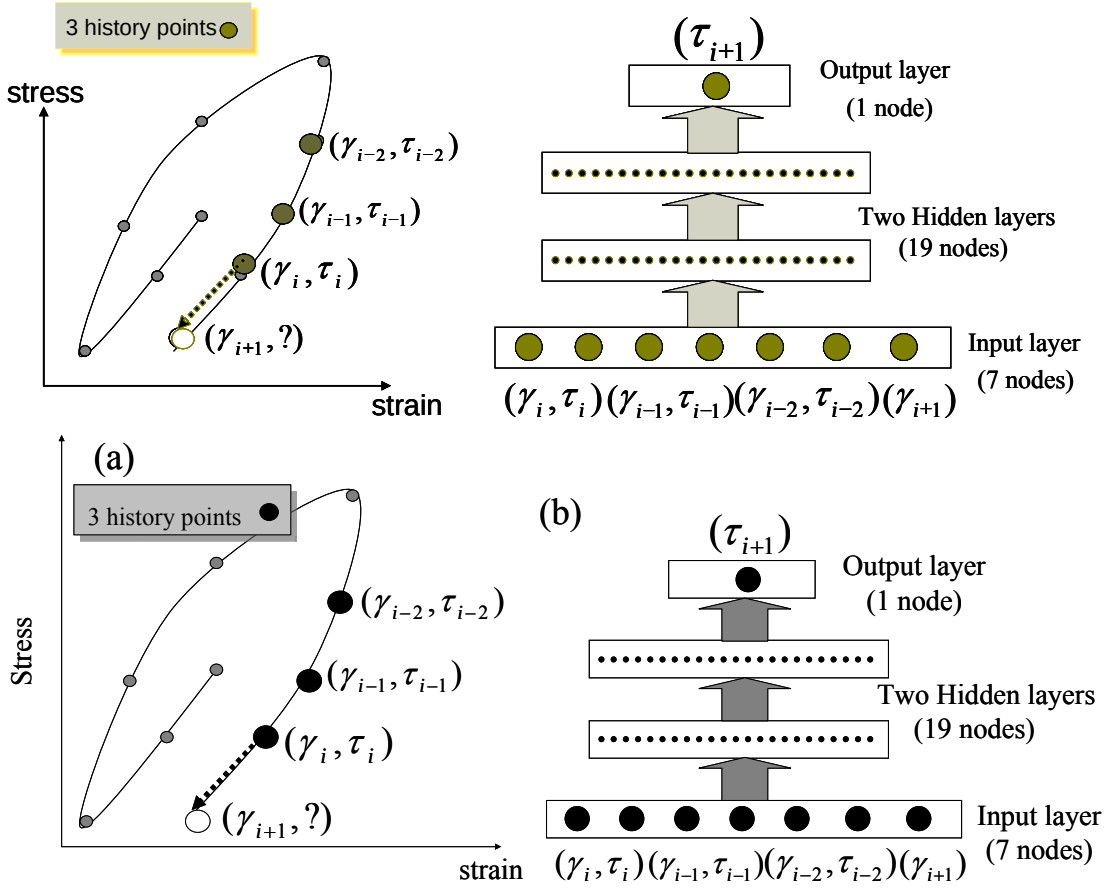

Figure 4 Illustration of (a) input parameters of general 3-point scheme and (b) the corresponding architecture of NN. (γ_i, τ_i) is current state of strain and stress. (γ_{i-1}, τ_{i-1}) and (γ_{i-2}, τ_{i-2}) are 2 history points which can be reverse points or immediate history points

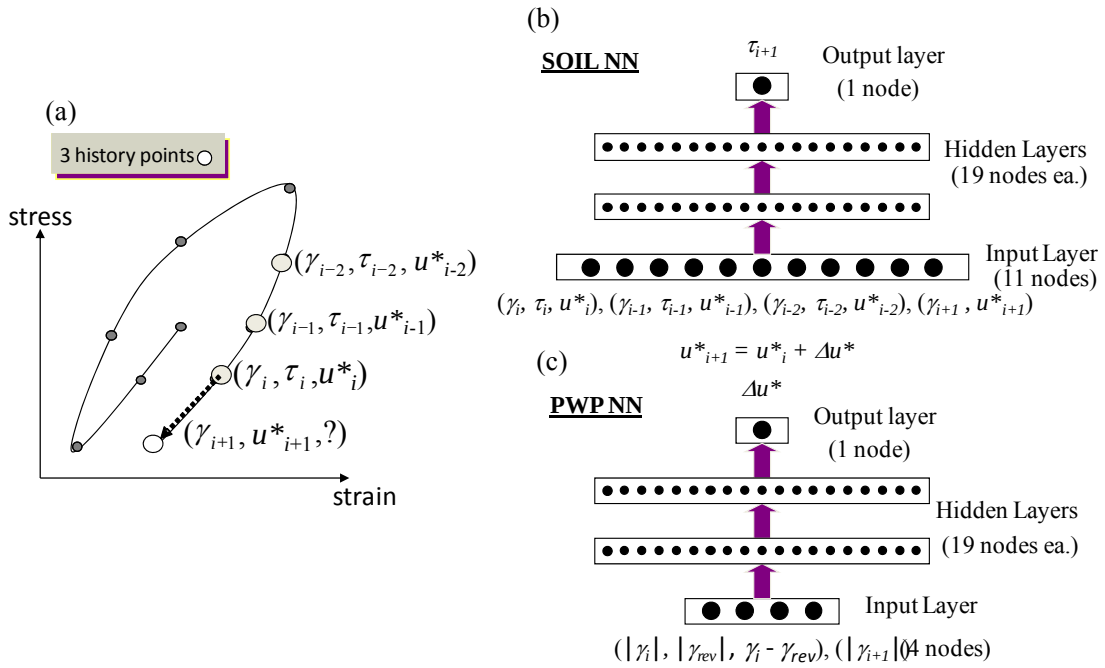

Figure 5 1-Point model demonstrated for pore pressures (a); 3-point model demonstrated for stress-strain-pore pressure coupled behavior (b). Proposed NN architectures for (c) pore pressure response model, and (d) stress-strain model illustrating how the pore pressure output is given as input to the soil model.

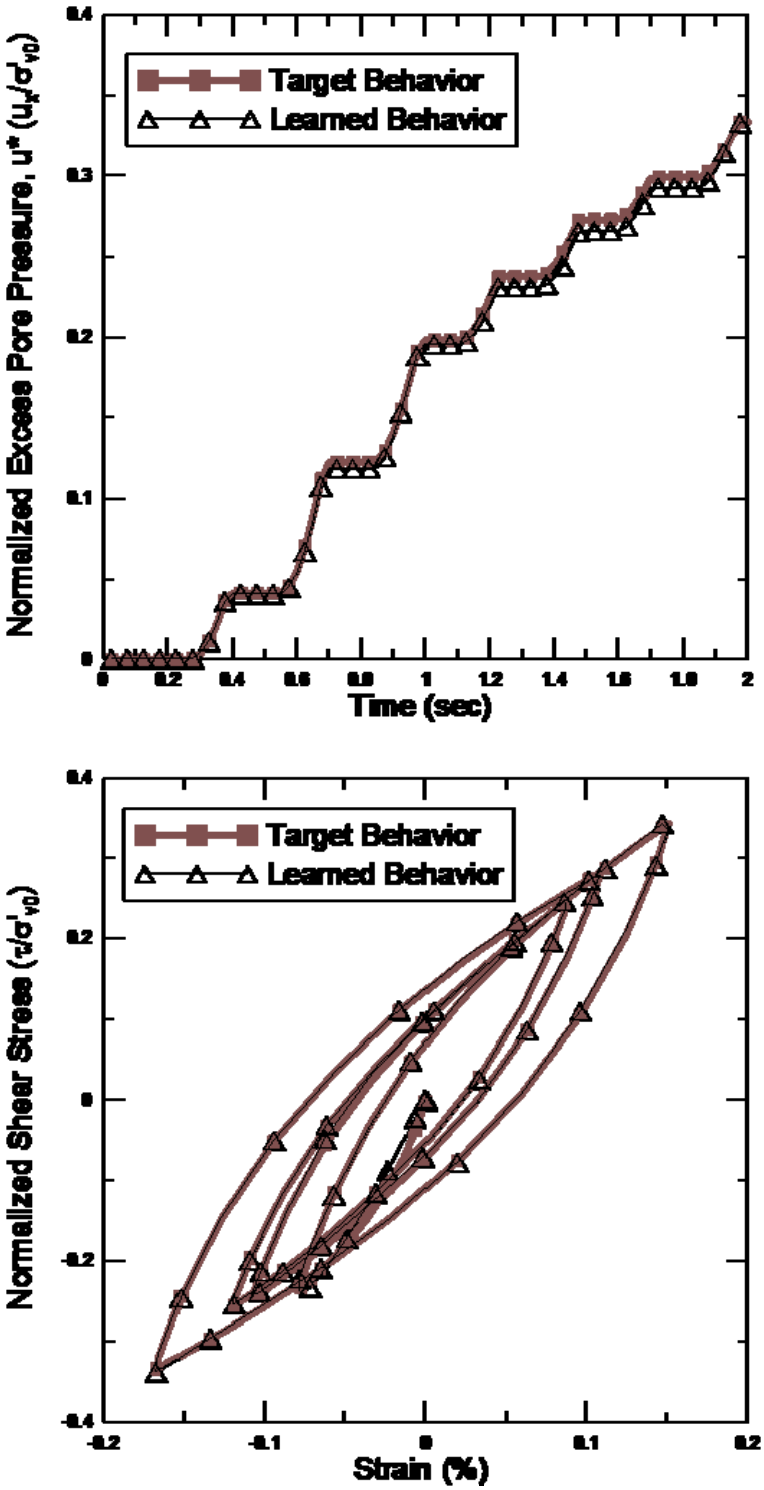

Figure 6 (a) Test results for NN pore water pressure model using the 1-point scheme, and (b) Test results for NN stress-strain model using the modified 3-point scheme

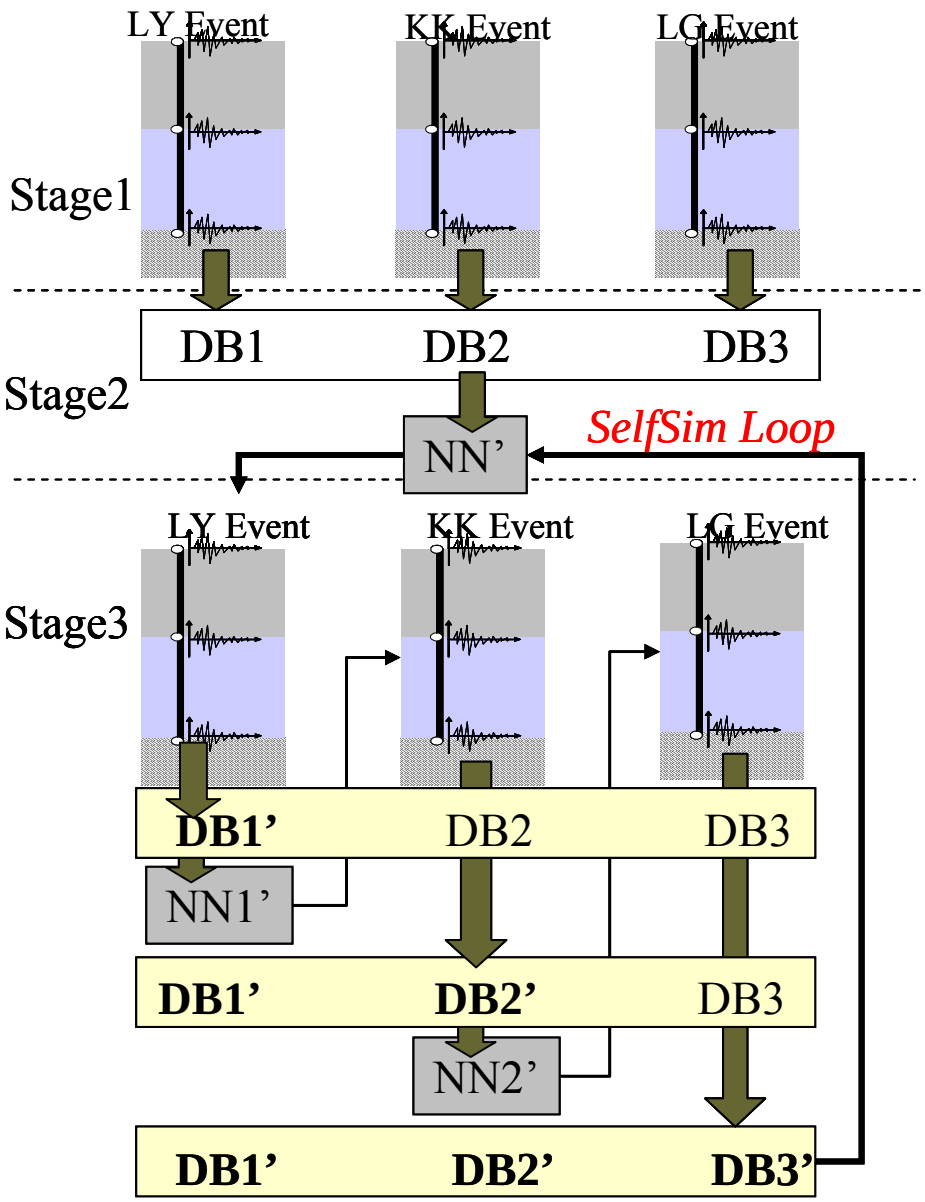

Figure 7 SelfSim learning of multiple events to improve SelfSim learning. Stage1: SelfSim learning of individual events. Stage2: combine data bases (DB) of extracted stress-strain behavior to train a new NN material model. Stage 3: SelfSim learning of individual events, and update of the combined data base used in retraining the NN material model.

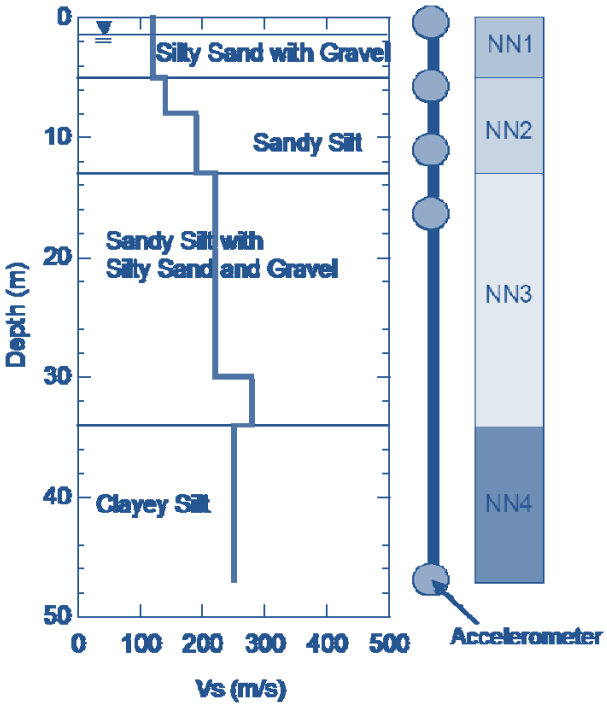

Figure 8 Lotung DHB array geology and shear wave profile (Tang 1987). The profile shows the four NN material models used in SelfSim learning.

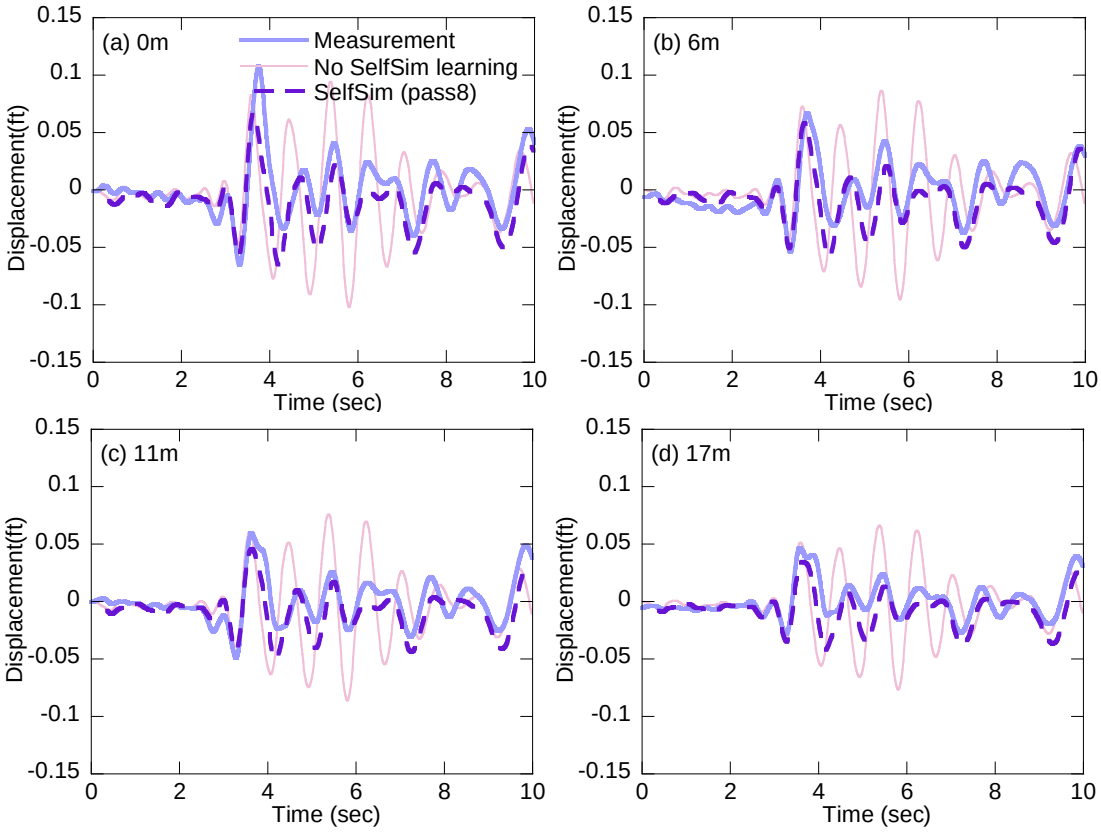

Figure 9 Comparison of measured and computed displacement of LLST7 NS component prior to and after SelfSim Stage1 learning of LLST7 NS component. Total Stress SelfSim Learning - Lotung Array, Taiwan

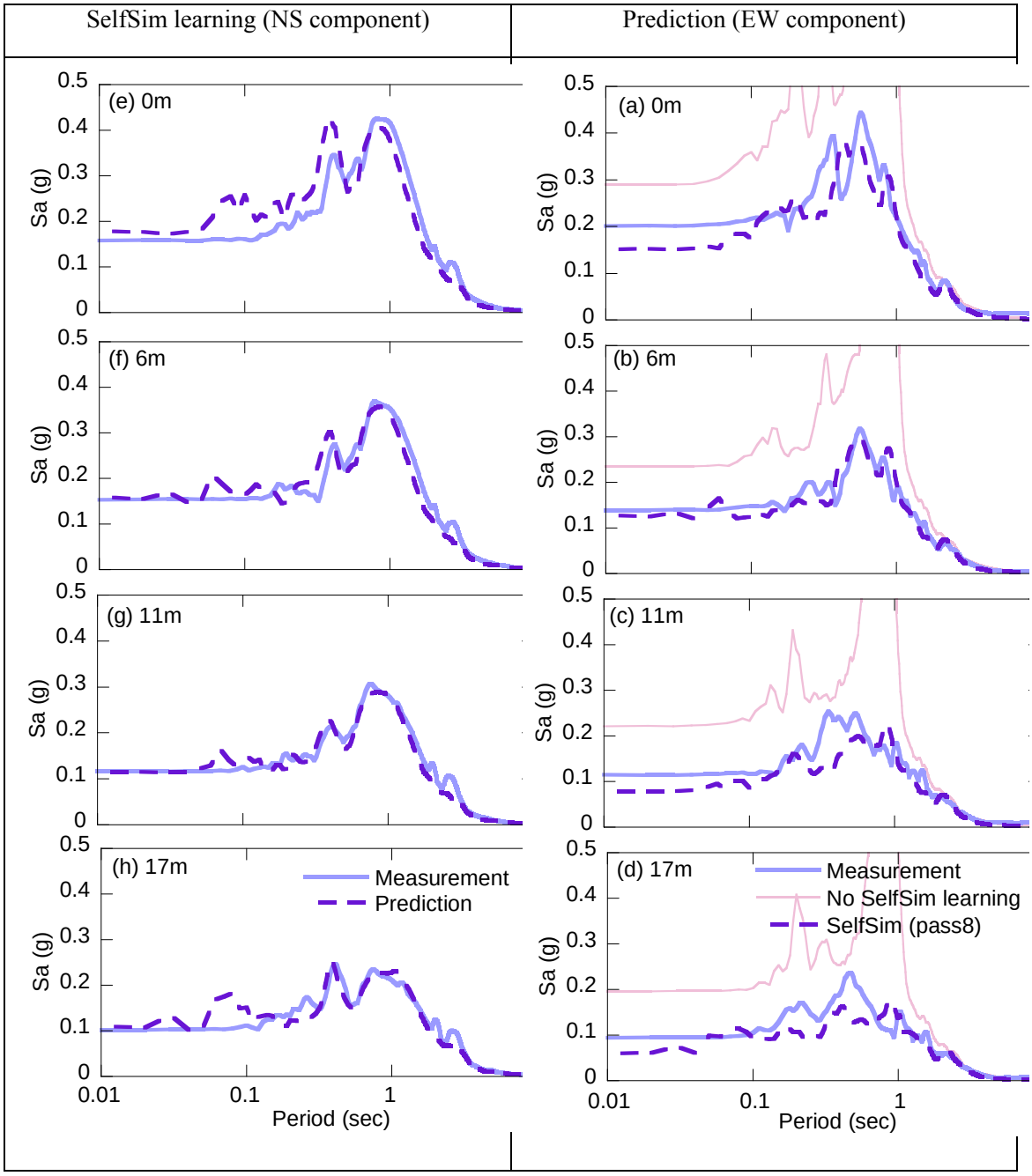

Figure 10 Comparison of measured and computed response spectra of LLST7 NS component prior to and after Stage1 SelfSim learning of LLST7 NS component (right column) and prediction of response spectra of LLST7 EW components using NN material model extracted by Stage1 SelfSim learning of LLST7 NS component (left column). Total Stress SelfSim Learning - Lotung Array, Taiwan

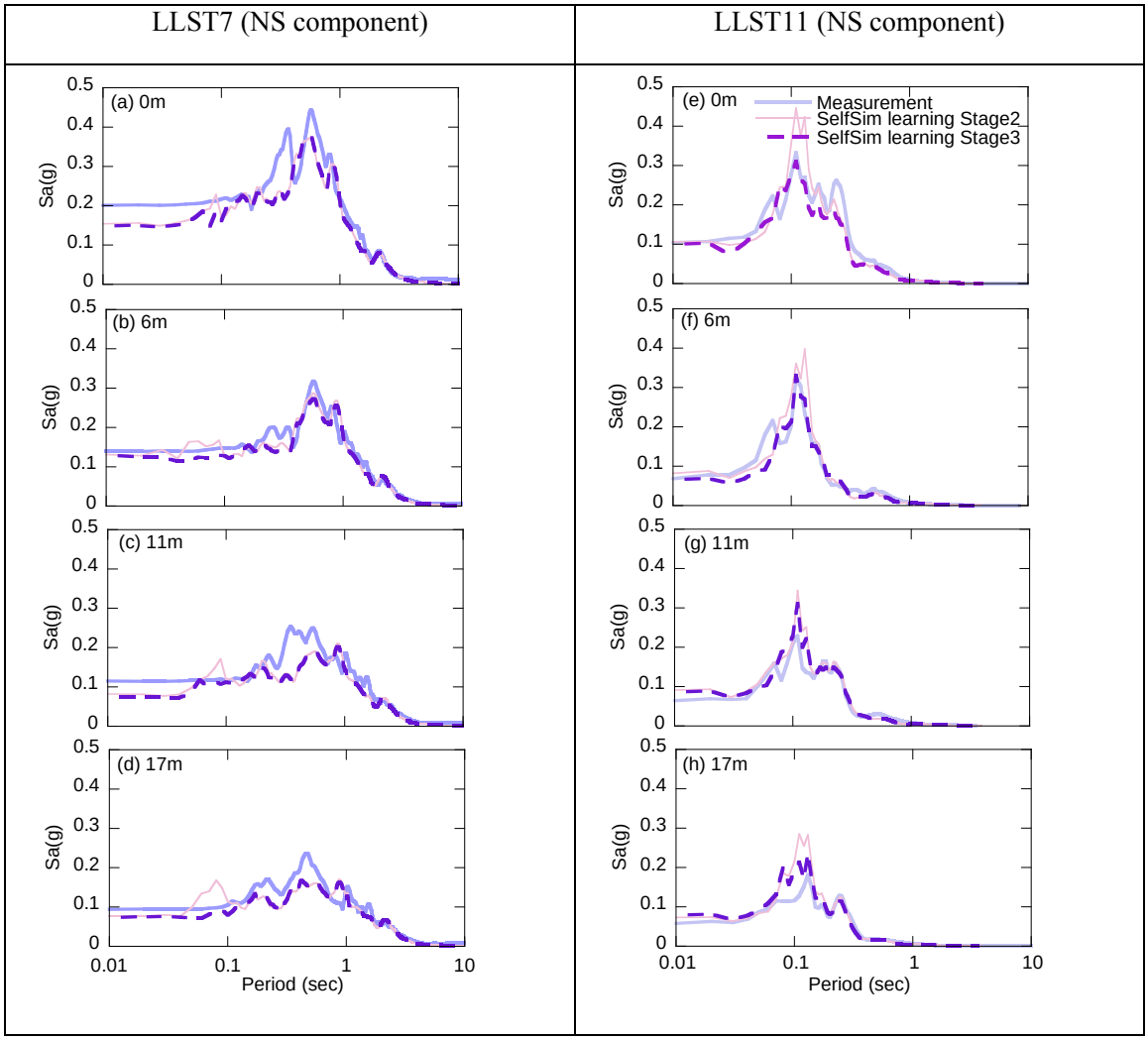

Figure 11 Comparison of response spectra of LLST7 and LLST11 NS component computed by Stage 2 combined NN material model trained with combined data from LLST7 NS component and LLST11 NS component (Prior to SelfSim loop) and Stage 3 combined NN material model extracted after three more SelfSim learning loops using LLST11 NS component and LLST7 NS component. Total Stress SelfSim Learning - Lotung Array, Taiwan.

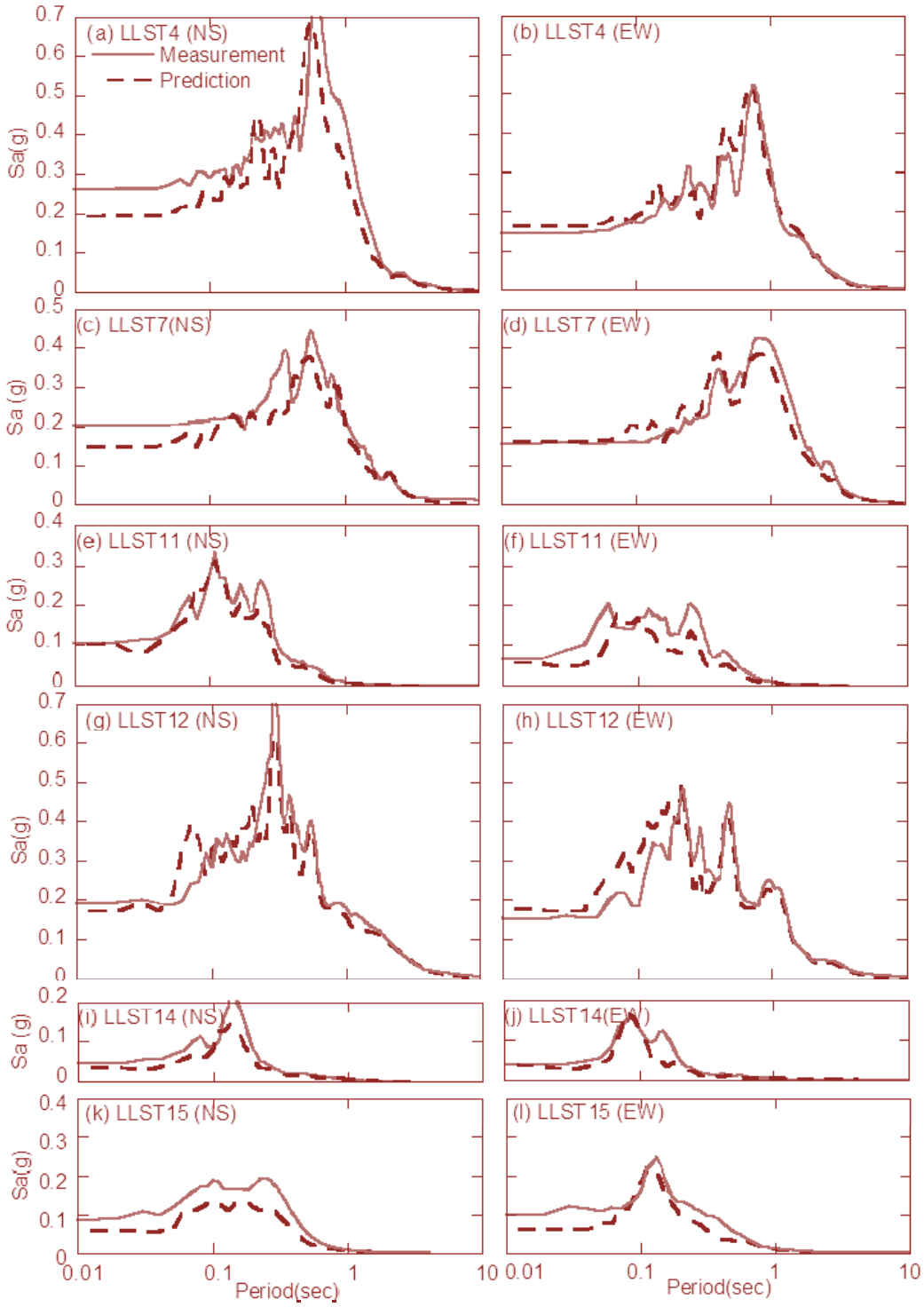

Figure 12 Prediction of surface response of LLST4, LLST7, LLST11, LLST12, LLST14, and LLST15 event using NN material model after Stage3 SelfSim learning of LLST7 NS component and LLST11 NS component. Total Stress SelfSim Learning - Lotung Array, Taiwan.

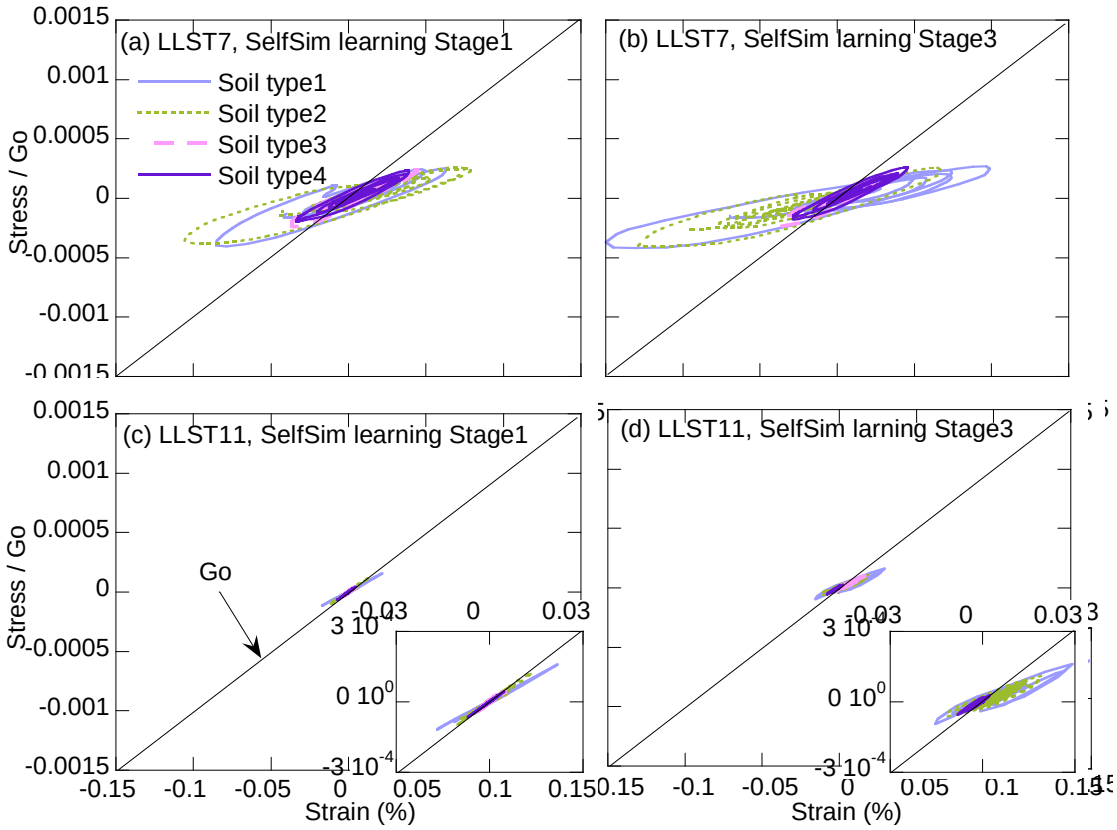

Figure 13 Extracted stress-strain curves of four soil types from SelfSim Learning, Stage 1 and Stage 3, Lotung array. Total Stress SelfSim Learning - Lotung Array, Taiwan

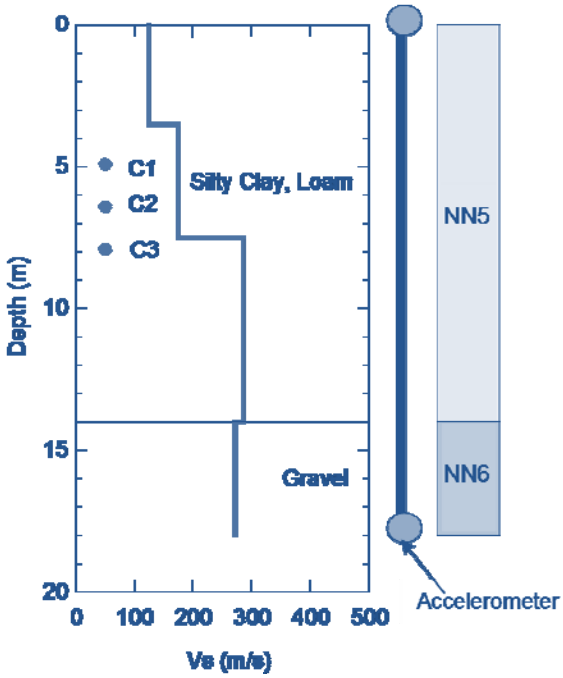

Figure 14 Geology and shear wave profile of La Cienaga array (ROSRINE) and two assigned NN models according to the geology profile. C1-C3 indicates the location of the specimen used for lab tests. Total Stress SelfSim Learning

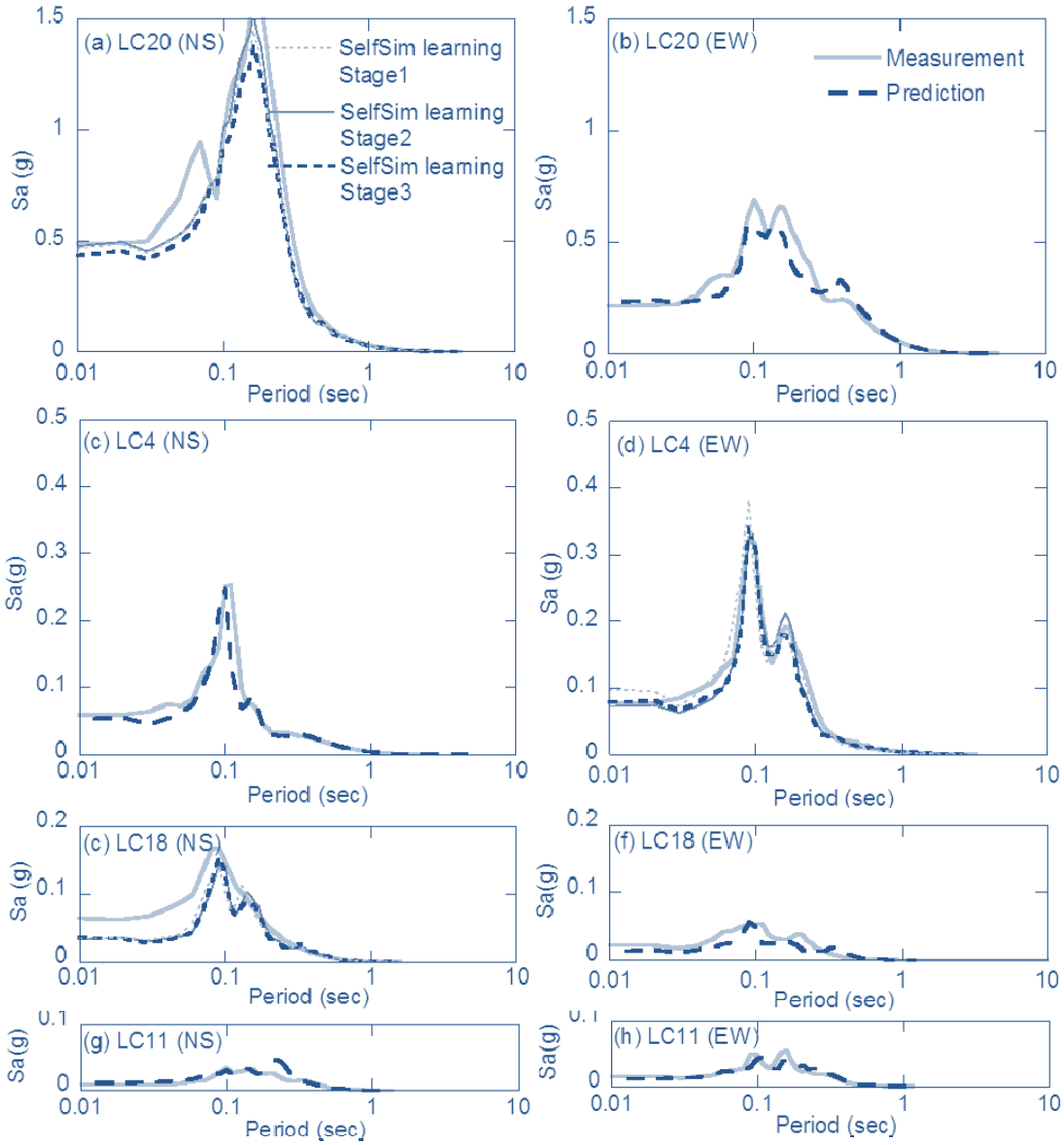

Figure 15 Comparison of surface response spectra of 3 events computed by Stage1 individual learning, Stage2 combined NN material model trained with combined data of (a) LC20 NS component, (d) LC4 EW component, and (e) LC18 NS component (Prior to SelfSim loop), and Stage3 combined NN material model extracted after four more SelfSim learning loops of (a) LC20 NS component, (d) LC4 EW component, and (e) LC18 NS component and prediction of four events using NN model after Stage3 SelfSim learning of LC20 NS component, LC4 EW component, and LC18 NS component, La Cienaga array. Total Stress SelfSim Learning - Lotung Array, Taiwan

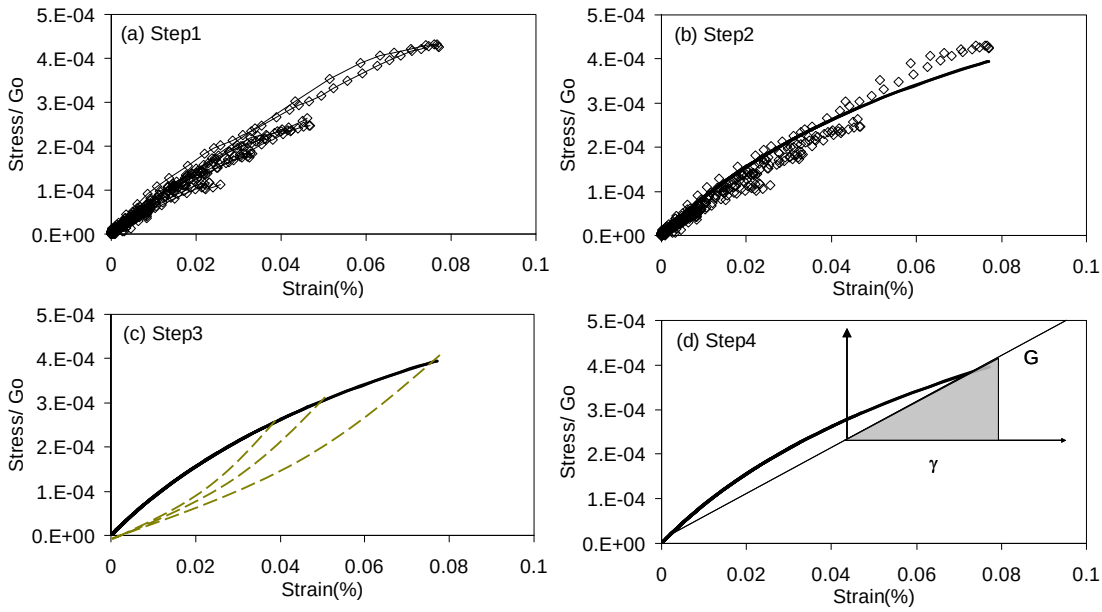

Figure 16 Illustration of Method 1 to extract soil behavior.

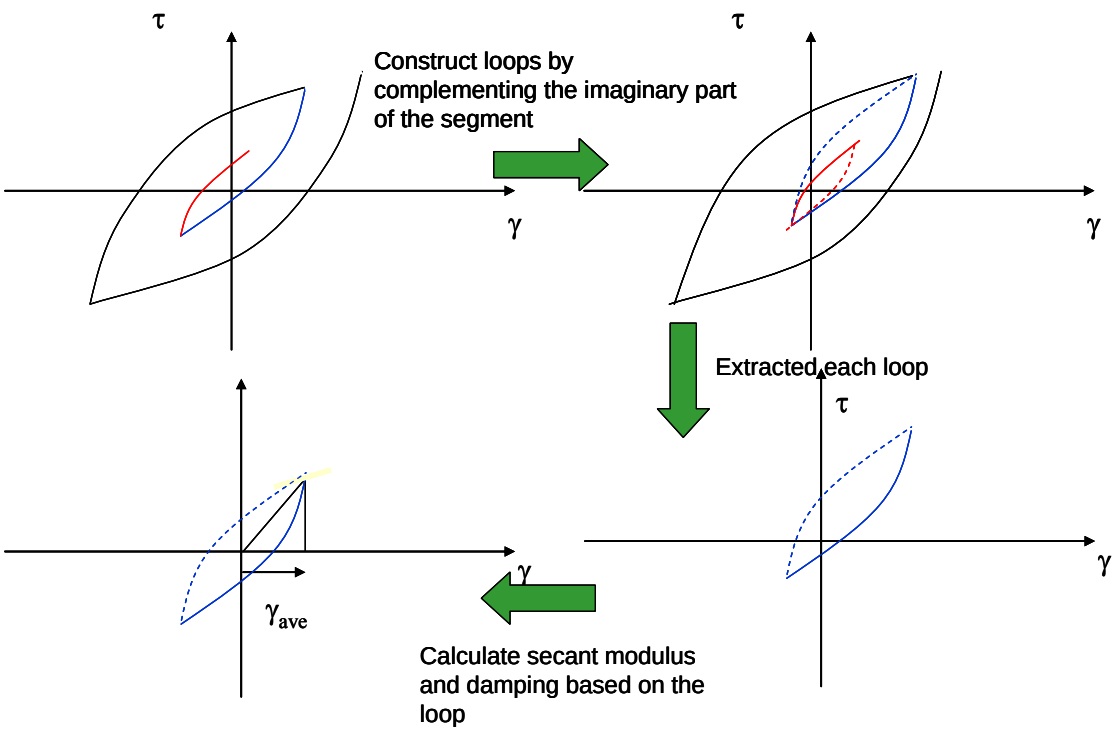

Figure 17 Illustration of method 2 to extract soil behavior

Figure 18 Compare extracted behaviors by methods 1 and 2 with properties from laboratory tests (Anderson and Tang 1989) and those from system identification (Elgamal et al. 2001), Lotung array.

Figure 19 Compare extracted behaviors by methods 1 and 2 with the properties from laboratory tests (ROSRINE), La Cienaga array.

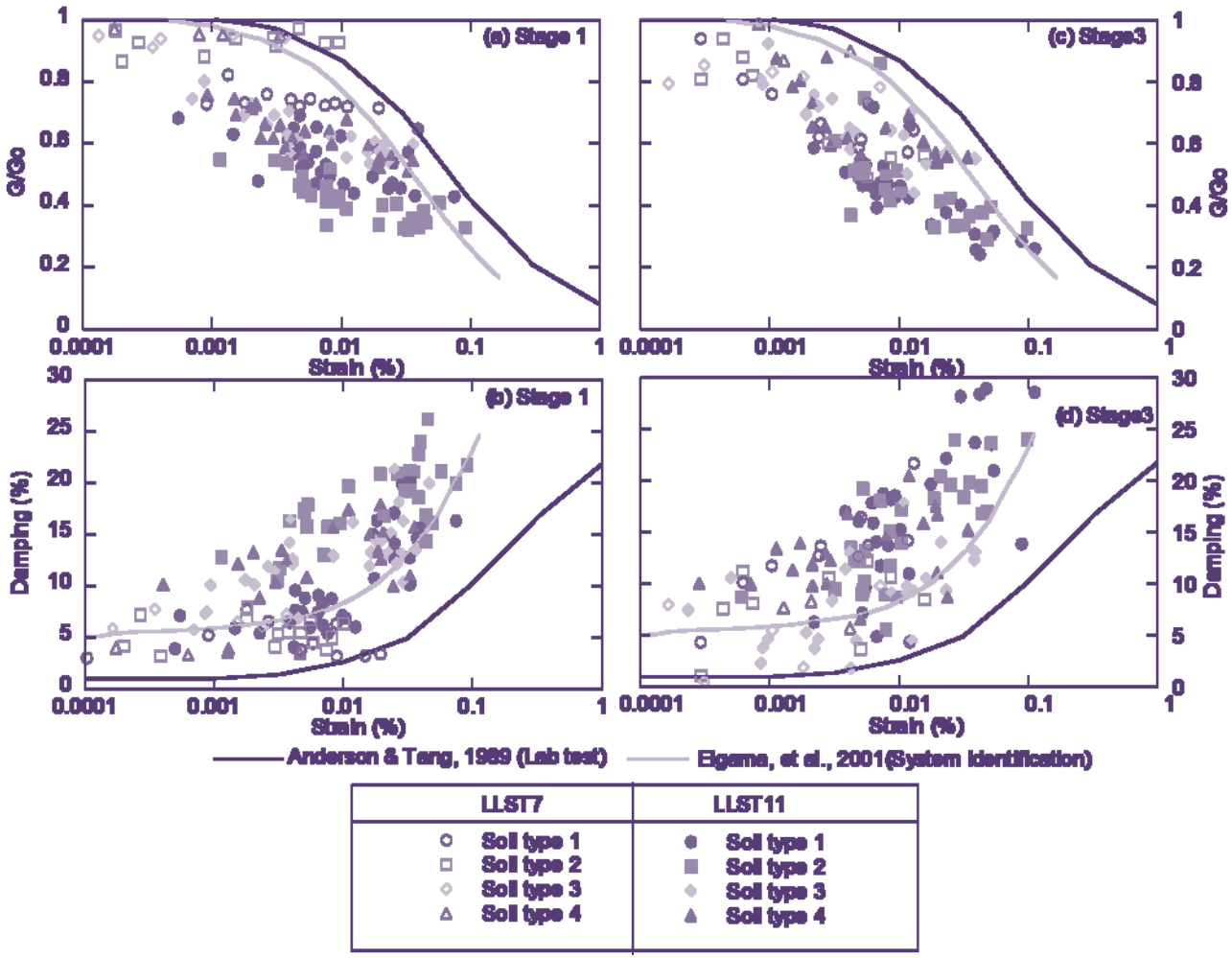

Figure 20 Evolution of extracted behaviors compared with the properties from laboratory tests (Anderson and Tang 1989) and those from system identification (Elgamal et al. 2001), Lotung array.

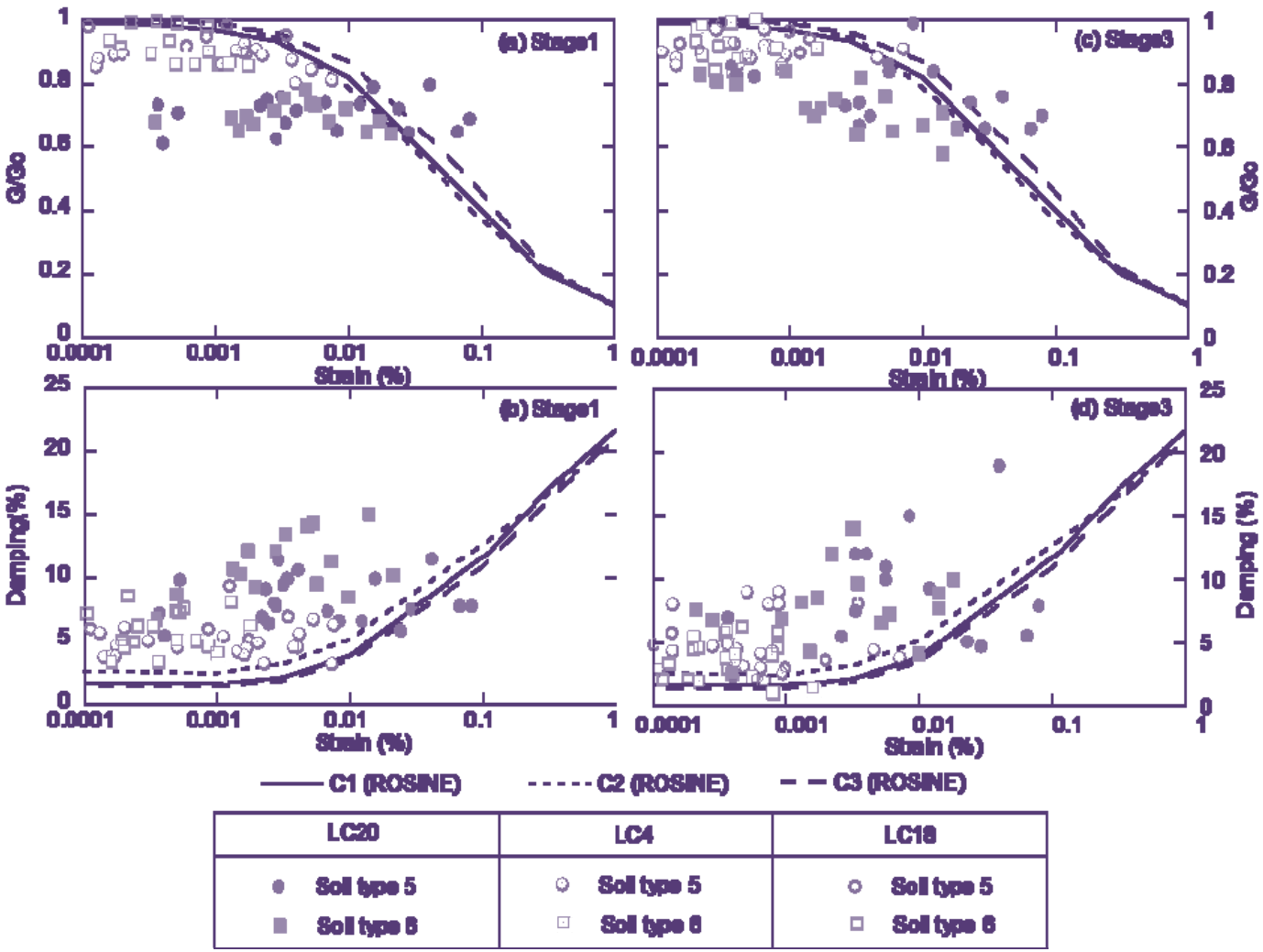

Figure 21 Evolution of extracted behaviors compared with the properties from lab test (ROSRINE), La Cienaga array.

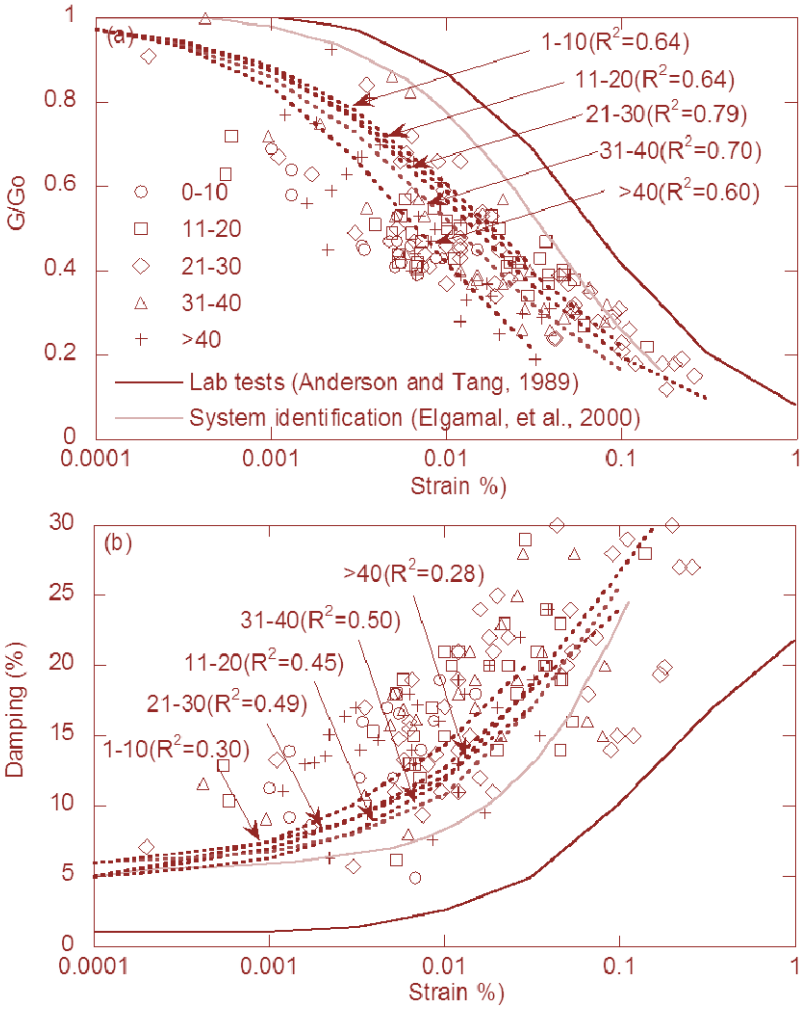

Figure 22 Extracted behavior of Soil type 1 in terms of number of cycles, Lotung array

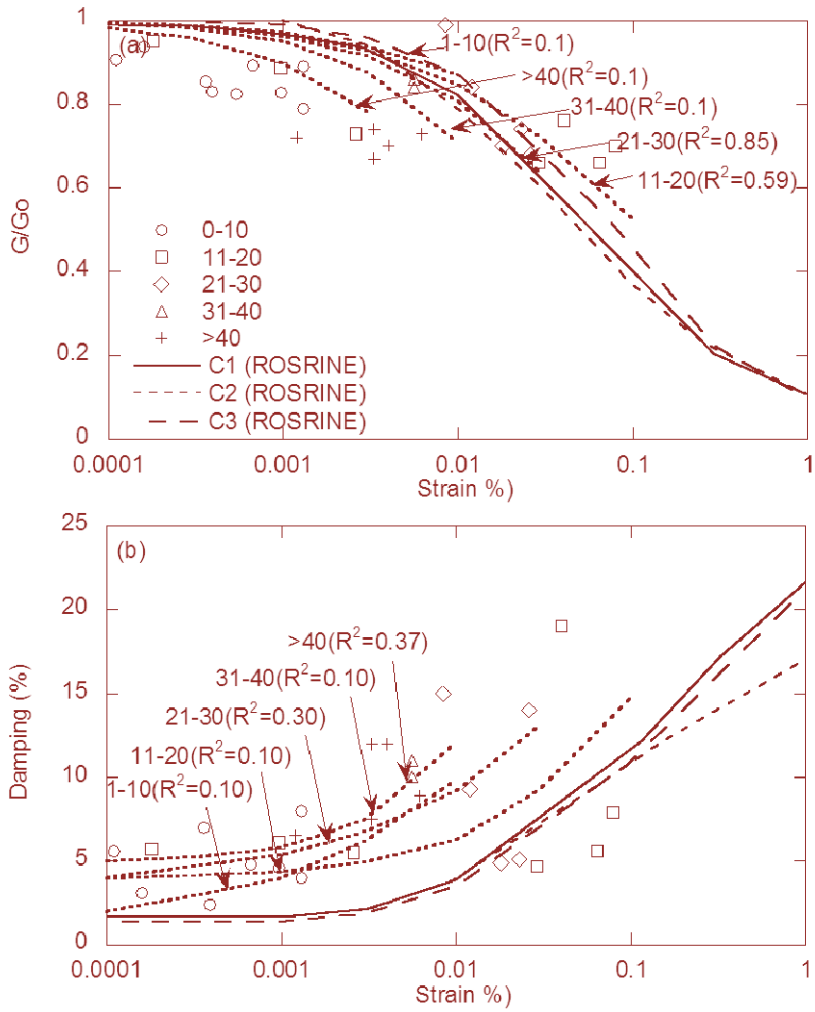

Figure 23 Extracted behavior of Soil Type 5 in terms of number of cycles, La Cienaga array

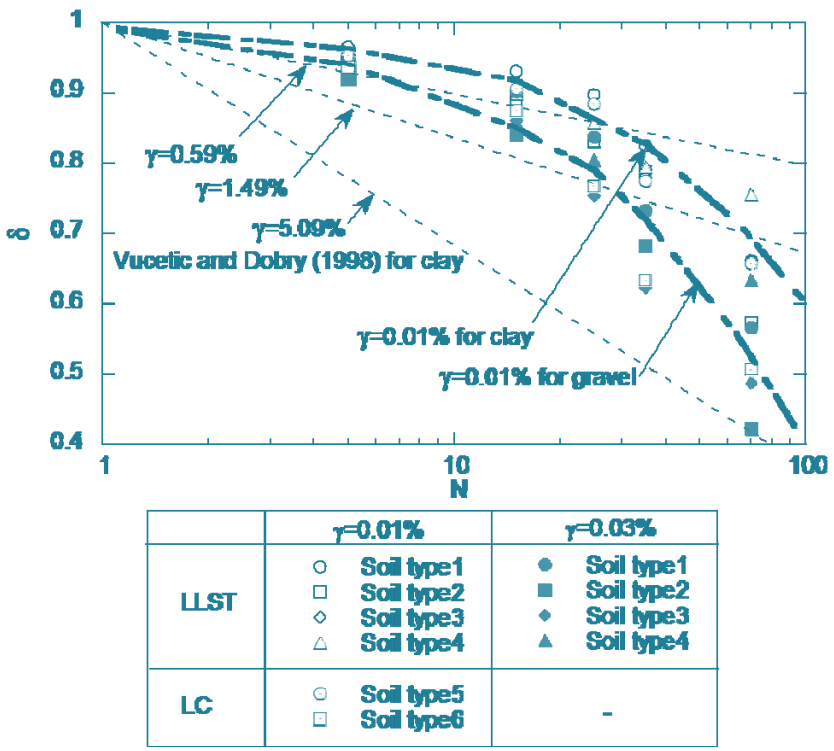

Figure 24 Comparison of soil degradation behavior extracted from downhole array and from lab test(Vucetic and Dobry 1988)

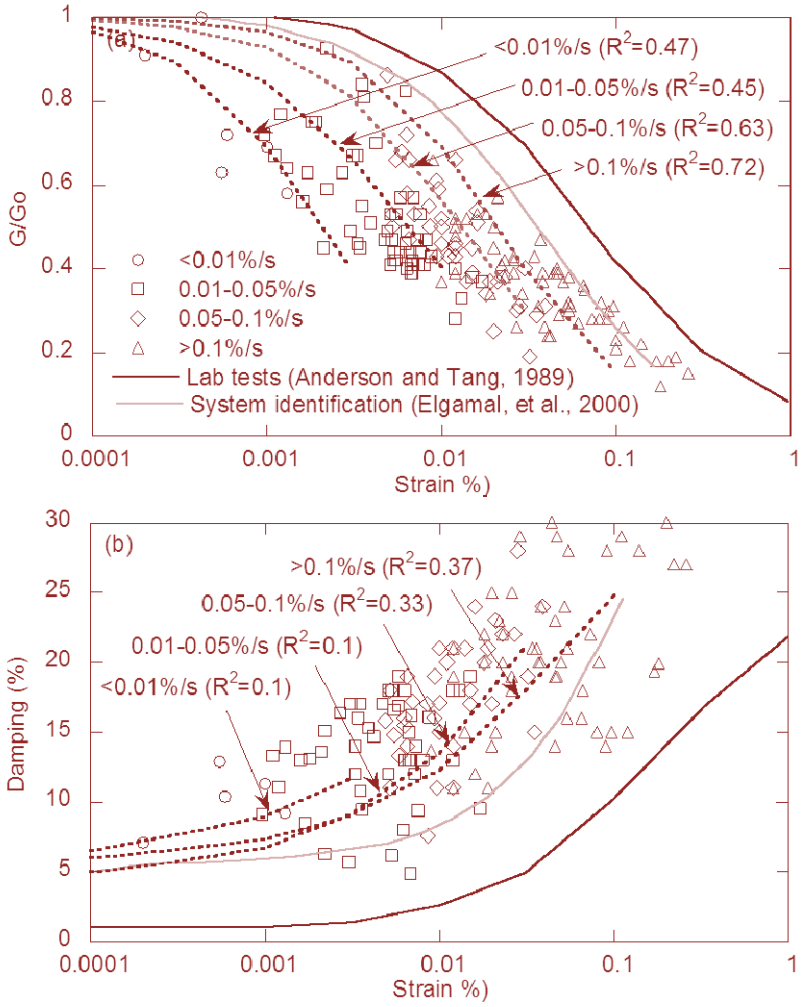

Figure 25 Extracted behavior of Soil Type 1 in terms of strain rate, Lotung array

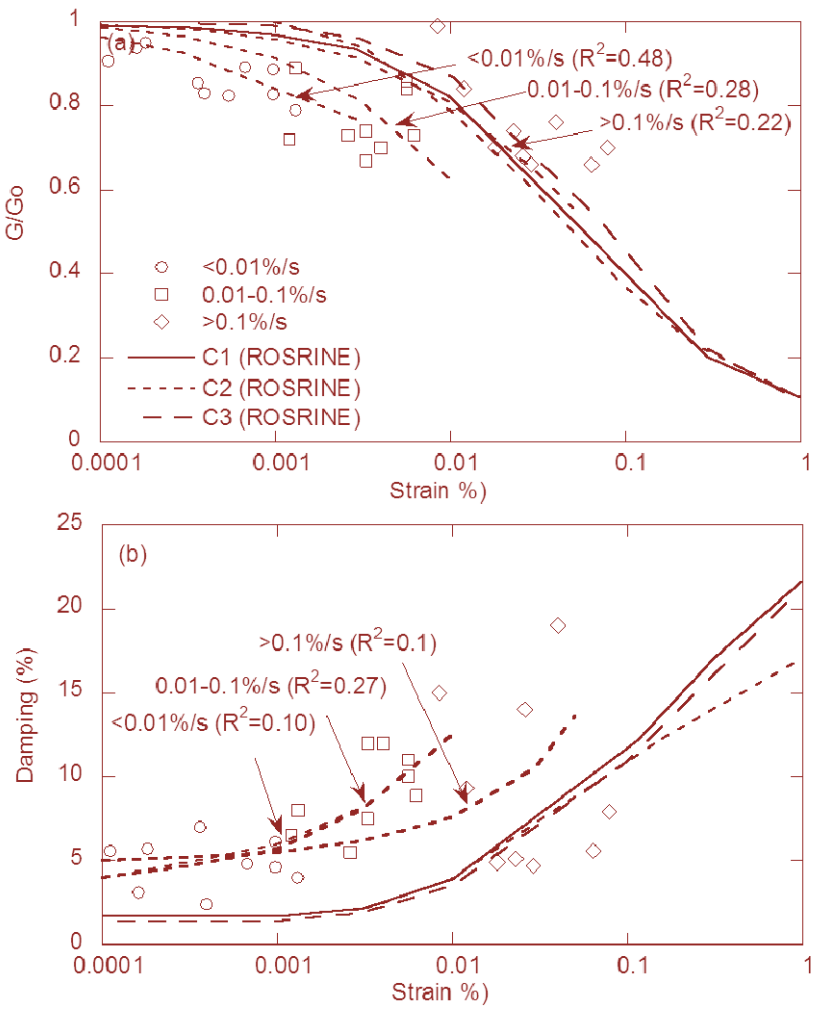

Figure 26 Extracted behavior of Soil Type 5 in terms of strain rate, La Cienaga array

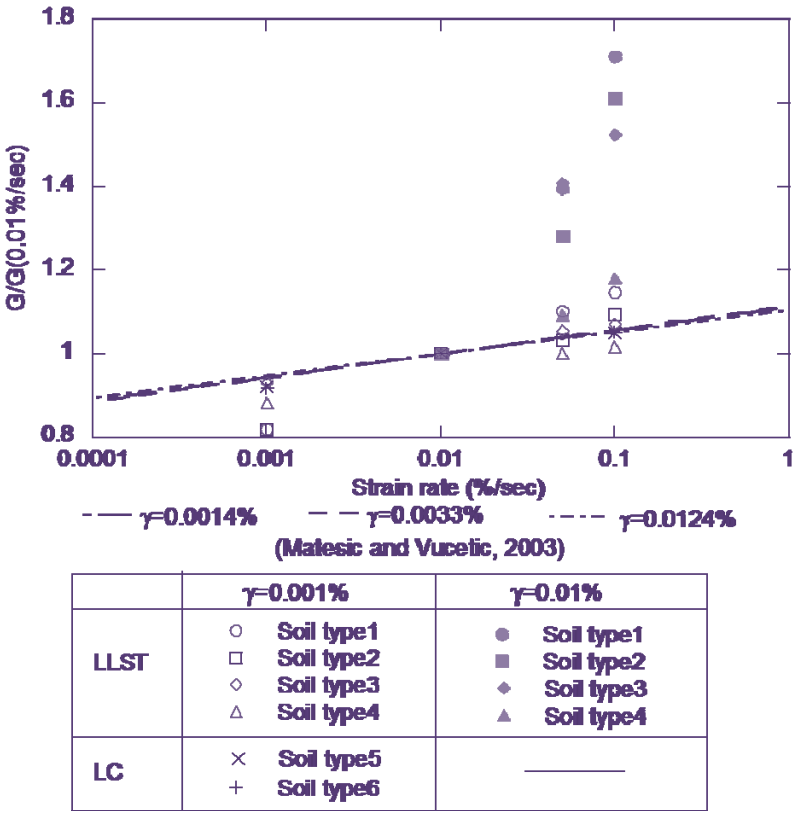

Figure 27 Comparison of strain-rate dependent behavior extracted from downhole array and from lab test (Matesic and Vucetic 2003)

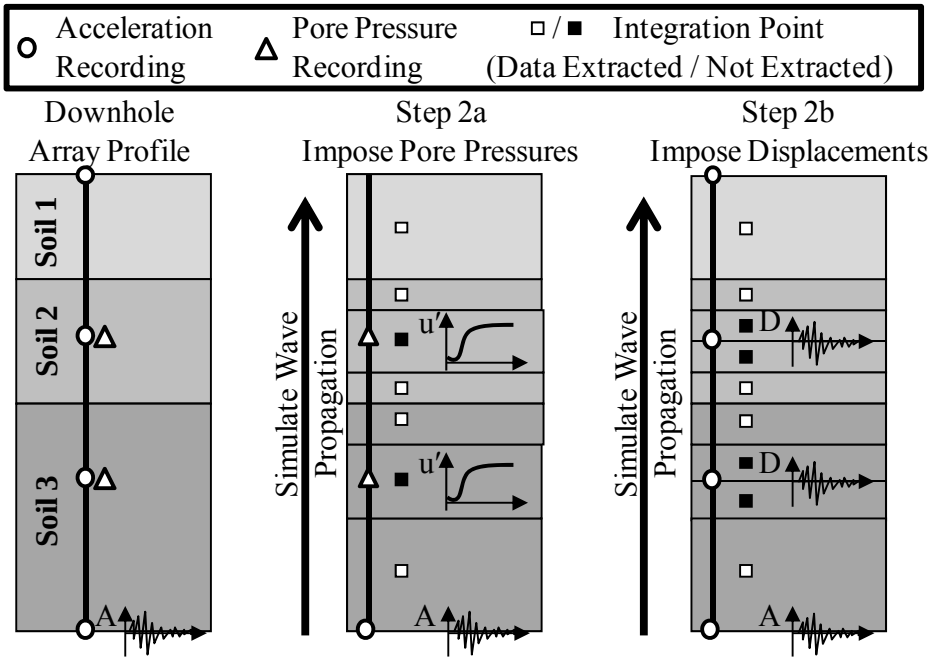

Figure 28 SelfSim mesh generation for pore pressure transducer and accelerometer measurements located at the same depth. Layers with imposed pore pressures (Step 2a) are sub-divided to impose displacements in Step 2b.

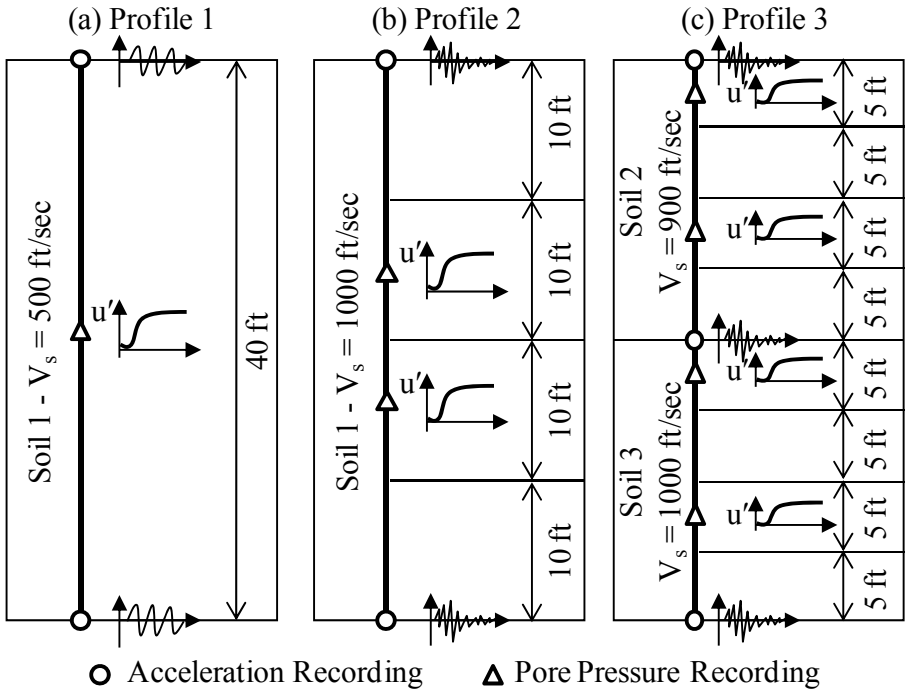

Figure 29 Three synthetic vertical arrays considered for SelfSim analysis.

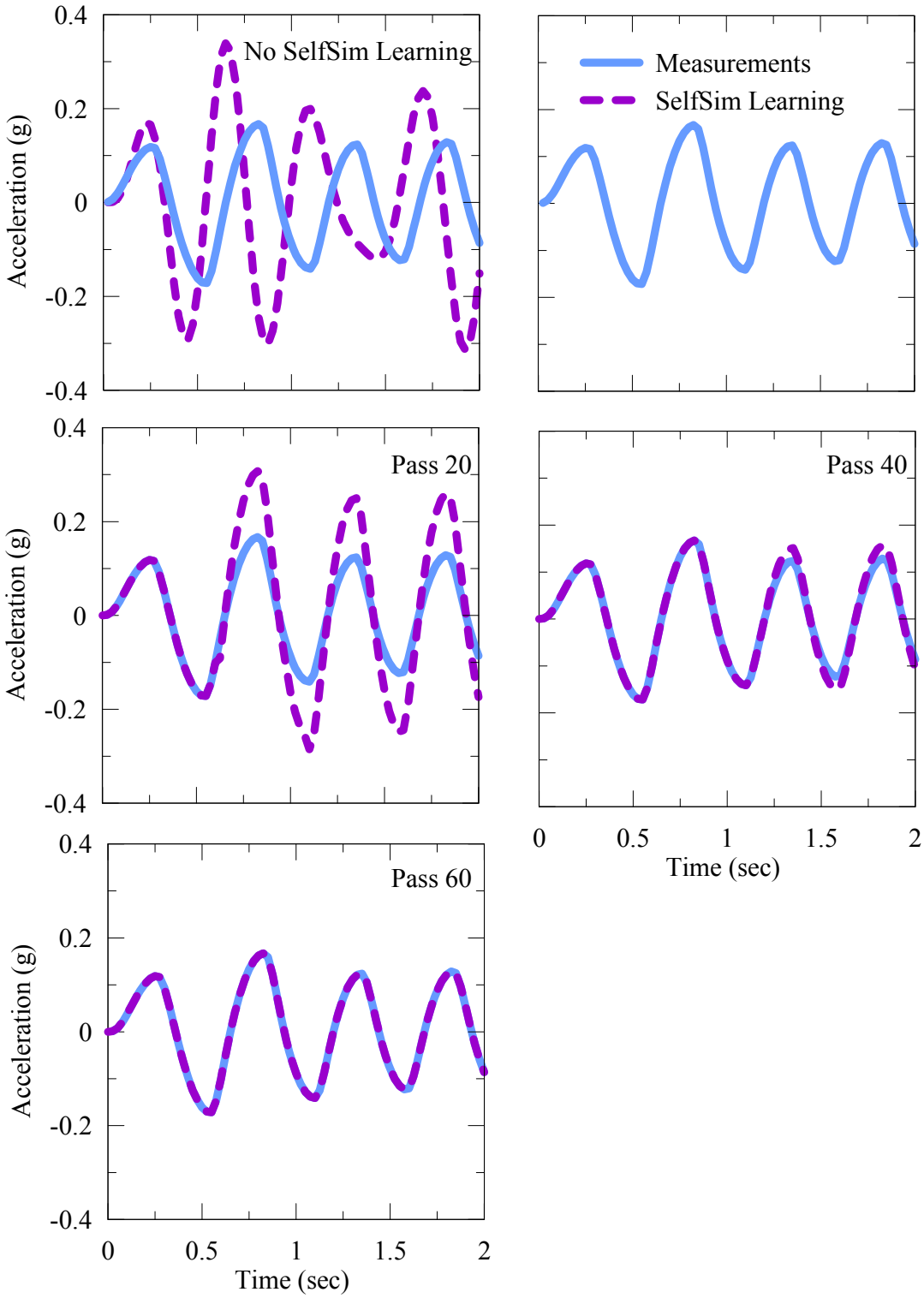

Figure 30 Learning of measured surface displacements, Profile 1, harmonic loading.

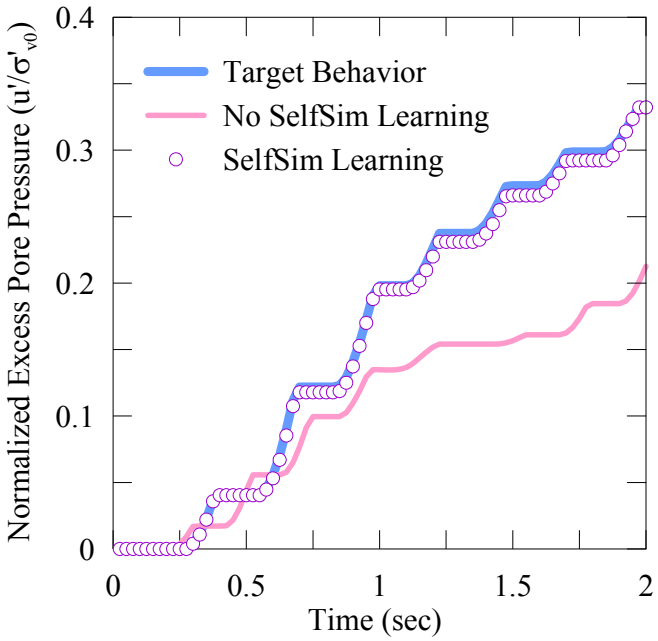

Figure 31 SelfSim learning of pore pressure measurements, Profile 1, harmonic loading.

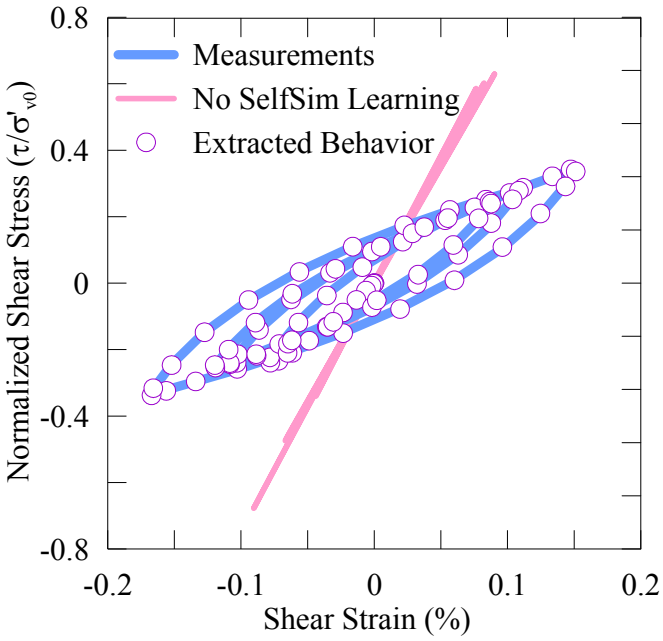

Figure 32 Extracted soil behavior, Profile 1, harmonic loading.

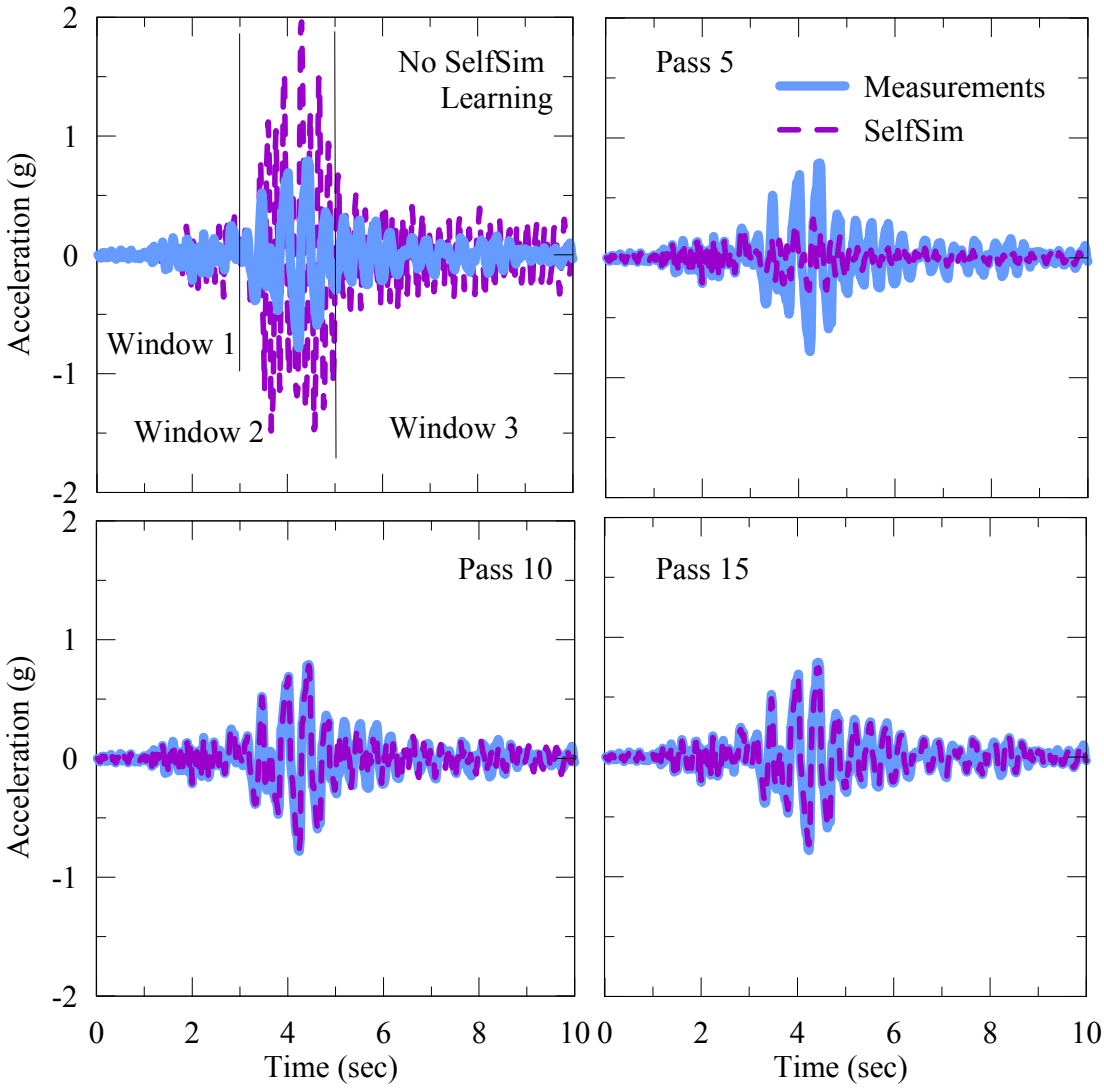

Figure 33 SelfSim learning of surface displacements, Profile 2, Loma Gilroy broadband motion.

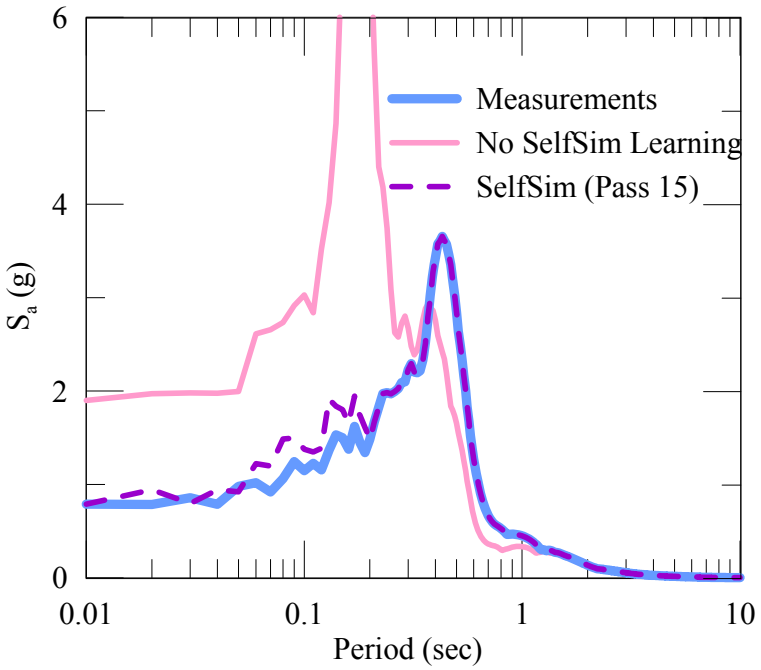

Figure 34 Evolution of surface response spectrum during SelfSim learning process from SelfSim learning (Pass 15), Profile 2.

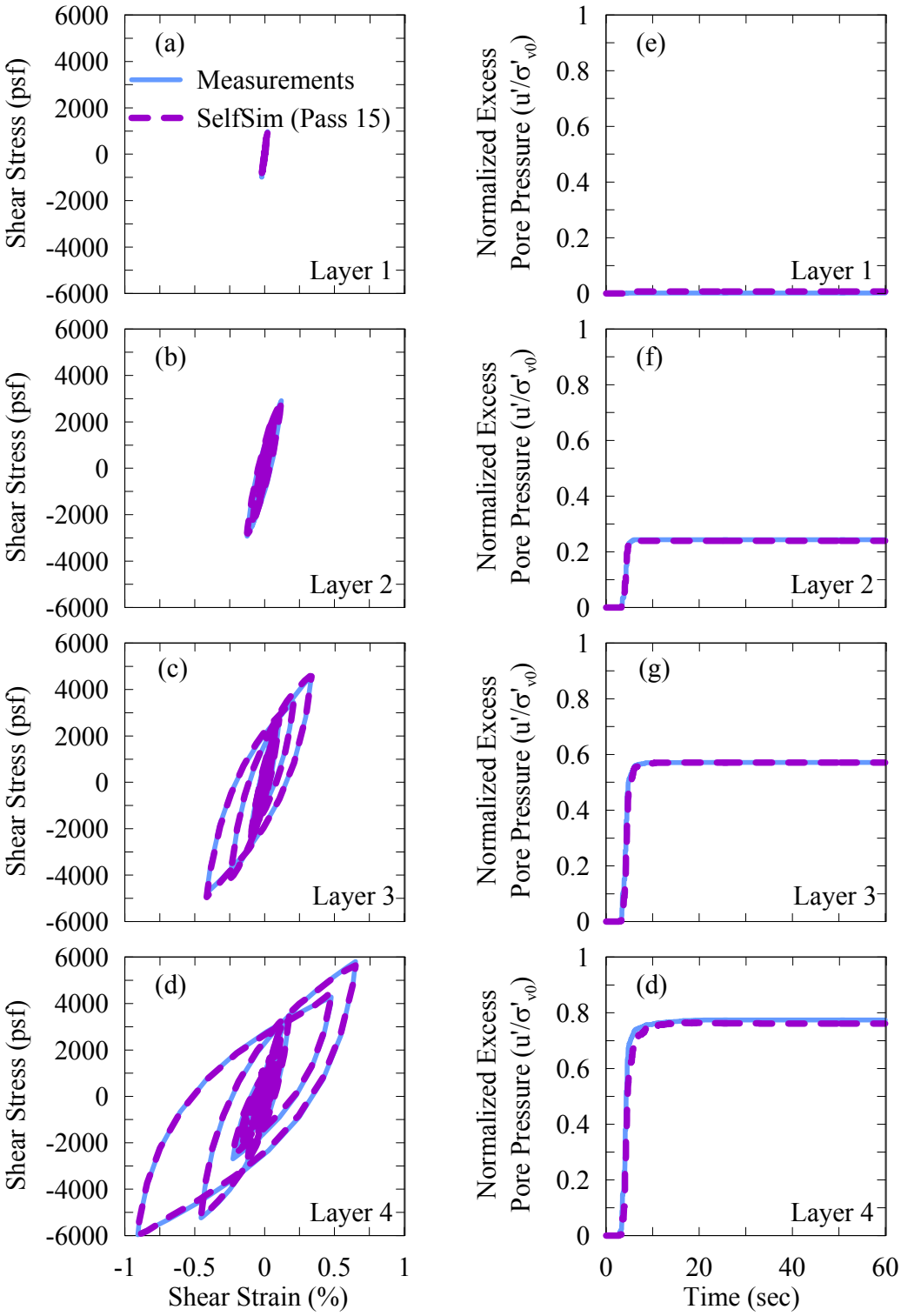

Figure 35 Comparison of learned pore pressure response and extracted and target strain-stress curve of each layer, Profile 2.

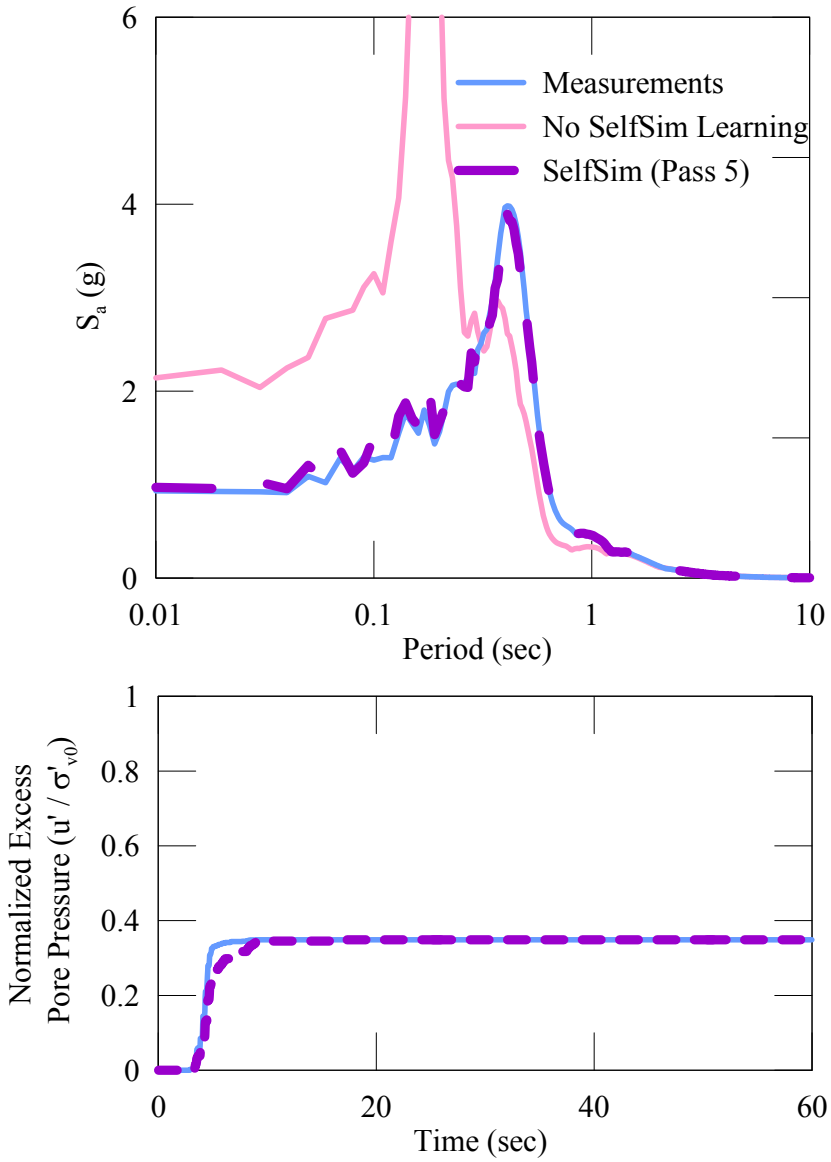

Figure 36 Learning of (a) response spectra and (b) pore pressure generation in layer 5 for LG event, Profile 3.

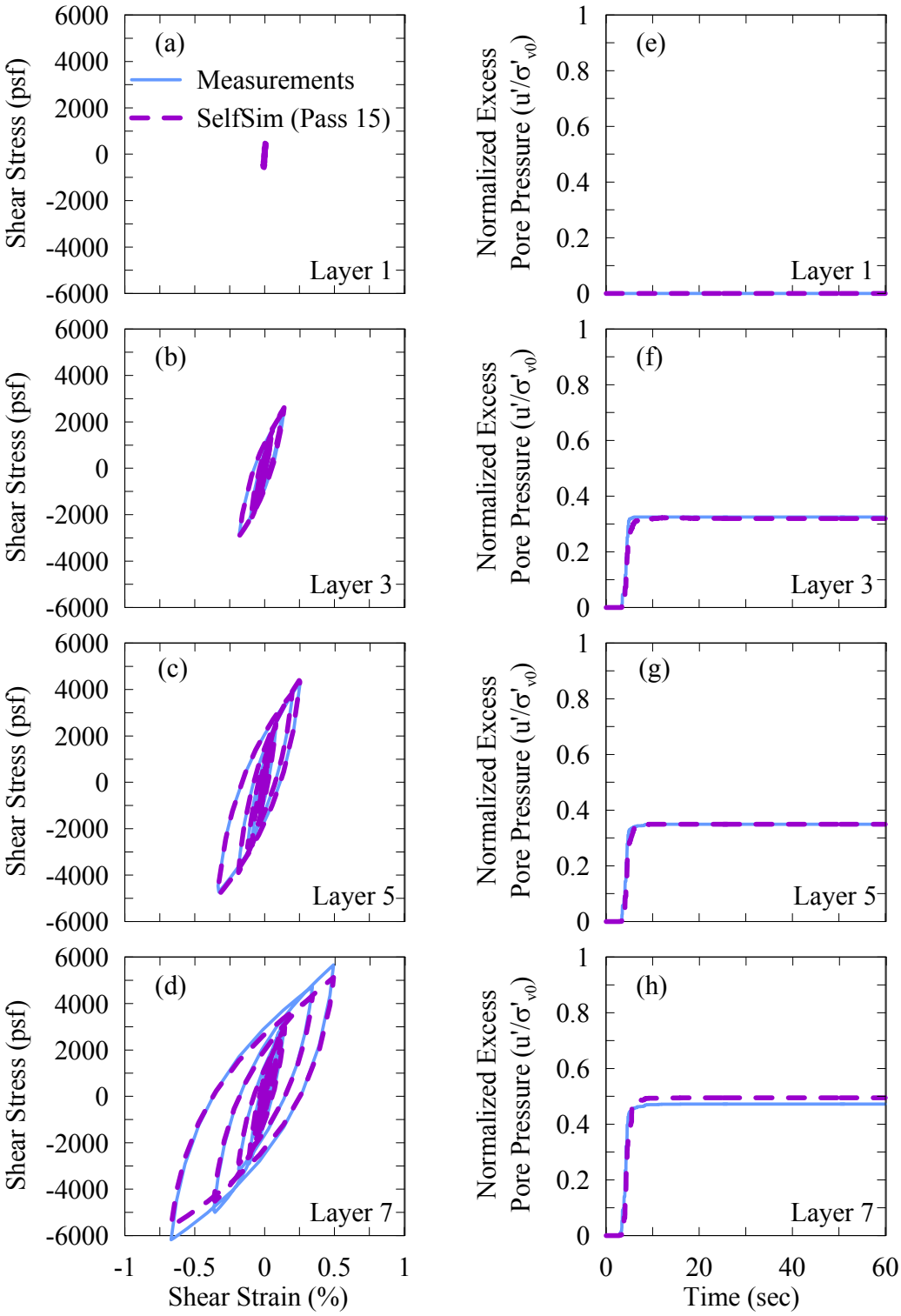

Figure 37 Comparison of extracted and target strain-stress curve and pore pressure response of 4 layers, Profile 3.

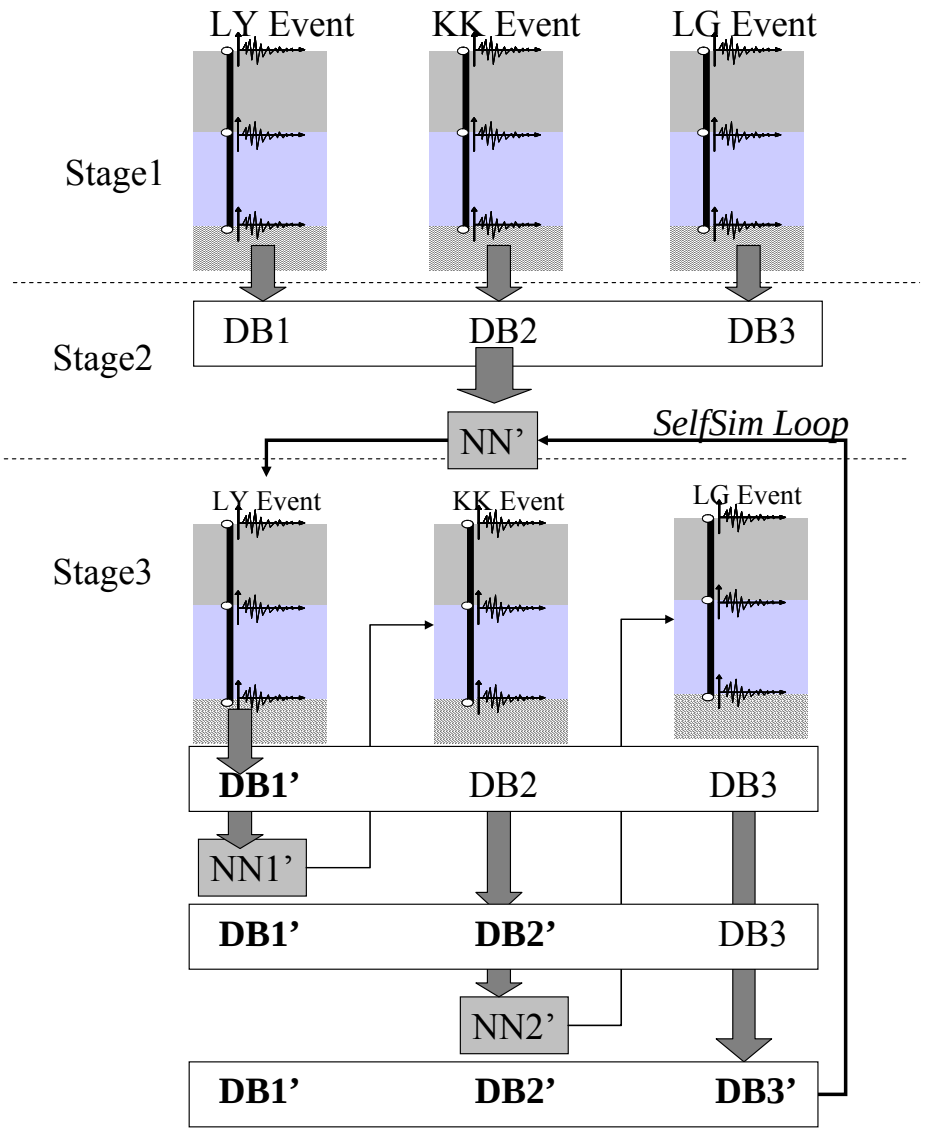

Figure 38 SelfSim learning of multiple events to improve SelfSim learning. Stage1: SelfSim learning of individual events. Stage2: combine data bases (DB) of extracted stress-strain behavior to train a new NN material model. Stage 3: SelfSim learning of individual events, and update of the combined data base used in retraining the NN material model.

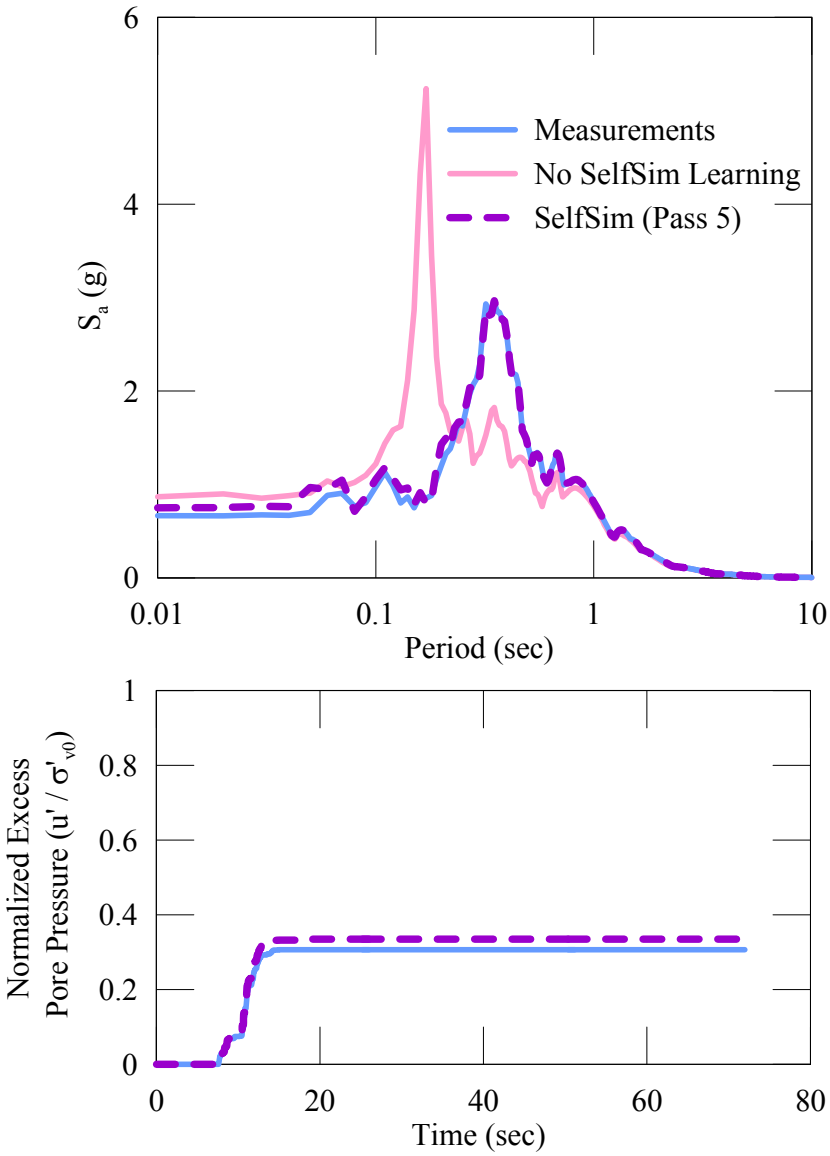

Figure 39 Comparison of (a) ground response and (b) pore pressure generation in layer 5 for KK event.

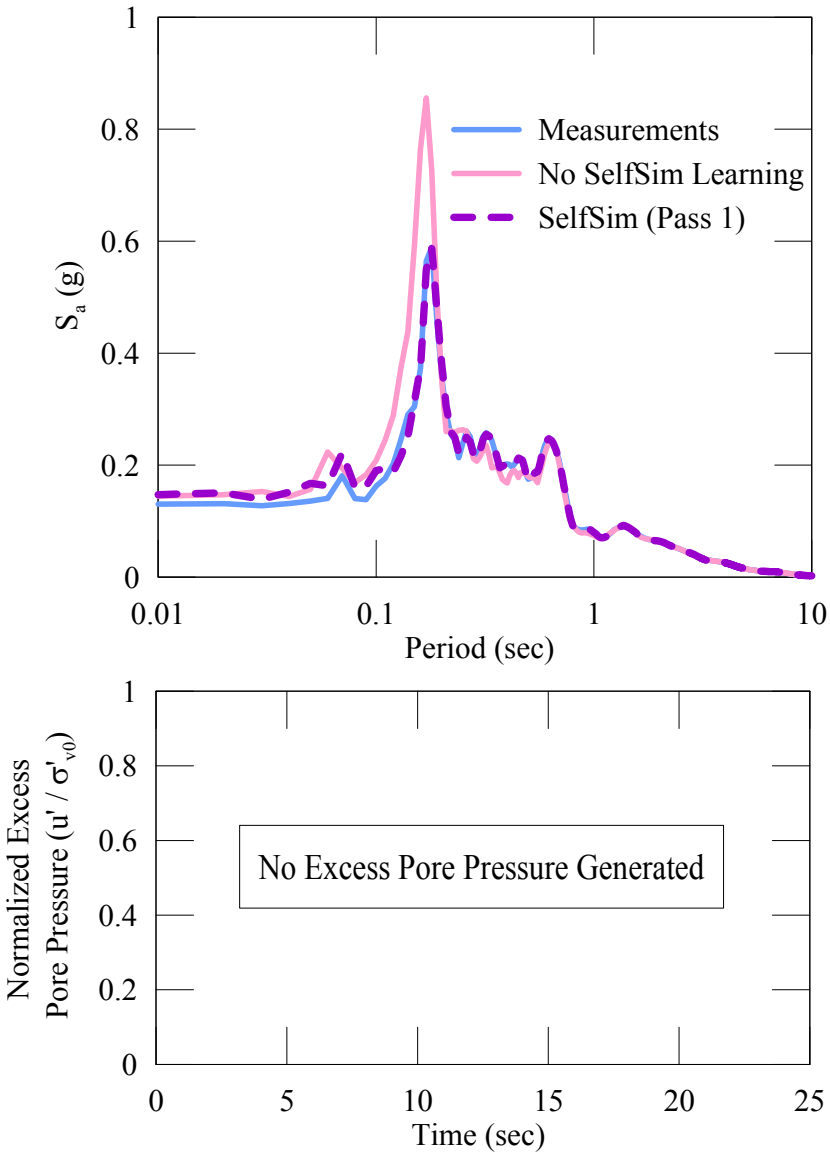

Figure 40 Comparison of ground response for LY event. No excess pore pressures were generated during this event.

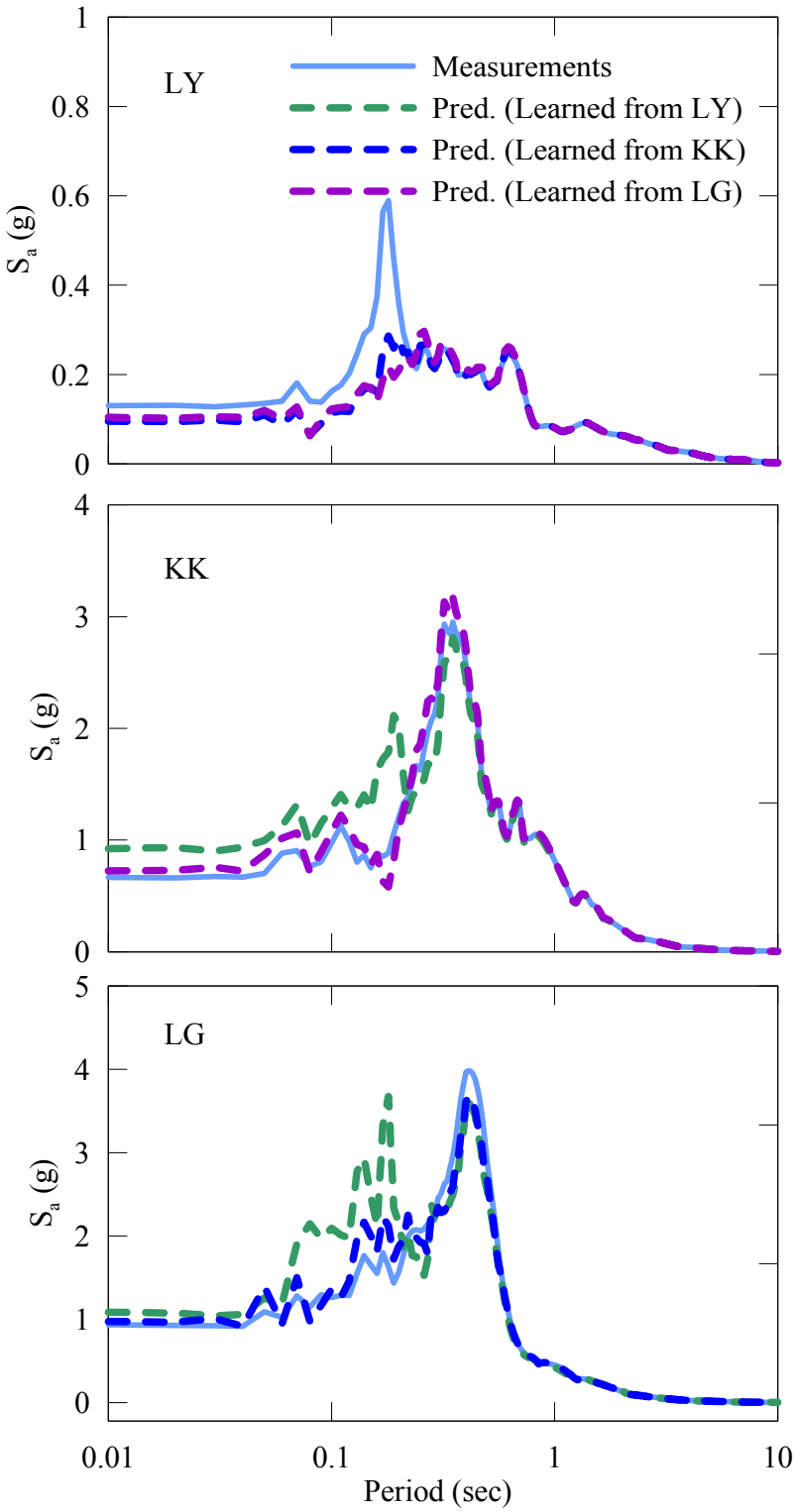

Figure 41 Predicted surface response spectra of a given event using SelfSim extracted NN material models from other events.

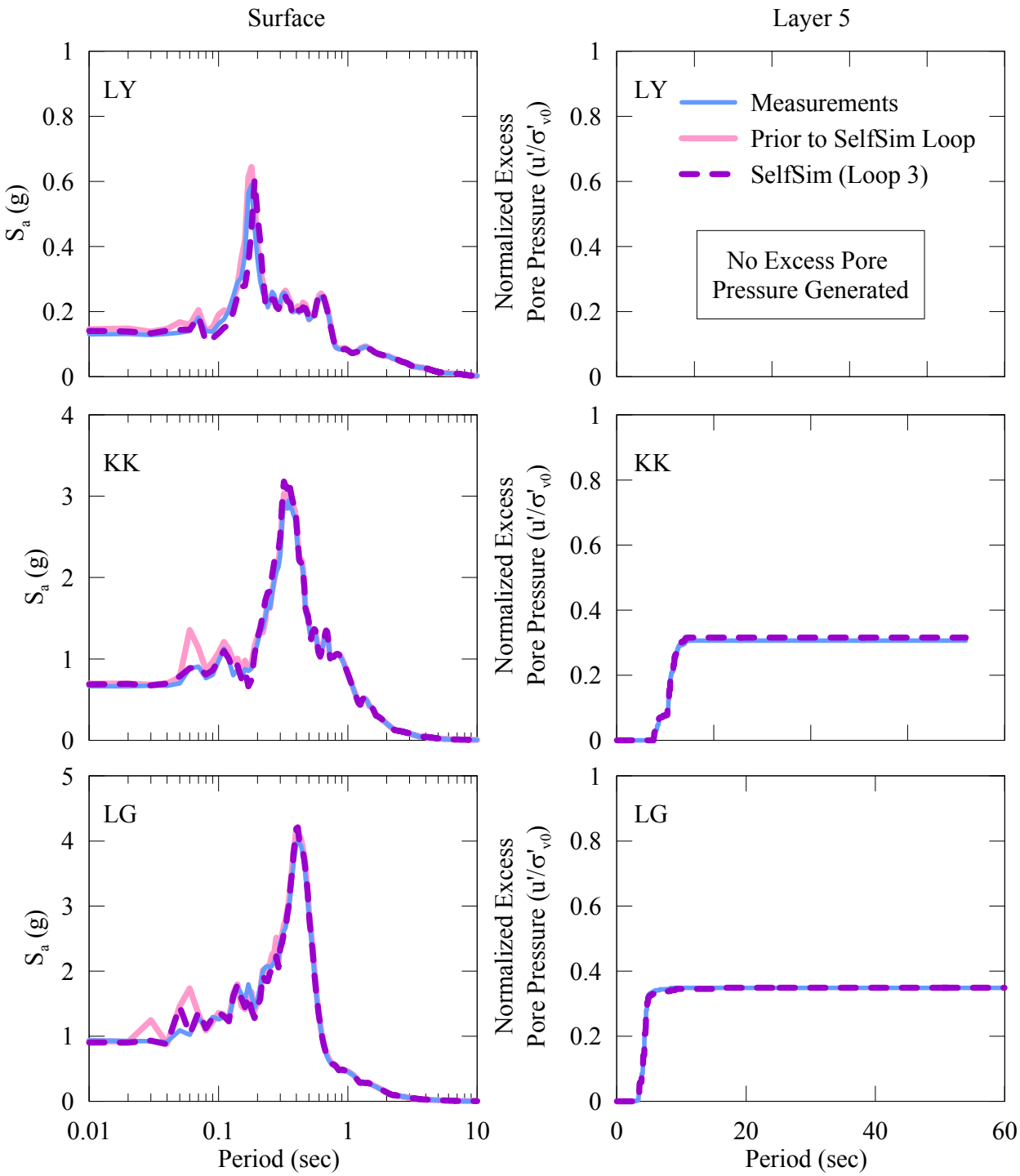

Figure 42 Comparison of surface response spectra (left column, a- c) and pore pressure response in Layer 5 (right column, d-e) of 3 events predicted by using a combined NN material model trained with combined data base (Prior to SelfSim loop) and combined NN material model extracted from SelfSim learning.

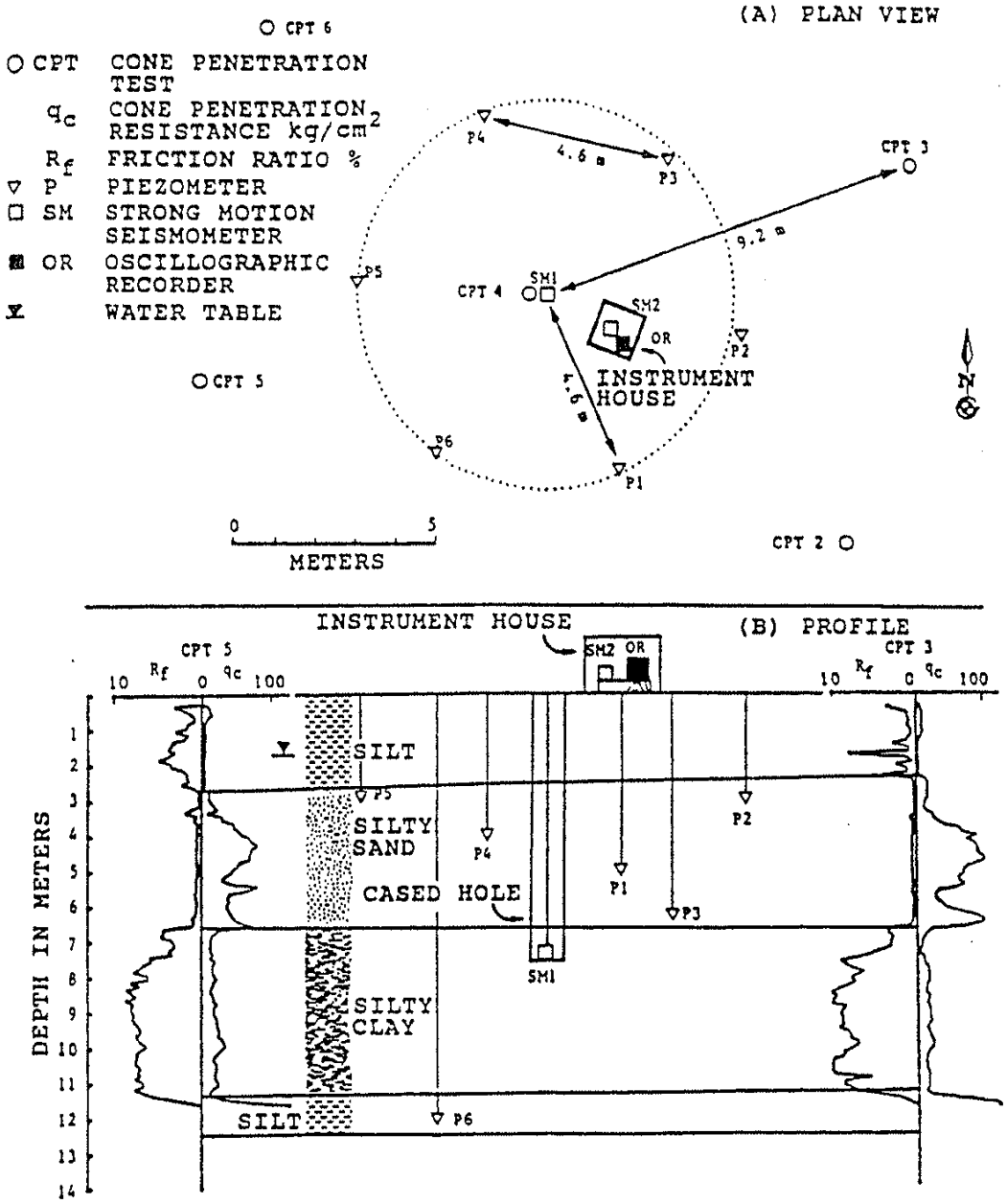

Figure 43 Soil profile at the Wildlife Site and the instrumentation (from Matasovic, 1993; after Benett et al., 1984).

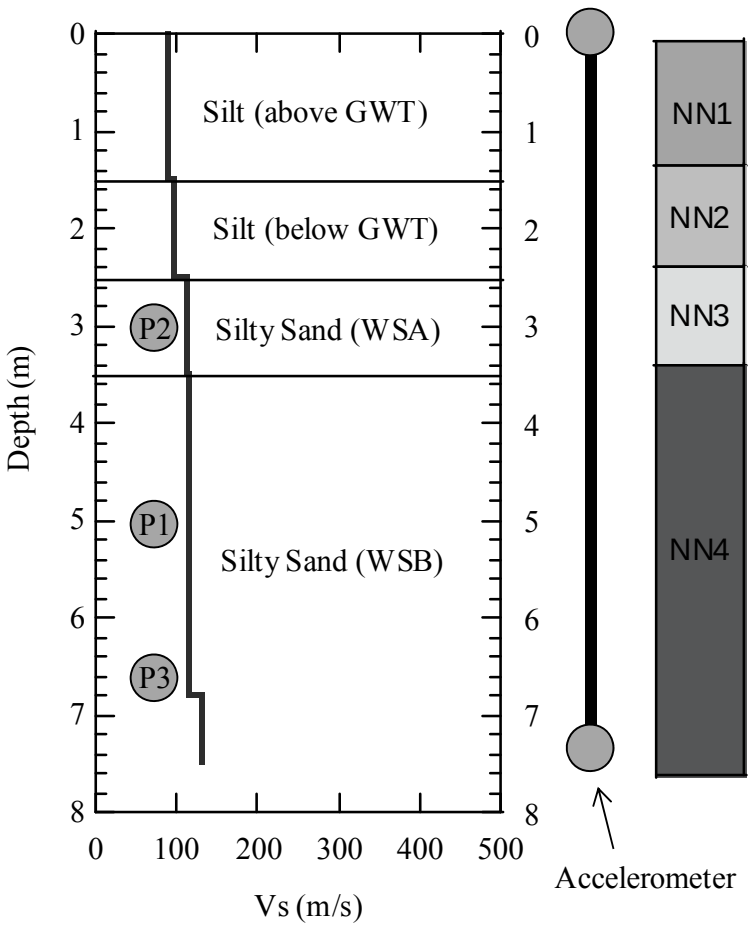

Figure 44 Geology and shear wave profile of Wildlife Liquefaction Array and four assigned NN models according to the geology profile. Accelerometers are located at the top and bottom of the considered profile. Pore pressure measurement locations are denoted as P1, P2, and P3.

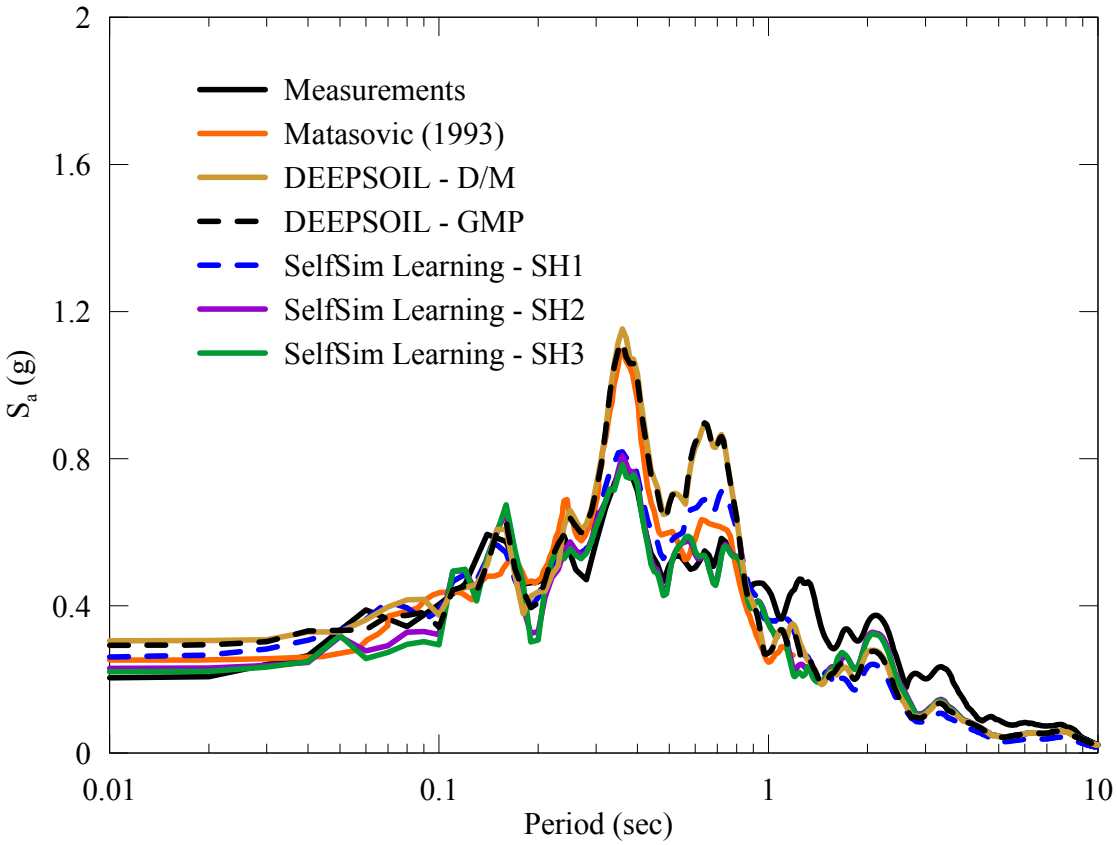

Figure 45 Comparison of surface response spectra of surface measurements, results from 1D site response analysis models, and the SelfSim algorithm for three scenarios (SH1, SH2, SH3) at the original Wildlife Site.

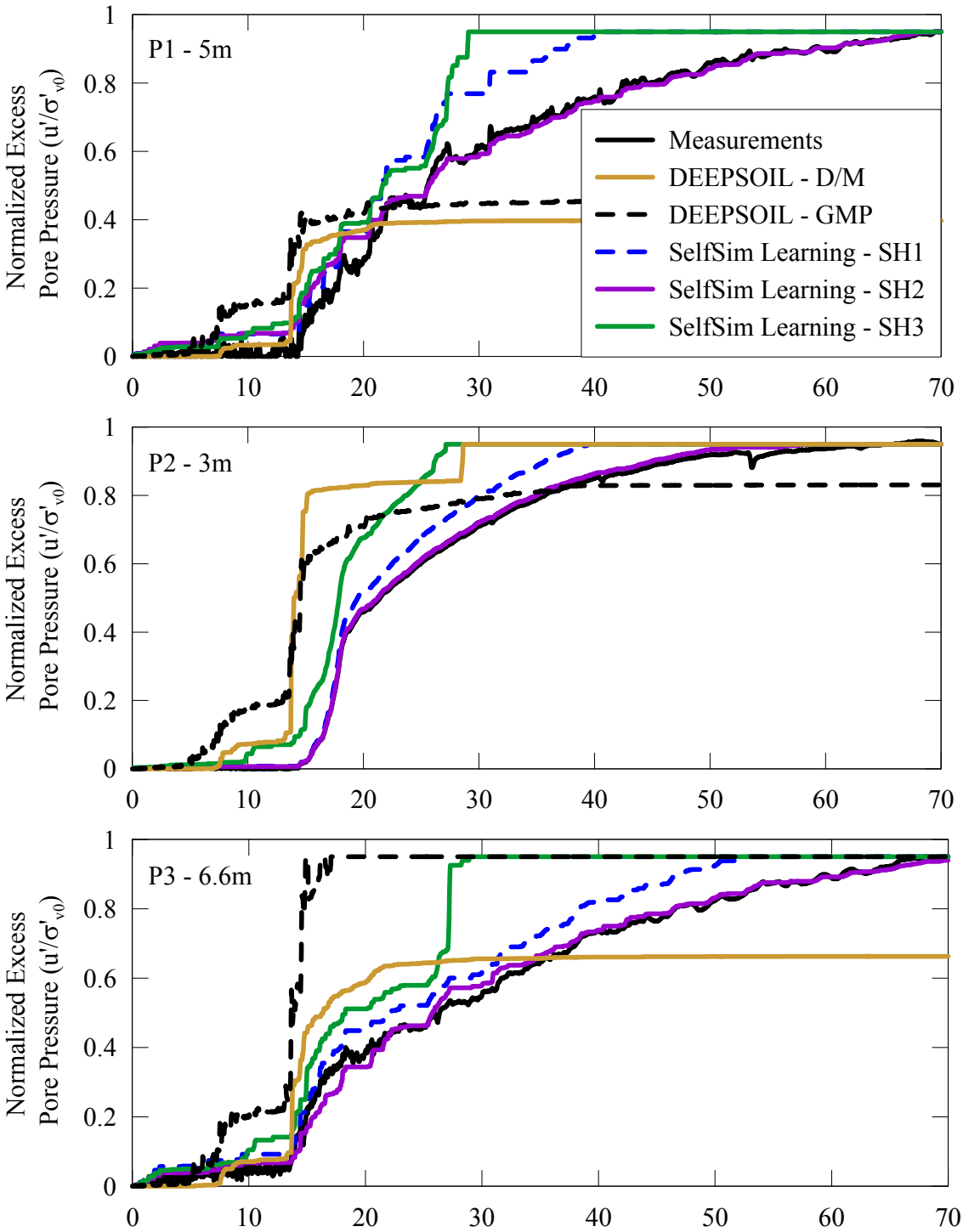

Figure 46 Comparison of pore pressure recordings with results from 1D site response analysis models, as well as the SelfSim algorithm for three scenarios (SH1, SH2, SH3).

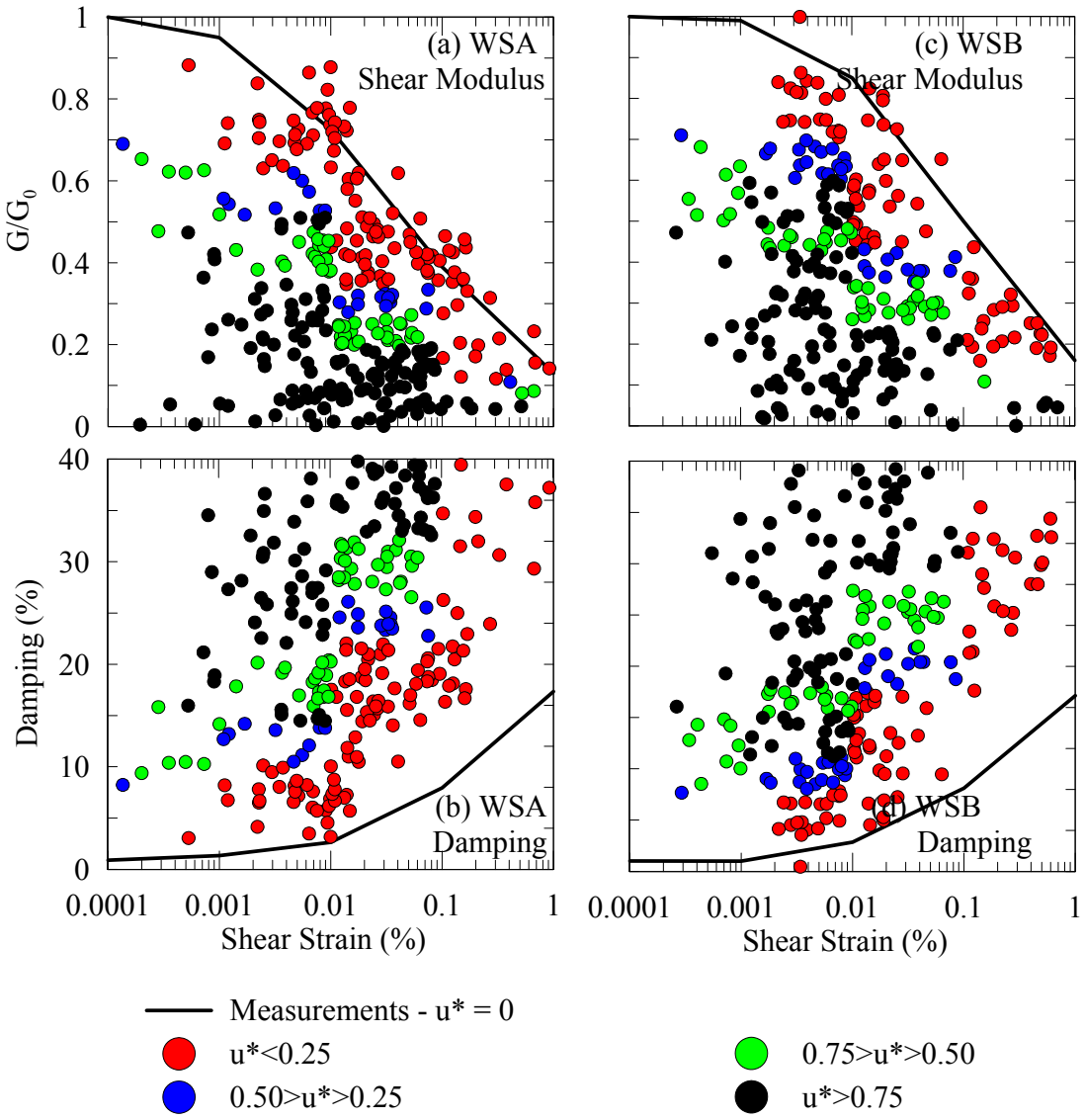

Figure 47 Extracted soil behavior from the SH2 (D/M Initialization) case of SelfSim learning demonstrating the degradation of shear modulus.